nagra National Cooperative for the Disposal of Radioactive Waste

TECHNICAL REPORT 94-07

Grimsel Test Site

Modeling of Groundwater Flow at the Subregional Scale:

Boundary Conditions, Transient and Thermal Effects, Inverse Modeling

December 1994

N.R. Correa (Ed.), A. Rivera, U. Kuhlmann
U. Schröder, F. Müri

Hardstrasse 73, CH-5430 Wettingen/Switzerland, Telephone +41-56-37 11 11

nagra National Cooperative for the Disposal of Radioactive Waste

TECHNICAL REPORT 94-07

Grimsel Test Site

Modeling of Groundwater Flow at the Subregional Scale:

Boundary Conditions, Transient and Thermal Effects, Inverse Modeling

December 1994

N.R. Correa (Ed.)[1], A. Rivera[2], U. Kuhlmann[3], U. Schröder[2], F. Müri[3]

1) Nagra, Wettingen

2) Colenco Power Consulting AG, Baden

3) VAW/ETH-Center, Zürich

Hardstrasse 73, CH-5430 Wettingen/Switzerland, Telephone +41-56-37 11 11

FOREWORD

Concepts for the disposal of radioactive waste in geological formations lay great weight on acquiring extensive knowledge of the proposed host rock and the surrounding rock strata. For this reason, Nagra has, since May 1984, been operating the **Grimsel Test Site (GTS)** which is located at a depth of 450 m in the crystalline rock of the Aar Massif of the Central Swiss Alps. The general objectives of the research being carried out in this underground laboratory include

— the build-up of know-how in planning, performing and interpreting field experiments in various scientific and technical disciplines and

— the acquisition of practical experience in the development of investigation methodologies, measuring techniques and test equipment which will be of use during actual repository site explorations.

The GTS is operated by Nagra and, on the basis of a German-Swiss cooperative agreement, various experiments are carried out by Nagra, the "Bundesanstalt für Geowissenschaften und Rohstoffe, Hannover" (BGR) and the "Forschungszentrum für Umwelt und Gesundheit, München" (GSF). The Grimsel projects of both GSF and BGR are supported by the German Federal Ministry for Research and Technology (BMFT). NAGRA 1985a (German version NAGRA 1985b) provides an overview of the German-Swiss investigation programme. In a special issue of the Nagra Bulletin 1988 (German version "Nagra Informiert 1+2/1988") the status of the programme up to 1988 is described.

VORWORT

Bei Konzepten, welche die Endlagerung radioaktiver Abfälle in geologischen Formationen vorsehen, ist die Kenntnis des Wirtgesteins und der angrenzenden Gesteinsschichten von grundlegender Bedeutung. Die Nagra betreibt deshalb seit Mai 1984 das **Felslabor Grimsel (FLG)** in 450 m Tiefe im Kristallin des Aarmassivs. Die generelle Zielsetzung für die Arbeiten in diesem System von Versuchsstollen umfasst insbesondere

- den Aufbau von Know-how in der Planung, Ausführung und Interpretation von Untergrundversuchen in verschiedenen wissenschaftlichen und technischen Fachgebieten, und

- den Erwerb praktischer Erfahrung in der Entwicklung und der Anwendung von Untersuchungsmethoden, Messverfahren und Messgeräten, die für die Erkundung von potentiellen Endlagerstandorten in Frage kommen.

Im Felslabor der Nagra werden, auf der Basis eines deutsch-schweizerischen Zusammenarbeitsvertrages, verschiedene Versuche von den beiden deutschen Partnern Bundesanstalt für Geowissenschaften und Rohstoffe, Hannover (BGR) und Forschungszentrum für Umwelt und Gesundheit GmbH, München (GSF) durchgeführt. Das Deutsche Bundesministerium für Forschung und Technologie (BMFT) fördert die Arbeiten der BGR und der GSF im FLG. Der NAGRA 1985a (englische Version NAGRA 1985b) enthält eine Übersicht des FLG und die Zusammenfassung der Untersuchungsprogramme mit Status August 1985. In der Ausgabe 1+2/1988 des Heftes "Nagra informiert" bzw. der englischen Spezialausgabe "Nagra Bulletin 1988" ist der Stand der FLG Arbeiten anfangs 1988 beschrieben.

AVANT-PROPOS

Lors d'études de concepts d'évacuation de déchets radioactifs dans des formations géologiques, on attache une grande importance à l'acquisition d'informations étendues sur la roche d'accueil et les formations rocheuses environnantes. C'est pour cette raison que la Cédra exploite depuis mai 1984 son **Laboratoire souterrain du Grimsel (LSG)** situé à 450 m de profondeur dans les roches cristallines du massif de l'Aar, situé au centre des Alpes suisses. Les principaux objectifs des recherches effectuées dans ce laboratoire concernent

— l'acquisition de savoir-faire dans diverses disciplines techniques et scientifiques pour la conception, la réalisation et l'interprétation d'expériences dans le terrain et

— la récolte d'expériences pratiques dans la mise au point de méthodologies d'investigation, de techniques de mesure et d'appareillages qui pourraient être utilisés lors de l'exploration de sites potentiels de dépôts finals.

Le LSG est exploité par la Cédra et diverses expériences y sont réalisées par celle-ci et deux institutions allemandes, la "Bundesanstalt für Geowissenschaften und Rohstoffe, Hannover" (BGR) et le "Forschungszentrum für Umwelt und Gesundheit, München" (GSF) dans le cadre d'un traité de collaboration germano-suisse. Les projets poursuivis au Grimsel par la BGR et le GSF sont supportés par le Ministère fédéral allemand de la recherche et de la technologie (BMFT). Les rapports NAGRA 1985a (version anglaise) et NAGRA 1985b (version allemande) présentent un aperçu du laboratoire souterrain et un résumé des programmes de recherches. La situation de ce programme en 1988 est présentée dans la publication "Cédra informe 1+2/1988" (version française) et "Nagra informiert 1+2/1988" (version allemande) ainsi que dans une édition spéciale en anglais (Nagra Bulletin 1988).

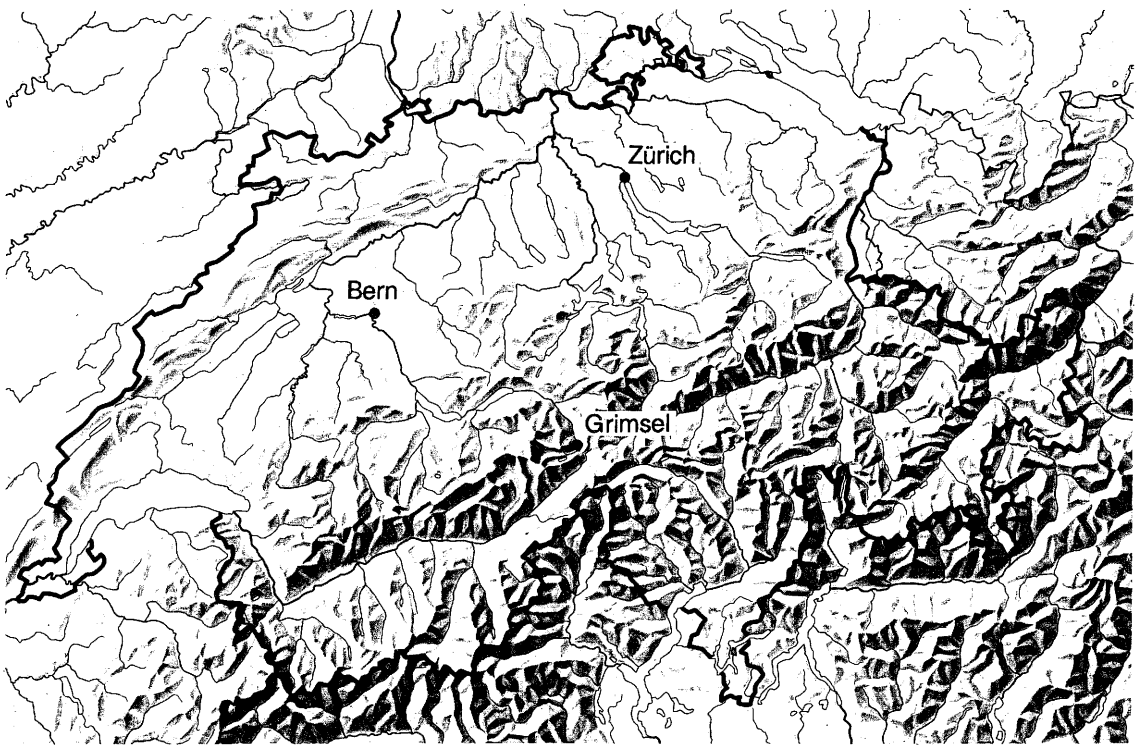

Location of Nagra's underground test facility at the Grimsel Pass in the Central Alps (Bernese Alps) of Switzerland (approximate scale 1 cm = 25 km).

Geographische Lage des Nagra Felslabors am Grimselpass (Berner Oberland) in den schweizerischen Zentralalpen (Massstab: 1 cm = ca. 25 km)

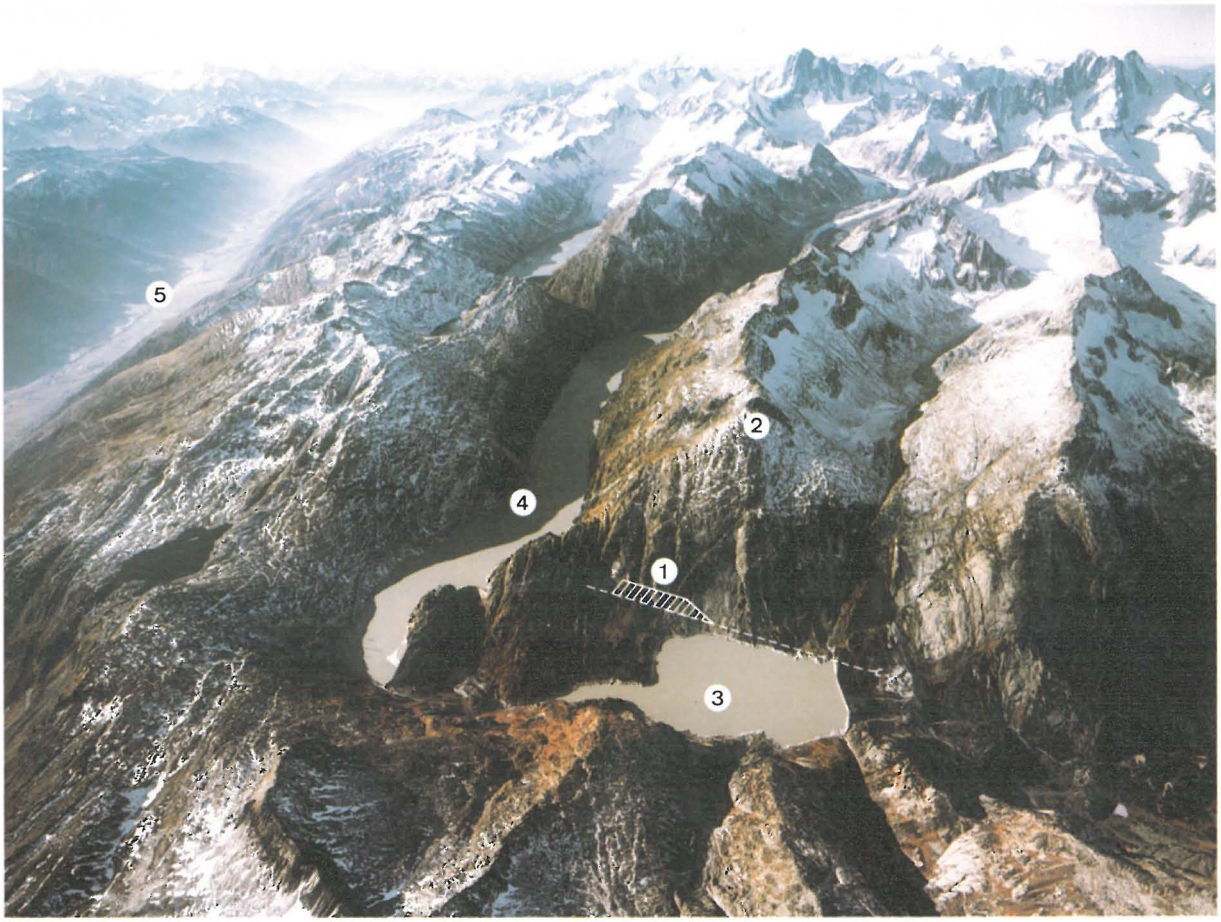

GRIMSEL-GEBIET

Blick nach Westen

1 Felslabor
2 Juchlistock
3 Räterichsbodensee
4 Grimselsee
5 Rhonetal

GRIMSEL AREA

View looking West

1 Test Site
2 Juchlistock
3 Lake Raeterichsboden
4 Lake Grimsel
5 Rhone Valley

FLG FELSLABOR GRIMSEL
GTS *GRIMSEL TEST SITE*

Situation

0 100 m

- Zugangsstollen/*Access tunnel*
- Fräsvortrieb/*by tunnel boring machine*
- Sprengvortrieb/*excavated by blasting*
- Zentraler Aaregranit ZAGR / *Central Aaregranite CAGR*
- Biotitreicher ZAGR / *CAGR with high content of biotite*
- Grimsel-Granodiorit / *Grimsel-Granodiorite*
- Scherzone/*Shear zone*
- Lamprophyr/*Lamprophyre*
- Wasserzutritt/*Water inflow*
- SB Sondierbohrung/*Exploratory borehole*
- US US Bohrung/*US borehole*

ZB	Zentraler Bereich/*Central facilities*
AU	Auflockerung/*Excavation effects*
BK	Bohrlochkranz/*Fracture system flow*
EM	El.magn. HF-Messungen/*-measurements*
FRI	Kluftzone/*Fracture zone investigation*
GS	Gebirgsspannungen/*Rock stresses*
HPA	Hydr. Parameter/*Hydr. parameters*
MI	Migration/*Migration*
MOD	Hydrodyn. Modellierung/*H. modeling*
NM	Neigungsmesser/*Tiltmeters*
UR	Untertageradar/*Underground radar*
US	Seismik/*Underground seismic testing*
VE	Ventilationstest/*Ventilation test*
WT	Wärmeversuch/*Heat test*

A — A Schnitt/*Section*

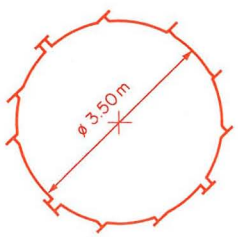

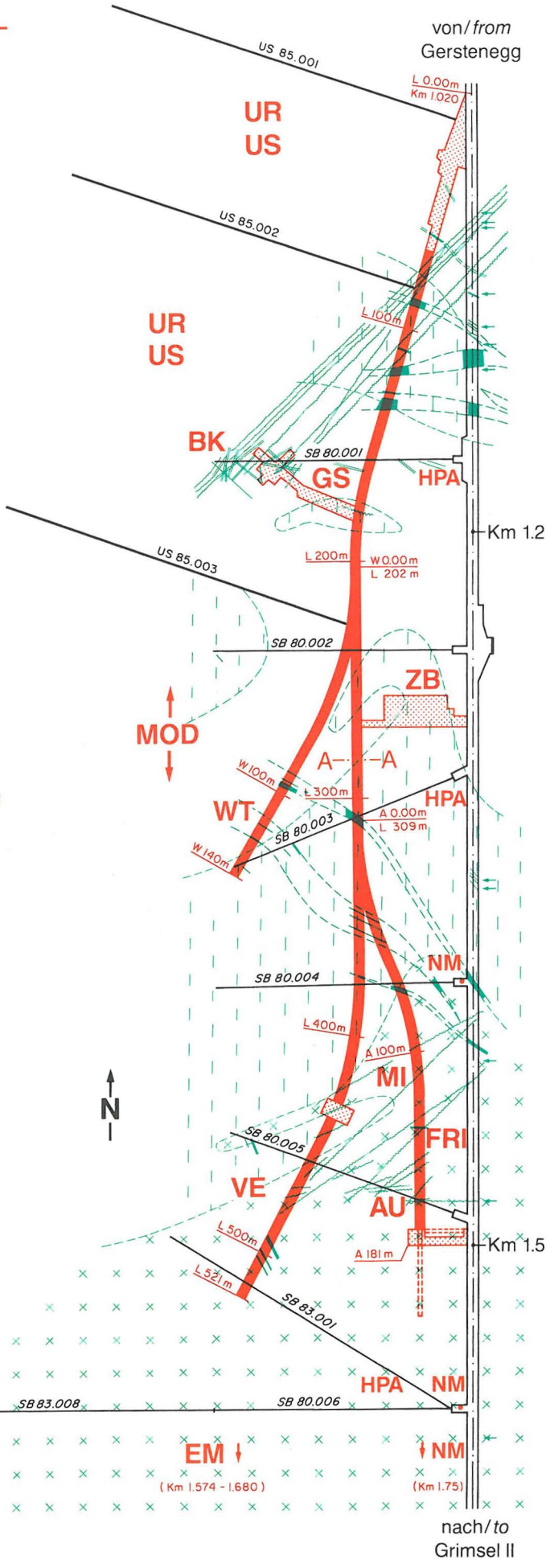

6/88

SUMMARY

This report presents the findings of four major works developed by various work teams during the period of 1991-1993, under project MOD phase III.

In the scope of the hydrogeological test program, project MOD was designed to investigate the adequate strategy for the hydrodynamic modeling of groundwater flow in a fractured rock body surrounding the Grimsel Test Site (GTS). The principal goals for phase III were to: investigate strategies for model calibration and validation; quantitatively evaluate groundwater transient effects due to the presence of drifts; analyse coupled thermo-hydraulic effects with variable-density fluid around an imaginary repository. An overall aim of project MOD from its very conception, was to gain experience and know-how and to create and/or adapt innovative numerical tools.

A literature review of model calibration and validation concepts, and scaling of hydrogeological parameters, allowed the elaboration of a strategy for model calibration and validation with the main conclusions from the state-of-the-art literature in this field. This methodology is applied to the sub-regional GTS model enabling an automatic calibration with the use of an inverse model. The groundwater transient effects due to the presence of drifts are evaluated quantitatively in one, two and three dimensions with analytical and numerical models. The latter exercise permits the application of complex numerical models that are tested by comparison with analytical solutions. In this case, an assorted type of boundary conditions and grid discretizations are tested in order to have a set of cases, as complete as possible, for this type of problems.

The effects of variable-density groundwater flow due to heat release from a fictitious high-level waste repository are evaluated. The numerical grid discretization needed for this type of nonlinear problem is first evaluated with the grid Peclet number criteria in three dimensions. This process-oriented study, aims at: determining the feasibility of performing 3-D coupled thermo-hydraulic computations with the available computer facilities; performing scoping thermo-hydraulic computations for a representative 3-D fictitious repository; and, comparing the resulting groundwater flow field with the isothermal flow field.

Finally, we conclude that the goals of project MOD phase III were achieved. The methodologies and tools developed during this work, as well as the modeling strategies and actual simulations give a useful framework for future site-specific hydrodynamic modeling studies within the scope of NAGRA. Processes related to transient hydrodynamic effects are better understood for models in one, two and three dimensions. Automated inverse modeling has proven to be a powerful tool for model calibration. The results on the scoping of computer load and grid discretization for large problems (3D) with complex hydrogeology, and transient or coupled problems, can be used to better

design future specific studies. In short, it is believed that considerable know-how and experience have been acquired during Project MOD III with a view to understanding the hydrodynamic behaviour of low permeable heterogeneous media around underground constructions.

ZUSAMMENFASSUNG

Dieser Bericht stellt die wichtigsten Ergebnisse dar, die im Zeitraum 1991-1993 innerhalb verschiedener Arbeitsgruppen im Rahmen vom Projekt MOD Phase III (Hydrodynamische Modellierung) erarbeitet wurden.

Im Rahmen eines übergeordneten hydrogeologischen Untersuchungsprogramms im Felslabor Grimsel (FLG) wurde das Projekt MOD initiiert, um eine geeignete Strategie und Vorgehensweise für die Modellierung der Grundwasserströmung in geklüftetem Gestein zu erarbeiten. Übergeordnetes Ziel des Projektes MOD war von Anfang an die Sammlung von Erfahrung und Know-how sowie die Entwicklung bzw. Anpassung von Software für numerische Simulationen. Die wichtigsten angestrebten Ziele des Projektes für die Phase III waren: die Untersuchung von transienten Effekten auf die Grundwasserströmung, welche durch Bau, Betrieb und Versiegelung von Stollen hervorgerufen werden; die Berechnung dichteabhängiger, gekoppelter thermo-hydraulischer Prozesse im Umfeld eines imaginären HAA-Endlagers; und die Erweiterung bzw. Vervollständigung bestehender Kalibrierungs- und Validierungkonzepte.

Durch eine Literaturstudie zum Stand der Technik über Modelleichung und -validierung, sowie über Skalierung von Prozessen und Modellparametern wurde eine Modellierungsstrategie für ein komplexes Standortmodell entwickelt. Diese Methodik wird anhand des subregionalen Modells FLG getestet, wobei eine automatisierte Eichung mittels Inverser Modellierung zur Anwendung kommt. Die durch Stollenbau, -betrieb und -versiegelung hervorgerufenen transienten Effekte auf die Grundwasserströmung werden mit ein-, zwei- und dreidimensionalen Modellen analysiert. In weiterführenden Arbeiten kamen komplizierte numerische Modelle zur Anwendung, deren Güte durch den Vergleich ihrer Resultate mit analytischen Lösungsansätzen dokumentiert wurde. Um allen Fragestellungen gerecht zu werden, und spezifische Probleme möglichst vollständig beantworten zu können, wurden mehrere Kombinationen von Randbedingungen und Netz-Diskretisierungen getestet.

Die Auswirkungen von dichteabhängigen Grundwasserströmungen, die durch die Freisetzung thermischer Energie eines imaginären Endlagers für hochaktive Abfallstoffe entstehen, wurde untersucht. Der Diskretisierungsbedarf bei diesem stark nicht-linearen, gekoppelten Simulationsproblem wurde zunächst durch das Peclet-Zahl Kriterium für das subregionale Modell FLG (drei-, zwei- und eindimensionale Finite-Elemente-Netze) ermittelt. Diese projektorientierte Studie sollte folgende Fragen beantworten:

- sind gekoppelte thermo-hydraulische Berechnungen in einem dreidimensionalen Finite-Elemente-Netz mit den vorhandenen Computerresourcen durchführbar;
- welchen Arbeitsaufwand erfordert die dreidimensionale Modellierung thermo-hydraulischer Prozesse im Umfeld eines imaginären Endlagers; und

— welche Unterschiede weisen ausschliesslich isothermal/thermohydraulisch beeinflusste Grundwasserfliesssysteme auf?

Alle angestrebten Ziele vom Projekt MOD konnten erreicht werden. Die Modellierungsstrategie, die entwickelte, angepasste bzw. getestete Software und die jeweiligen Simulationsergebnisse geben wertvolle Hinweise und Rahmenbedingungen für künftige Standortmodelle von Endlagern. Es wurden umfangreich Erfahrungen über transiente Effekte von Tunnelsystemen auf die Grundwasserströmung gesammelt, die mit ein-, zwei- und dreidimensionalen Modellen gewonnen wurden. Die automatisierte Inverse Modellierung hat sich für die Modellkalibrierung als sehr wertvoll erwiesen und bewährt. Die Ergebnisse über die numerische Computerauslastung von komplexen dreidimensionalen Problemen und deren Diskretisierungsbedarf können benutzt werden, um künftige Modellarbeiten an konkreten Standorten zu realisieren.

Im Verlauf des Projektes wurden vertiefte Kenntnisse des hydrodynamischen Verhaltens und der Modellierung eines gering durchlässigen und heterogenen Gesteinskörpers im Umfeld eines Untertagebauwerks gewonnen.

RESUME

Ce rapport présente les résultats des quatre principaux travaux effectués par plusieurs équipes de travail pendant la période 1991-1993 à l'intérieur du projet MOD, phase III.

Dans le cadre du programme hydrogéologique, le projet MOD a pour but d'étudier une stratégie adaptée à la modélisation hydrodynamique des écoulements dans les roches fracturées entourant le Site du Laboratoire Souterrain du Grimsel (GTS). Les objectifs principaux pendant cette phase ont été de rechercher des stratégies pour le calage et la validation des modèles, d'évaluer quantitativement les effets d'écoulement transitoires dus à la présence de tunnels, d'analyser les effets couplés thermo-hydrauliques avec des fluides de densité variable autour d'un dépôt fictif. On a réalisé également le calage automatique du modèle régional du GTS par la méthode inverse. Dès la conception du projet MOD, un des objectifs d'ensemble a été aussi d'acquérir l'expérience et les connaissances dans la création et l'adaptation d'outils numériques innovateurs.

Une révision approfondie des concepts de calage et de validation, ainsi que de l'effet d'échelle des paramètres hydrogéologiques, a permis l'élaboration d'une stratégie pour calibrer et valider le modèle du GTS, avec prise en compte des principales conclusions de la littérature la plus récente dans ce domaine. Cette méthodologie a alors été appliquée au modèle sub-régional du GTS, ce qui a permis un calage automatique avec un modèle inverse. Les effets transitoires de l'écoulement d'eau souterraine dus à la présence de tunnels ont été évalués quantitativement dans une, deux et trois dimensions avec des modèles analytiques et numériques. Ce dernier exercice a permis l'application de modèles numériques sophistiqués, testés par comparaison avec les solutions analytiques. Dans ce cas, des conditions aux limites et la discrétisation des mailles assorties ont été testées pour pouvoir ainsi disposer de cas aussi variés que possible pour ce type de problèmes.

Les effets de l'écoulement d'eau souterraine de densité variable due à la libération de chaleur d'un dépôt fictif de déchets radioactifs de haute activité sont évalués. La discrétisation numérique nécessaire pour ce type de problème non-linéaire est d'abord évaluée à l'aide du critère du nombre Peclet pour les mailles en trois dimensions. Cette étude du type d'orientation d'un processus physique a comme but de déterminer la possibilité d'effectuer des calculs tridimensionnels couplés thermo-hydrauliques avec les ressources du matériel informatique disponible, d'exécuter des simulations couplées thermo-hydrauliques pour un modèle tridimensionnel représentatif d'un dépôt potentiel, et de comparer le champ de l'écoulement d'eau souterraine qui en résulte avec un champ d'écoulement isothermal.

En conclusion nous pensons que les objectifs ont été atteints. Les méthodologies et outils développés durant ce travail, ainsi que les stratégies et simulations, peuvent être utiles pour des études futures de modélisation hydrodynamique de sites spécifiques dans le cadre des objectifs de la CEDRA. Les processus liés aux effets transitoires sont mieux compris pour les modèles en une, deux et trois dimensions. La modélisation automatique du modèle inverse se révèle être un outil puissant pour le calage des modèles. L'évaluation des besoins en informatique et de discrétization des mailles pour des problèmes en trois dimensions avec hydrogéologie complexe et problèmes transitoires ou couplés, peut maintenant être utiliseé pour des études futures de ce type. Nous croyons qu'un savoir-faire et une expérience considérables ont été acquis au cours de ce projet en vue de mieux comprendre le comportement hydrodynamique des milieux hétérogènes autour de constructions souterraines.

TABLE OF CONTENTS

LIST OF TABLES

LIST OF FIGURES

LIST OF AUTHORS

Chapter 1
INTRODUCTION AND REPORT OVERVIEW
A. Rivera, U. Kuhlmann and F. Mueri

Chapter 2
PREVIOUS MODELING WORK
A. Rivera

Chapter 3
GROUNDWATER TRANSIENT EFFECTS AROUND THE KWO TUNNEL AT GTS
A. Rivera, N.R. Correa and U. Schroeder

Chapter 4
COUPLED THERMO-HYDRAULIC EFFECTS
A. Rivera, N.R. Correa and U. Schroeder

Chapter 5
CALIBRATION OF THE SRM WITH THE KWO TUNNEL
U. Kuhlmann, N.R. Correa and A. Rivera

Chapter 6
GENERAL CONCLUSIONS AND RECOMMENDATIONS
A. Rivera and N.R. Correa

CHAPTER 1

INTRODUCTION AND REPORT OVERVIEW

A. Rivera, U. Kuhlmann and F. Mueri

1 INTRODUCTION AND REPORT OVERVIEW

1.1 Background and scope

The investigation program "Hydrodynamic Modeling (MOD)" at the Grimsel Test Site (GTS) was designed by NAGRA as part of the GTS phase which was initiated in 1988.

The construction of underground structures such as access and exploration tunnels in a geological medium provides valuable information concerning the hydrogeological characterization of the host rock. A rock laboratory at a potential radioactive waste disposal site can maximize such information and also assist in the proper characterization of the near- and far-field host rock environment.

Phase II of the MOD project was designed as a specific example within the general framework of hydrogeological characterization at the Grimsel Test Site. Some of the important issues investigated during this period include: (a) methods for representing complex structures (e.g., tunnels) in a hydrogelogical model; and (b) the use of a hierarchical modeling approach to investigate groundwater flow on different spatial scales.

The modeling activities in the MOD-II project were carried out using FEM301, a finite-element model for simulating steady-state groundwater flow in a three-dimensional porous medium. Although a simple steady-state model conceptualization is adequate for a first analysis, second-generation models were forseen in phase III for more realistic representations of complex, physical phenomena taking place in a hypothetical repository environment, such as transient effects, coupled hydro-thermal effects, or the effects of drifts to unconfined aquifers. Additionally, the developing of procedures for model calibration were needed to acquire practical know-how in hydrodynamic modeling.

During phase III of the MOD project, other more sophisticated numerical codes were used, including: conceptual models with free-surface boundary conditions, groundwater transient effects, coupled hydro-thermal effects, and automatic inverse-model calibration. The numerical models used during this phase include: NAMMU, GW3D, MOVEMESH, FRACMESH and CASA.

The results of the MOD-II project for the period 1988-1990 are documented in NTB 91-03 (VOBORNY et al., 1991). The present report is an edited version of the major studies developed during the MOD-III project for the period 1991-1993.

1.2 Report organisation and persons involved

Table 1.1 gives an overview of the studies, during the period 1991-1993, reported internally at different dates. The persons involved in the work come from different oraganizations. Because of the diverse nature and complexities of the tasks, credit is given to the persons involved in each study by naming the authors at the beginning of the respective chapters in this report.

This report is divided into three main chapters. A. RIVERA summarizes the previous modeling work on a regional scale of the GTS model, originally developed by VOBORNY et al. (1991), on Chapter 2.

Chapter 3 by A. RIVERA, N.R. CORREA and U. SCHROEDER presents a quantitative analytical and numerical evaluation of the groundwater transient effects around tunnels, in one, two and three dimensions. The sub-regional model formulation and selection is presented. Hydraulic information on the GTS, for the period 1983-1987, is reviewed and summarized. The hierarchically derived initial and boundary conditions from the regional to the sub-regional scales are discussed. Three-dimensional transient simulations are performed with the SRM, including the KWO access tunnel discretized in one and three dimensions. Groundwater transient effects caused by a fictitious repository are simulated in three dimensions.

Chapter 4 by A. RIVERA, N.R. CORREA and U. SCHROEDER describes coupled hydro-thermal effects due to the presence of a hypothetical repository. An attempt is also made to perform a fully three-dimensional coupled hydro-thermal numerical simulation with the SRM.

Chapter 5 by U. KUHLMANN, N.R. CORREA and A. RIVERA presents an automatic-inverse modeling approach to calibrating the SRM using volumetric fluxes measured along the KWO access tunnel.

Finally, chapter 6 by A. RIVERA and N.R. CORREA presents the general conclusions and recommendations derived from this report.

The last section in this chapter, by U. KUHLMANN and F. MUERI, presents an overview of a strategy for model calibration, validation, and scaling of hydrological processes and parameters. Additional information is given in RIVERA et al., 1993a.

Table 1.1 The four major studies of the MOD-III project during 1991-1993

TITLE	DATE	AUTHOR
Status Report 1991.	April 1992	W. Huerlimann, A. Rivera, S. Mishra and N. Correa
Status Report 1992: Transient Effects, Boundary Conditions, Validation Concepts.	March 1993	A. Rivera, W. Huerlimann, J. Troesch, U. Kuhlmann, F. Mueri and N. Correa
FLG: Hydraulic Information at the Sub-Regional Scale of the Grimsel Site.	September 1993	B.W. Chalmers and N.R. Correa
Three-dimensional Groundwater Transient Simulations with the Sub-Regional Model Including the KWO Tunnel.	December 1993	A. Rivera, U. Schroeder and N. Correa

1.3 Overview for modeling strategy

In accordance with the objectives of the MOD project, for the period of 1991-1993, a modeling framework has been elaborated which is summarized below. A comprehensive description including methodological details are given in RIVERA et al., 1993a.

General concept

Groundwater flow and transport modeling involves making numerous assumptions, both for the selection of processes and for the representation of the hydrogeological structures in which they occur. Thus, predictions of the impact of future stresses on groundwater systems are prone to errors which may be related to the correctness of the conceptual model (model structure), to the accuracy of model parameters, or the uncertainties of future stresses.

In this context, the need for evaluating the validity of the assumptions of a numerical model is evident. In subsurface flow modeling, the term model validation often refers to the process demonstrating that the models "represent adequately the real system" (IAEA, 1982), i.e., both for the flow processes and for the hydrogeological structure. Here, adequacy means not that the model can be validated in the generic sense, but that it should be judged in the context of its intended application, i.e., with respect to a given process and/or a specific site.

It is often accepted that the validation process "is carried out by comparison of model predictions with independent field observations and experimental measurements" (IAEA, 1988). Such computations are restricted to the conditions under which the experiments have been or will be conducted so that scale effects in time and space may be important obstacles in modeling the groundwater flow and the solute transport. In practice, comparative validation needs to be quantified, not only in terms of the computed discrepancies, but also in terms of the scope of the test.

Modeling framework

Being aware that comparison of model output with field experiments alone does not suffice, we share the philosophy of USUNOFF et al. (1992) who call for a systematic approach where the various uncertainties are explicitly recognized throughout the modeling process. The framework below summarizes the required steps of such an approach, placing all the emphasis on the correct assessment of uncertainties. Clearly, each step of the strategy should be examined, in addition, by applying other more qualitative validation methods (e.g. peer review). The steps are:

(1) *Formulate purpose of model predictions, identify prediction capabilities, define performance measures and acceptance*

criteria for calibration, validation and prediction
(2) Identify physical process(es)
(3) Select computer code(s)
(4) Review data, quantify input uncertainty
(5) Scale input parameters and build conceptual model
(6) Select field experiments or observations for calibration and validation
(7) Calibrate model
(8) Quantify remaining output uncertainties
(9) Select model
(10) Perform validation tests
(11) Predict and quantify prediction uncertainties

According to this approach a model can be accepted (or be considered to have been 'validated') if (i) it fulfils some calibration criteria, then, (ii) passes the validation tests and, finally (iii) the uncertainties of the predictions are sufficiently small[1]. It is clear that the need for alternative conceptualization or additional data may arise from large uncertainties in the parameters or in the conceptual model and that this need can be identified after calibration, model selection or during prediction. Thus, the modeling process is iterative.

Hierarchical approach

Within this framework, the present conceptualisation considers a hierarchical modeling approach, as illustrated in Chapters 2 and 3, where several local models (MI, BK, VE, scale < 100 m) embedded in a sub-regional model (scale < 1000 m). The latter represents the kernel of a regional model, which is able to simulate groundwater flow to the biosphere within an area of several km^2 (VOBORNY et al., 1991; RIVERA et al., 1993a,b).

While boundary conditions for the regional model are assumed to be sufficiently well known, prescribed heads at the inner model boundaries have to be interpolated from regional and sub-regional simulations, respectively. Clearly, these predicted heads are highly uncertain, particularly in the transient state. Thus, quantification of the uncertainties related to the boundary conditions will be one of the key issues throughout the calibration process. A statistical approach to this issue is discussed in section 3.3.3.

Data Selection and scaling

Hydrogeological properties are usually measured or derived at discrete points in the domain of interest so that they provide information on a very limited scale. The salient question is how to determine the appropriate (averaged)

[1] What is meant by sufficiently small depends on model objectives and other issues (social, political, etc.). Its discussion is beyond the scope of this work.

value corresponding to a certain subdomain of the numerical model. This process is known as scaling and involves transition from the scale of variability of the physical property and/or measurement to the scale of the model parameters (parametrization scale). In fact, most hydrogeological (physical) parameters show a scale effect, a consequence of the continuum approach commonly used to groundwater flow modeling.

Every physical parameter may have its own characteristic scale transition behaviour and therefore needs a specific scaling method. In this context, the physical properties of interest are, e.g., the hydraulic conductivity or permeability, the storativity, the effective pore volume and the dispersion coefficient. Note that the appropriate scaling method depends not only on the magnitude relations, but also on the spatial distribution of the measurement points, the possible correlation among the data, the required precision of the scaled value, and the type of problem and expected results under investigation.

In inverse modeling, as described in Chapter 5, scaling has to be applied in order to obtain *prior information* on the model parameters. Numerous methods to evaluate scale-effects are available and have been reviewed in RIVERA et al., 1993a.

Model calibration

Once a conceptual model has been defined, the numerical model is left in terms of a finite number of unknown model parameters (e.g., for hydraulic conductivity, storativity, and boundary conditions). Calibration refers to the process of estimating these parameters from measurements of the system response, as well as from prior information on the parameter values. Calibration of the GTS model has been carried out with the CASA programs (KUHLMANN, 1992) for saturated groundwater flow. Here, the implemented inverse modeling methodology follows the Maximum Likelihood (ML) estimation theory. ML estimations minimize an objective function (goodness-of-fit function) which represents the weighted sum of squared residuals between calculated performance measures and their measured counterparts. In addition to the estimation of hydrogeological parameters, the programs allow the assessment of statistical parameters describing the error structure of the measurements and prior information.

Error analysis

Once 'optimum' parameter values have been estimated, the quality of the results has to be evaluated by an a-posteriori error analysis also provided by CASA. A lower limit for the parameter uncertainties can be approximated by its covariance matrix, a by-product of the statistical formulation of the inverse problem. In addition, the computation of the correlation matrix is useful in many cases. An example of this application is shown in section 5.5.

Concluding remarks

The main conclusion from the modeling strategy presented here is that most steps follow a systematic approach (without the steps that involve conceptualization). The proposed strategy is based on:

i) the definition of performance measures that are related to the intended use of the model,
ii) the definition of acceptance criteria for input data and model structure,
iii) the explicit treatment of uncertainties, and
iv) a continual iteration in the modeling process to diminish uncertainty in the model structure and performance.

Each further modeling step should allow discrimination of the less plausible conceptual model, thus reducing the spectrum of hypothesis as to the valid conceptual and numerical models. Considering the conceptual model as a theory of the natural system (that can be proven wrong but cannot be proven right), the validation process should be taken as support for the model that allows the modeler to increase the confidence in predictions.

In the best case, after the available information has been fully integrated into the modeling tasks, the model performance should meet the acceptance criteria previously defined. Otherwise, an evaluation of the contribution of existing observations (data) with respect to the identified parameters needs to be done, which parallels an evaluation of the sufficiency of existing data to meet the acceptance criteria.

If additional data are needed to meet the acceptance criteria, future field experiments or a data collection strategy may be designed based on the last best-calibrated model. The optimum number, location and frequency of further samplings may be generated based on model reliability requirements and cost minimization. SUN and YEH (1990a,b, 1992) and YEH and SUN (1990) developed and tested the theoretical framework for carrying out these experimental/sampling design and reliability analyses.

CHAPTER 2

PREVIOUS MODELING WORK

A. Rivera

2 PREVIOUS MODELING WORK

2.1 Scope and objectives

Within the scope of the hydrogeological testing program, The MOD project was designed to investigate an adequate strategy for hydrodynamic modeling of groundwater flow in a fractured rock body surrounding the Grimsel Test Site (GTS). Thus, the principal objectives for phase II of project MOD were:

- to develop and test new numerical tools and techniques related to mesh generation and pre- and post-processing of data, and to determine appropriate calibration/validation procedures and criteria;
- to support the interpretation of hydrological in-situ experiments within the GTS test program; and
- to increase the general understanding of the hydrological behaviour of low-permeable fractured rock around underground constructions.

The findings of phase II of project MOD, developed during the period 1988-1990, are documented in the Nagra Technical Report NTB 91-03 (VOBORNY et al., 1991). These authors provide a thorough overview of an approach for modeling low-permeable, fractured media around an underground facility.

Their conceptual model includes a hierarchical-modeling approach from regional to local to site-specific sub-models and adopts a hybrid modeling approach allowing inclusion of various types of fractures or faults and drains in a three-dimensional finite element grid. The results of their GTS models on regional and local scales are briefly presented here.

2.2 The Grimsel area

The Grimsel Test Site (GTS), Nagra's underground research facility, is situated 1 730 m above sea level in the Central Aar Massif of the Swiss Alps. The GTS is located in a region which is not under consideration for nuclear waste disposal. The Test Site was selected due to the general relevance of the geology as well as the excellent logistic support (including ready access and the infrastructure provided by a nearby underground hydroelectric power station, KWO).

The GTS lies at 8°19'E - 46°35'N under about 450 m of crystalline rock overburden. The site was selected after a series of 100-m-long, sub-horizontal exploration boreholes had been drilled from various adits to the access tunnel for an underground power station. Excavation for the access to the power station began in the summer of 1974 and the initial exploratory boreholes were drilled in 1980. The Grimsel Test Site facility was built between 30th May 1983

and 20th June 1984, by full-face drilling of a tunnel system about 800 m long with a diameter of 3.5 m. (FRICK et al., 1992, page 2-1).

2.3 Regional model

The regional model includes an area of approximately 30 km^2 covering Grimsel lake, Raeterichsboden lake, the regional Baechlisbach shear zone, part of the Aare river, and the Alplistock and Juchlistock massifs; the layout of the horizontal mesh is reproduced here in Figure 2.1. The vertical extent of the model is from a maximum surface elevation of 2900 m a.s.l. down to an elevation of 500 m a.s.l.

The model assumes impermeable boundary conditions at the bottom and lateral model walls. The model is fully saturated; thus, a hydraulic head boundary condition is prescribed along the top surface with values corresponding to ground elevation. The main access tunnel (KWO tunnel) is simulated in one dimension, by prescribing an atmospheric pressure boundary condition at the corresponding nodes along the 1D line representing the tunnel.

The assignment of hydraulic properties to the hydrogeological units was based on review of the available data base for the GTS laboratory. Measurements of hydraulic conductivities were taken from packer tests in exploration boreholes performed from the main access tunnel, and from in-situ experiments. Besides the low-permeable granite matrix, the regional model includes the two main fracture systems K (joints) and S (schistosity-related). These principal systems, together with the Baechlisbach shear zone, are considered to govern the large-scale hydraulic anisotropy of the massif.

These same units and parameters were used for the extended numerical analysis presented in Chapter 3 of this report. The adopted hydrogeological units in the model, with the corresponding hydraulic properties, are given in Chapter 3, Table 3.11 (from VOBORNY et al., 1991).

The regional GTS model steady-state results form the basis for the sub-regional model (SRM) presented in Chapter 3. The boundary conditions of the SRM are derived from these results, as will be shown in sections 3.2 & 3.3.

2.4 Local model

The local model covers an area of approximately 0.4 km^2; it includes the complete GTS area, but only about half of the length of the main access tunnel. This local model was focused on the detailed geology in and around the GTS; the main exercise was to define an approach with which the main geological characteristics could be discretized in two and three dimensions in the numerical model. The range of the local model was determined essentially

by the extent of the laboratory tunnel and the reach of the exploration boreholes. Figure 2.1 also shows the area covered by the local model, in a black rectangle entitled "GTS".

The boundary conditions for the local model are taken directly from the regional model, thus, the extent of this could be chosen arbitrarily. However, a great effort was invested in establishing a methodology with which to adjust head values at the boundaries, prescribed from a large-scale model with coarser discretization, into the finer local model.

A series of parameter variation sets allowed the calibration of the model to fit the observed total outflow into the GTS tunnel and a section of the main access tunnel (KWO tunnel). Additionally, observed head profiles in a vertical borehole were also used for the calibration process.

It was found that the simulated groundwater flow through the local model was basically controlled by the transmissivities adopted for the discrete tectonic structures and the imposed boundary conditions.

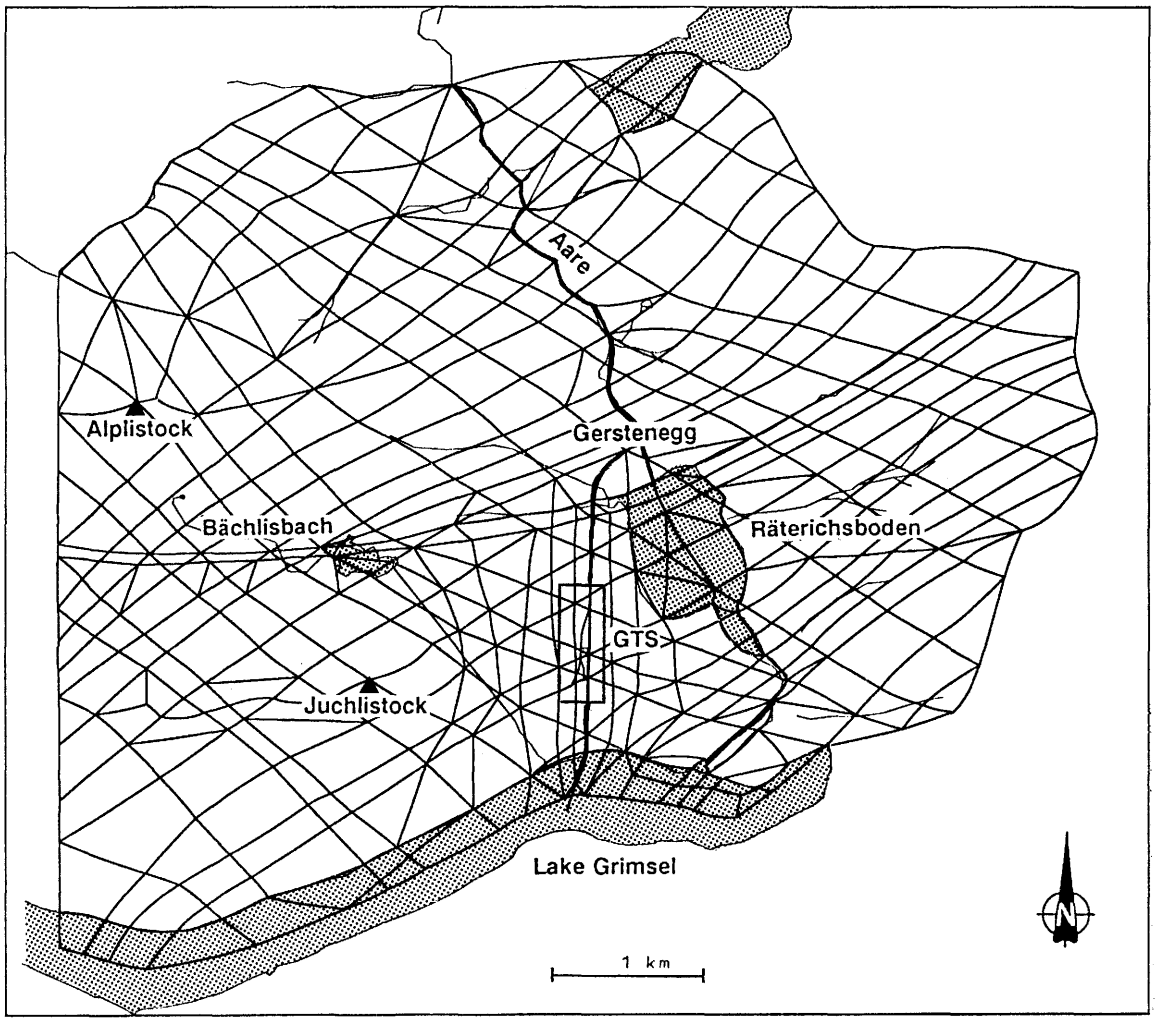

Figure 2.1 Regional and local GTS models: horizontal discretization of the grid (from VOBORNY et al., 1991).

CHAPTER 3

GROUNDWATER TRANSIENT EFFECTS AROUND THE KWO TUNNEL AT THE GTS

A. Rivera, N.R. Correa and U. Schroeder

3 GROUNDWATER TRANSIENT EFFECTS AROUND THE KWO TUNNEL AT THE GTS

3.1 One dimensional analytical and numerical calculations

The objective is to perform transient scoping calculations in one dimension to gain insight into time scales and the spatial discretization needed for different diffusivity ratios; and to compare an analytical solution with a numerical solution using NAMMU (NAMMU, 1993). An analytical solution for one-dimensional flow, useful in the interpretation of variations (increase/decrease) of the hydraulic head in aquifers, is presented and compared with a numerical solution for the same conditions.

3.1.1 Analytical solution

Consider a semi-infinite confined aquifer of homogeneous, isotropic porous medium, initially in equilibrium at the hydraulic head h_o with a reservoir as one boundary (Figure 3.1a). The equation governing the one-dimensional groundwater flow for this case is

$$\frac{\partial^2 h}{\partial x^2} = \frac{S_s}{K}\frac{\partial h}{\partial t}; \qquad x, t \geq 0 \qquad (3.1)$$

where K is the hydraulic conductivity, S_s is the specific storage coefficient, and t is the time.

For a sudden decrease in the head at the reservoir boundary (Figure 3.1a), equation (3.1) has the following solution (de MARSILY, 1986)

$$h(x,t) = h_o\, erf\left[\frac{x}{2\,(K/S_s\, t)^{1/2}}\right] \qquad (3.2)$$

with initial and boundary conditions

$h(x,0) = h_O$, $x > 0$ (initial condition)
$h(0,t) = 0$, $t \geq 0$ (at the boundary)

where h_o is the initial head and erf[ ] is the error function.

3.1.2 Numerical solution with NAMMU

In order to mimic the transient analytical solution with a numerical solution, the space has to be discretized in such a way as to account for the decreasing hydraulic gradient. A total length, L, of 500 m is represented by a geometrically increasing grid of quadratic one-dimensional elements as shown in Figure 3.1b. A total of 99 elements with 199 nodes were used with the node locations

varying from a minimum distance of 0.01 m at the boundary to a maximum of 18 m.

The boundary conditions are chosen from a no-flow condition at t=0 and a prescribed constant head h(0,t)=ho-Δh at the reservoir boundary. The time-dependent problem is solved using Gear's method, implemented in NAMMU, which automatically selects the time step and the order of the difference scheme to maximize the step length subject to an acceptable precision (error criterion). The simulated total times were long enough to allow the transient problem to reach a steady state according to the diffusivity ratios tested.

Results

Five different cases were simulated and were chosen from diffusivity ratios calculated with parameter values derived from rock properties similar to those at the GTS.

A range of values for specific storage coefficient was estimated using its definition

$$S_s = \rho g \phi (\beta_1 + \alpha/\phi) \qquad (3.3)$$

where ϕ is porosity, ρ is fluid density, g is the acceleration due to gravity, β is fluid compressibility, and α is rock compressibility. For jointed to sound rock, α ranges from 1E-11 Pa^{-1} to 1E-8 Pa^{-1} (FREEZE AND CHERRY, 1979); taking values of ϕ from 0.1% to 2%, a specific weight of fluid ρg=1E+4 Pa, and neglecting fluid compressibility, a range of values for specific storage coefficient were calculated and are presented in Table 3.1.

With these values and the hydraulic conductivity, K, for the hydrogeological units simulated in the block model (HÜRLIMANN et al., 1992), a range of values for diffusivity ratios (κ=K/S_s) were selected and are presented in Table 3.2. The five simulated cases range from 1E-5 to 0.1 m^2/s.

The results from the five simulated cases are presented in Figures 3.2 to 3.4. The agreement between the analytical and the numerical solutions seems excellent at times when the effect of the sudden decrease has not yet reached the opposite boundary. Figure 3.4b also shows the effect of the pulse at a distance of 30 m from the reservoir for the five diffusivity ratios; from this last Figure one can see the time needed for the head to reach a new steady-state condition at that distance.

Table 3.1: Range of values for specific storage coefficient

ϕ	α (Pa^{-1})	S_s (m^{-1})
0.005	1E-11 1E-10 1E-9 1E-8	1.2E-7 1E-6 1E-5 1E-4
0.01	1E-11 1E-10 1E-9 1E-8	1.4E-7 1E-6 1E-5 1E-4
0.02	1E-11 1E-10 1E-9 1E-8	2E-7 1E-6 1E-5 1E-4
0.001	1E-11 1E-10 1E-9 1E-8	1E-7 1E-6 1E-5 1E-5

Table 3.2: Range of values for diffusivity ratios

K (m/s)	S_s (m^{-1})	κ (m^2/s)
1E-10	1E-7 1E-6 1E-5	1E-3 1E-4 1E-5
1E-9	1E-7 1E-6 1E-5	1E-2 1E-3 1E-4
1E-8	1E-7 1E-6 1E-5	0.1 1E-2 1E-3
1E-7	1E-7 1E-6 1E-5	1. 0.1 1E-2

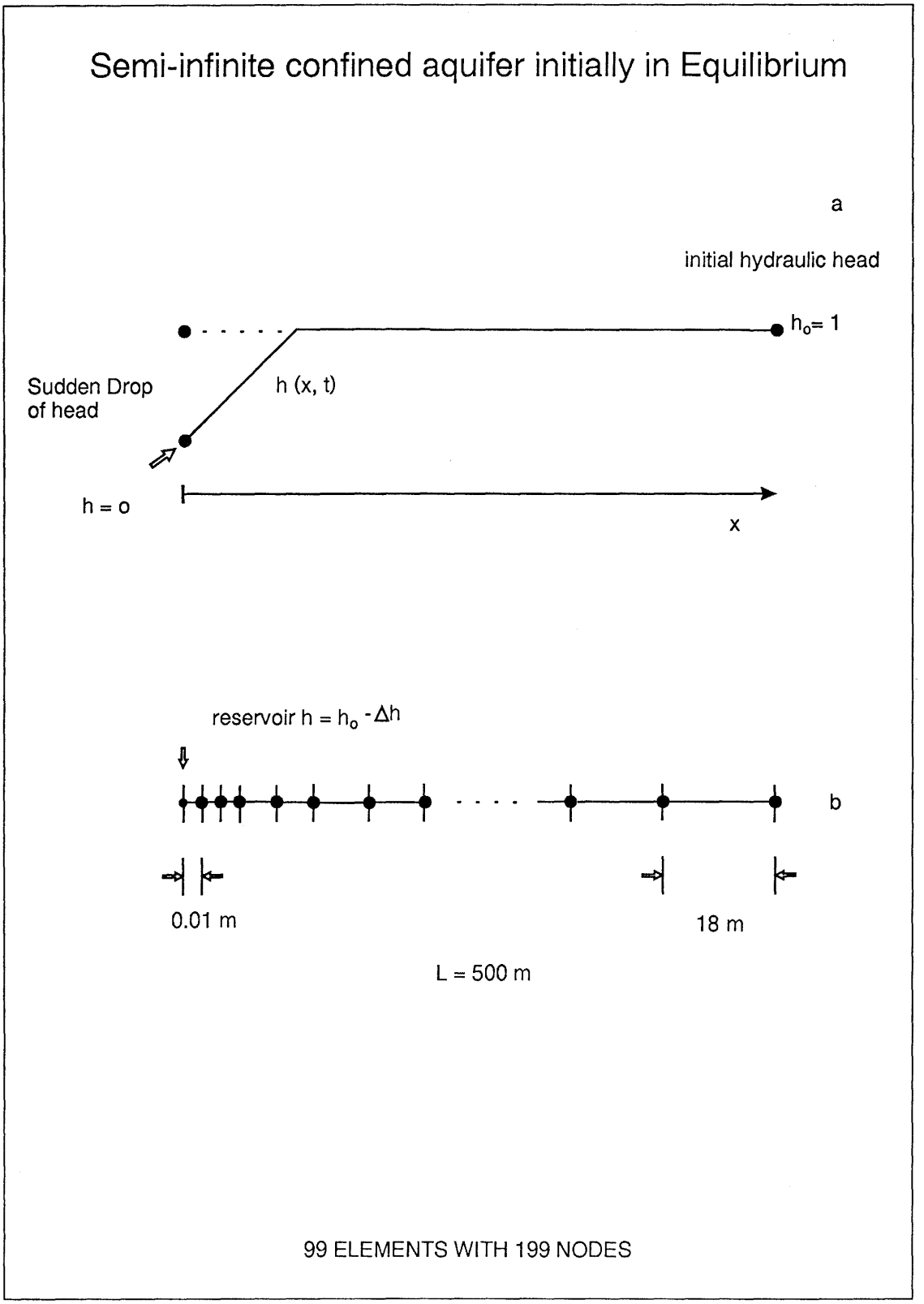

Figure 3.1 (a) Reservoir in contact with a confined aquifer; (b) numerical discretization with one-dimensional line elements.

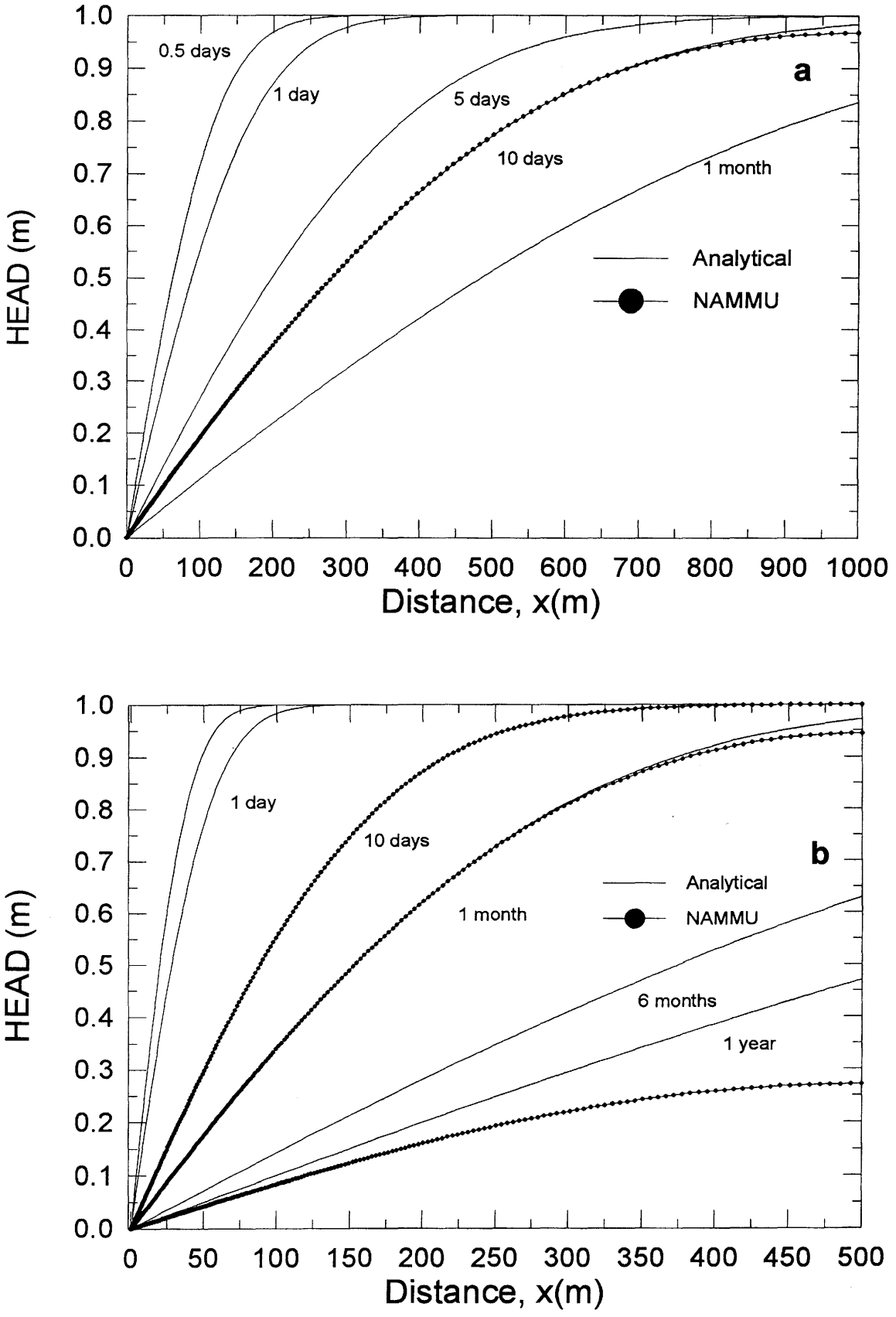

Figure 3.2 Comparison between the analytical and numerical solutions in 1D: (a) κ=0.1; (b) κ=1.E-2.

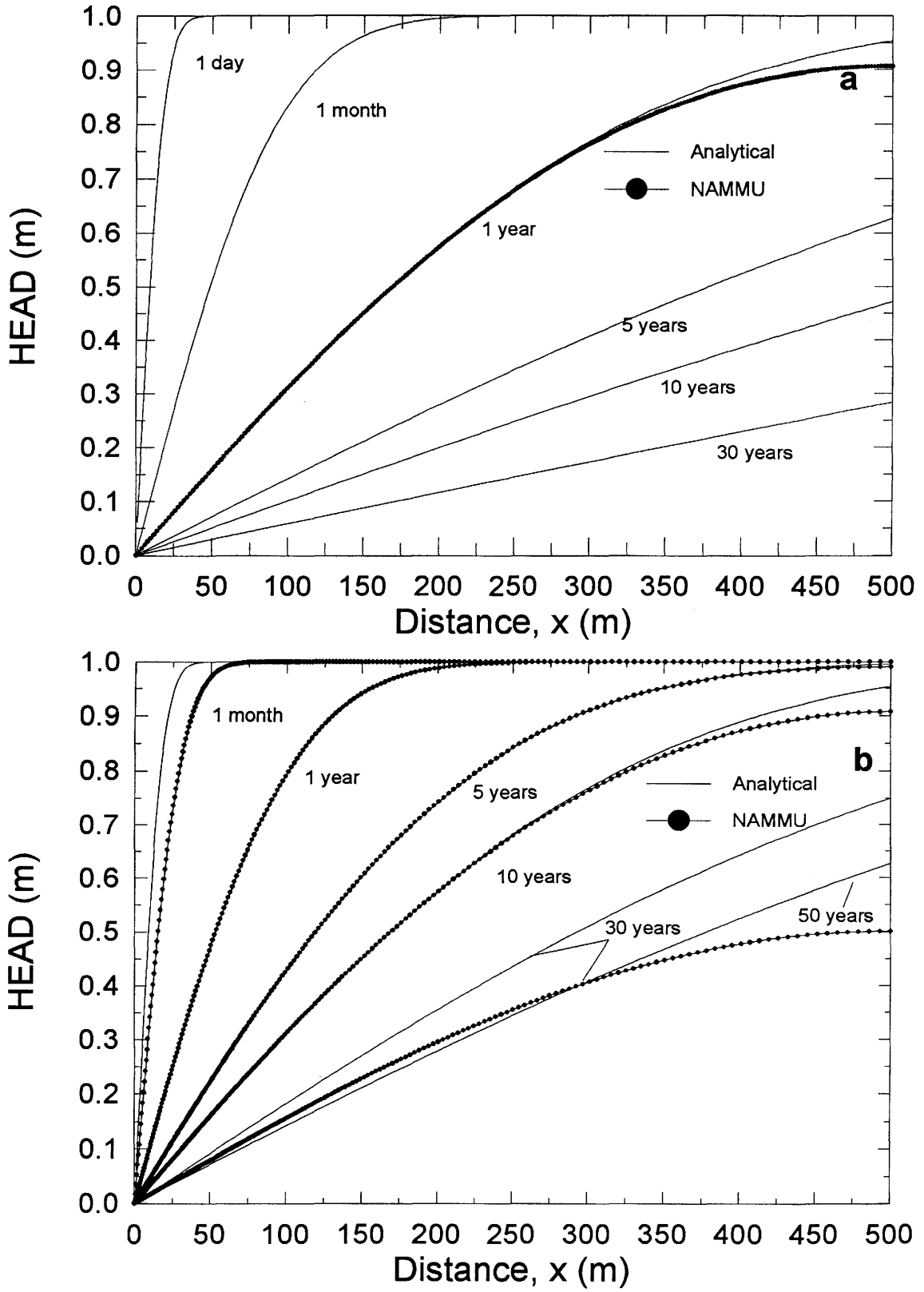

Figure 3.3 Comparison between the analytical and numerical solutions in 1D: (a) κ=1.E-3; (b) κ=1.E-4.

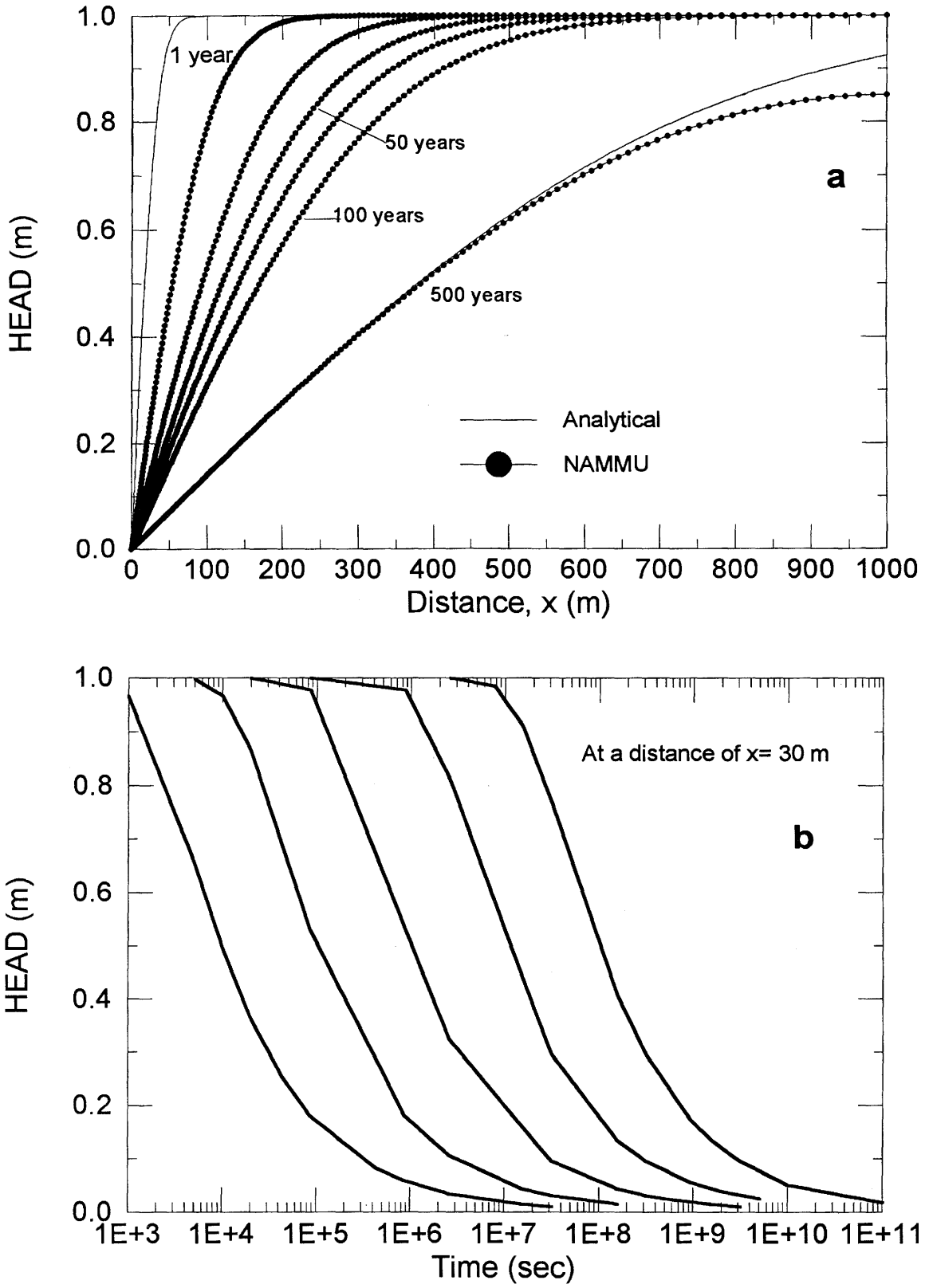

Figure 3.4 (a) Analytical vs numerical solution with $\kappa = 1.E\text{-}5$; (b) Effect of the pulse at a distance of 30 m with the five κ values.

3.2 Two-dimensional transient simulations

Transient effects caused by the presence of drifts were numerically investigated in two dimensions. Data from the "block model" (Figure 3.5; HÜRLIMANN et al., 1992), were used as basis for these investigations.

3.2.1 Fixed-head boundary conditions

Definition of the 2D problem

A NW-SE vertical cross section of a sub-model from the GTS regional model, referred to as the "block model" (HÜRLIMANN et al., 1992), was chosen to numerically investigate transient effects due to tunnels in two dimensions (Figure 3.5). Figure 3.6a presents an horizontal section of the block model showing the location of the vertical cross section through the GTS tunnel. This vertical section will be referred to hereafter as cut33. Figure 3.6b shows the original space discretization of cut33 with six layers, 78 quadratic elements, and 273 nodes. Note the location of the tunnel (not to scale) at the intersection of elements 44, 45, 50 and 51. The horizontal and vertical sections from the tunnel, indicated in Figure 3.6b, will be used to display the results of the simulations in this section and in section 3.2.2.

Parameter values and boundary conditions

The parameter values and the cases investigated in the 2D cut simulations are summarized in Tables 3.3 and 3.4, respectively. The values of hydraulic conductivity are taken from the regional model (VOBORNY et al., 1991) and correspond to the granitic matrix, defined as the "base case" by these authors. The hydraulic conductivities (K) were transformed into rock permeabilities (k) in order to apply the code NAMMU, by using the relation $k = 10^{-7} \cdot K$.

Table 3.3: Hydraulic conductivity and permeability values for the granite matrix

LAYER	K (m/s)	k (m^2)
1	1.E-10	1.E-17
2	5.E-11	5.E-18
3	1.E-11	1.E-18
4	5.E-12	5.E-19
5	1.E-12	1.E-19
6	1.E-12	1.E-19

Three cases were selected by defining three different diffusivity ratios (κ) with

specific storage coefficients previously defined in section 3.1.1 (eq. 3.3 and Table 3.1). For each case, the storage coefficient was the same for all the layers but the diffusivity ratio was different because of the different conductivities. No attempt was made to simulate systems of fractures or faults.

Finally, the boundary conditions for all the simulations presented in this section are: prescribed head (fixed) at the top of the vertical section and a no-flow condition at the bottom and lateral bounds.

Table 3.4: Cases simulated with three different diffusivity ratios

CASE	α (Pa^{-1})	S_s (m^{-1})	K (m/s)	κ (m^2/s)
1	1.E-11	1.E-7	1.E-10 5.E-11 1.E-11 5.E-12 1.E-12 1.E-12	1.E-3(1) 5.E-4(2) 1.E-4(3) 5.E-5(4) 1.E-5(5) 1.E-5(6)
2	1.E-10	1.E-6	1.E-10 5.E-11 1.E-11 5.E-12 1.E-12 1.E-12	1.E-4(1) 5.E-5(2) 1.E-5(3) 5.E-6(4) 1.E-6(5) 1.E-6(6)
3	1.E-9	1.E-5	1.E-10 5.E-11 1.E-11 5.E-12 1.E-12 1.E-12	1.E-5(1) 5.E-6(2) 1.E-6(3) 5.E-7(4) 1.E-7(5) 1.E-7(6)

$\kappa = K/S_s$, diffusivity ratio;

(1) Layer 1; (2) Layer 2; (3) Layer 3; (4) Layer 4; (5) Layer 5; (6) Layer 6

In order to use these diffusivities in the numerical simulation, different parameters that are used internally in NAMMU must be evaluated. The diffusivity coefficient is not given as a physical property in NAMMU; instead NAMMU evaluates it internally as follows.

According to the theory of consolidation, the compressibility of a soil or rock (e.g., decrease in porosity) is "elastic". The relative variation in volume of a soil element then becomes,

$$dV/V = -\alpha\overline{\sigma} \qquad (3.4)$$

where $\bar{\sigma}$ is the effective stress; accordingly, α can be written in terms of porosity and pressure as,

$$\alpha = \frac{dV/V}{\Delta\bar{\sigma}} = \frac{d\phi/\phi}{dP} \qquad (3.5)$$

In NAMMU, equation (3.5) is used to estimate rock compressibility from input values for porosity, fluid compressibility, fluid density and a gravitational factor (see eq. 3.3); the final diffusivity coefficient is obtained, using (3.3) combined with hydraulic conductivity values.

Thus, for each of the three cases investigated, equation (3.5) was evaluated separately and three different values for compressibility were given.

Effects of space discretization in the vicinity of the KWO tunnel

An important issue during the transient simulations was the appropriate refinement of the grid around the tunnel. In order to investigate the influence of the FE discretization in the vicinity of the tunnel on the numerical accuracy, several refinements had to be performed until an optimum grid was chosen for the results to be stable and realistic. An approach was selected in which the transient simulations were performed following an increasingly finer grid around the KWO tunnel, starting from the original one, and comparing the simulation results between coarser and finer grids.

This proved to be a highly time-consuming task. To refine the grid after each simulation an automatic grid-generator code "MESH" (FINSTERLE, 1991) was used.

Table 3.5 summarizes the size of a series of six different grids used for the simulations.

Table 3.5: Grids used in the 2-D transient simulations

GRID	No. of Elements	No. of Nodes
Original	78	273
cut33_2	207	569
cut33_3	256	673
cut33_4	958	2617
cut33_5	1054	2817
cut33_6	1687	4588

Up to refinement cut33_5 the results were indeed improved, but the results of the finer grid, cut33_6, were not different than those for the former, thus indicating that an optimum refinement of the grid for the problem investigated

had been reached. Cut33_5 was then selected to perform the transient 2-D simulations.

The grid corresponding to cut33_5 is shown in Figure 3.7 with three different scales. The sides of the elements closest to the tunnel are 0.7 m long.

The simulation of the influence of the tunnel was done following an approach proposed by KUHLMANN (1992). In this approach the tunnel is simulated with a series of elements comprising an area similar to the area of the tunnel. The drawdown due to the presence of the structure is prescribed at the centre of this area, and a hydraulic condutivity two, three or more orders of magnitude higher than that of the rock material surrounding the structure is applied inside the tunnel. Figure 3.7 also shows an enlarged area in the vicinity of the tunnel for the grid cut33_5; according to this approach the shadowed area shown in the Figure is the area where the hydraulic conductivity (Km) is two to three orders of magnitude higher than that of the surrounding rock to mimic the tunnel. The hydraulic conductivity inside the tunnel was fixed as Km=100K.

The boundary condition adopted in the tunnel was an hydraulic head equals to atmospheric pressure at the tunnel elevation, corresponding to a constant head of h=1730 m prescribed at the central node of the selected area (see Figure 3.7).

The initial condition for the transient simulations was the steady-state solution without the tunnel. In the first time step, a drawdown is prescribed at the drift node and is kept constant thereafter. The transient simulation continues until a new steady state is reached.

Results

Case 1

This case corresponds to a hydraulic diffusivity of 5.E-4 m^2/s and 1E-4 m^2/s for layers 2 and 3, respectively (see Table 3.4); the location of the tunnel intersects these two layers.

Figure 3.8 presents the results in a vertical and a NW-SE horizontal section from the tunnel to the top and lateral boundaries, respectively (head vs distance). These results correspond to simulations done with cut33_5.

Approximately 100 years are needed to re-equilibrate the flow system to a new steady-state condition as shown in Figure 3.8. The transient simulation was run for longer periods of time (e.g. 200, 500, 1000 years), but only very little change occurred after 100 years. Thus, it was concluded that the transient solution indeed reaches the steady-state solution with tunnel in this period of time.

Case 2

This case corresponds to a hydraulic diffusivity of 5.E-5 m^2/s and 1E-5 m^2/s for layers 2 and 3, respectively (see Table 3.4).

Figure 3.9 presents the results in a vertical and a NW-SE horizontal section from the tunnel to the top and lateral boundaries, respectively (head vs distance). Approximately 500 years are needed to re-equilibrate the flow system to a new steady-state condition as shown in Figure 3.9. The transient simulation was run for longer periods of time (e.g. 700, 800, 1000 years), but only very little change occurred after 500 years. Thus, it was concluded that the transient solution indeed reaches the steady-state solution with tunnel in this period of time.

Case 3

Figure 3.10 presents the results in a vertical and a NW-SE horizontal section from the tunnel to the top and lateral boundaries, respectively (head vs distance). These results correspond to simulations done with cut33_5. In this case approximately 3000 years are needed to re-equilibrate the flow system to a new steady-state condition as shown in Figure 3.10. The transient simulation was run for longer periods of time (e.g. 3200, 3500, 4000 years), but only very little changes occurred after 3000 years. Thus, it was concluded that the transient solution indeed reaches the steady-state solution with tunnel in this period of time.

Figure 3.11 shows the results as plots of head evolution in time at selected locations 6m, 12m, 25m, 50m, 100m and 200m horizontal distance from the tunnel.

The main uncertainties related to the present numerical exercises are:

- The adopted boundary conditions: fixed at the top of the model and no flow at the lateral boundaries;
- the adopted initial and boundary condition at the tunnel;
- the evolution with time of the hydraulic head during the construction and operation of the tunnel is unknown;
- the nature of the two-dimensional model.

We will see in section 3.2.2 how a moving free surface (infiltration) boundary condition modifies the results as compared to the fixed-head boundary condition.

The preliminary numerical investigations described in this study reveal that, due to the presence of a tunnel, transient hydrodynamic conditions in the rock matrix at the site will occur during approximately 3000 years for case 3 with a diffusivity of 5E-6 m^2/s. This is the worst case scenario; the presence of

fractures with greater K values may accelarate this process, thus reducing the duration of the transient effects. These results show that, at a first glance, it may be important to pursue numerical investigations of transient effects on the groundwater flow caused by the excavation of drifts and their sealings in proposed sites.

Head recovery after the sealing of the tunnel

In order to investigate the head recovery after the sealing of the tunnel, the conditions from case 3 were used because this is the most likely repository situation in terms of the known parameters; this is also the extreme situation in terms of the diffusivity for the three cases simulated. The initial conditions for this case are the results of the simulation with the head (atmospheric pressure) prescribed at the tunnel. The simulation is stopped at t=30 years (30 years operation before sealing of the tunnel) and the evolution of the hydraulic head is simulated in time until it reaches a new steady-state condition. In order to do this with the numerical model, the boundary condition at the tunnel is simply removed at the end of the 30-year simulation.

It was apparent, according to the numerical simulations, that it would take about 500 years for the head to recover about 95% of its original condition with the tunnel being sealed. Figure 3.12 shows the results at 25-m and 200-m horizontal distances from the tunnel. Figure 3.13 shows the results in horizontal and vertical sections. The small difference in the simulated head after the sealing of the tunnel at the new steady-state, 25 m up (Figure 3.12a), is a consequence of the combination of the distance and the discretization of the time and the space in the numerical model.

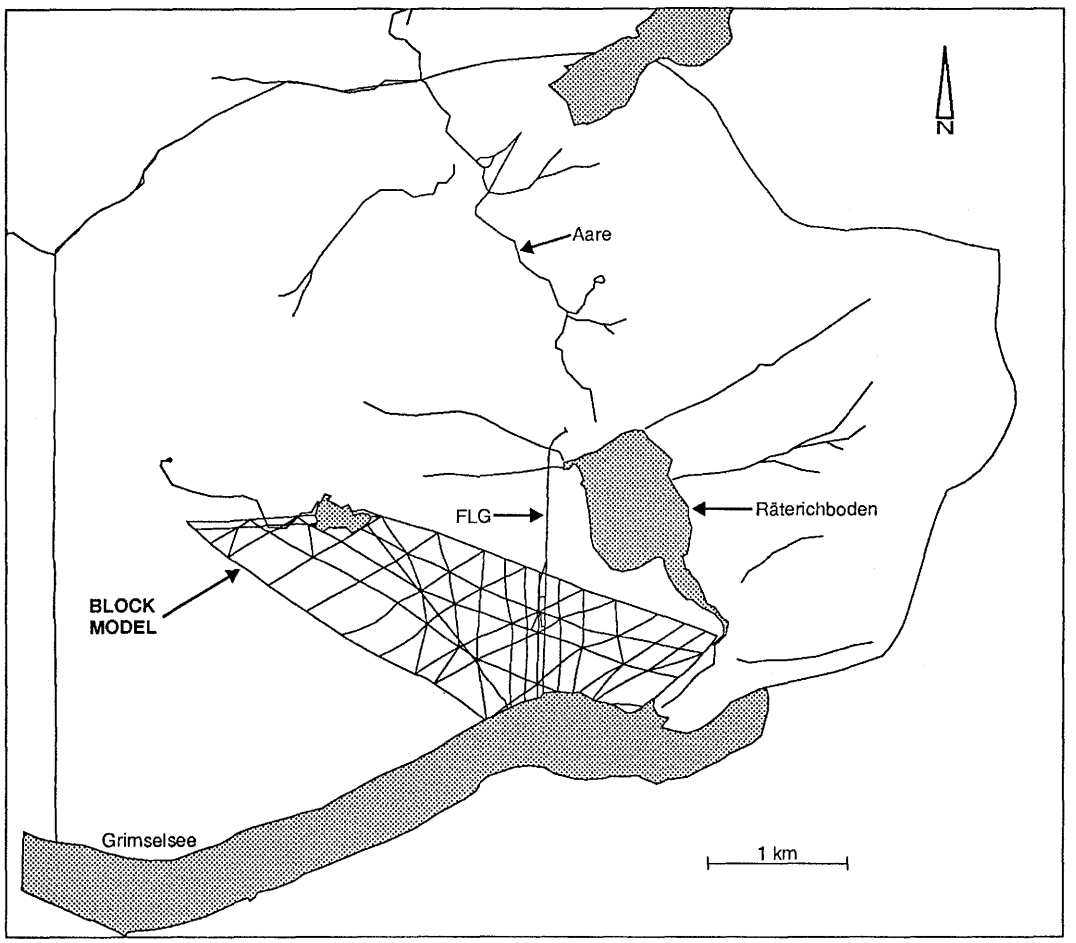

Figure 3.5 Location of the block model into the regional model (after HUERLIMANN et al., 1992).

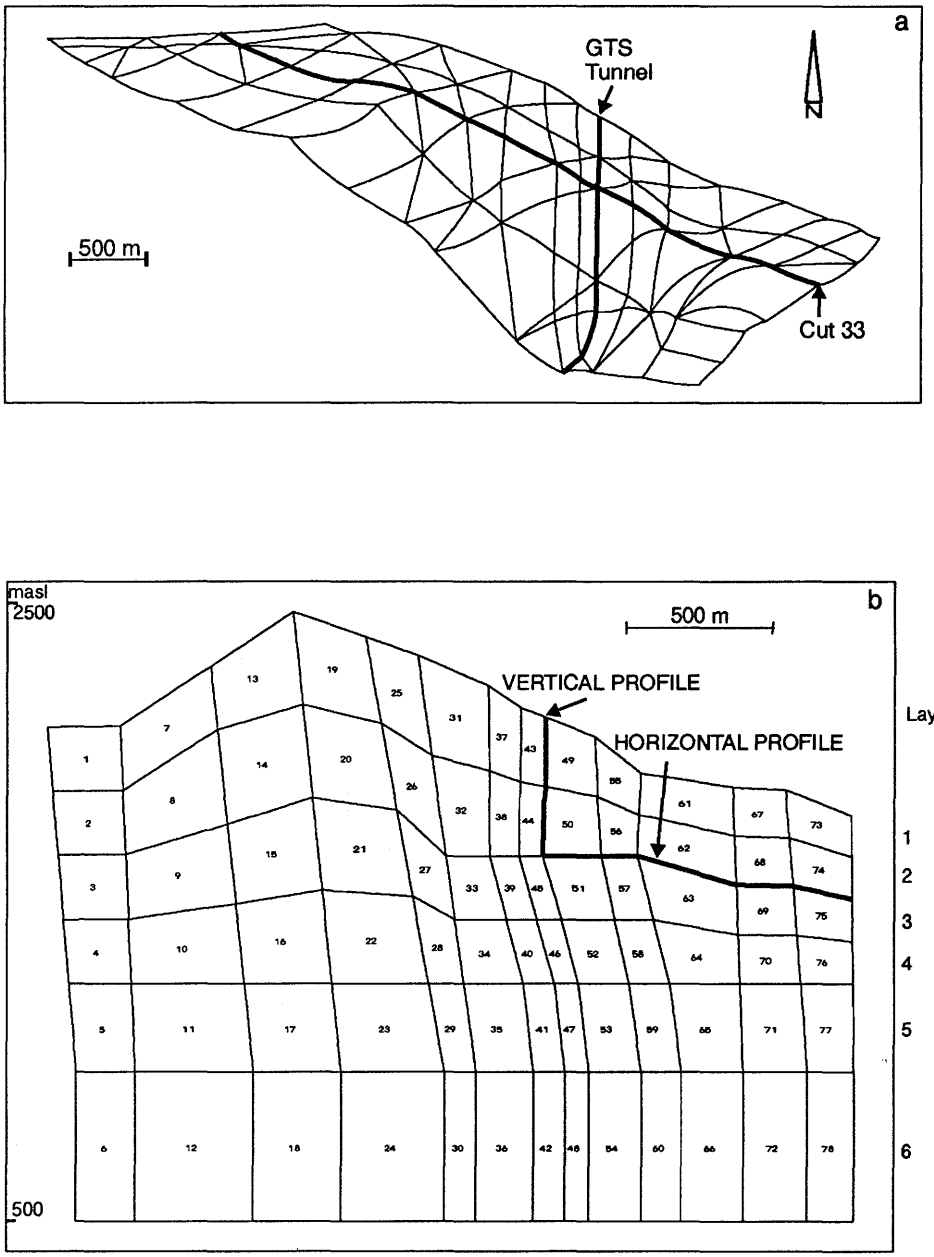

Figure 3.6 (a) Horizontal section through the block model (top); (b) original grid of the vertical cross-section cut33.

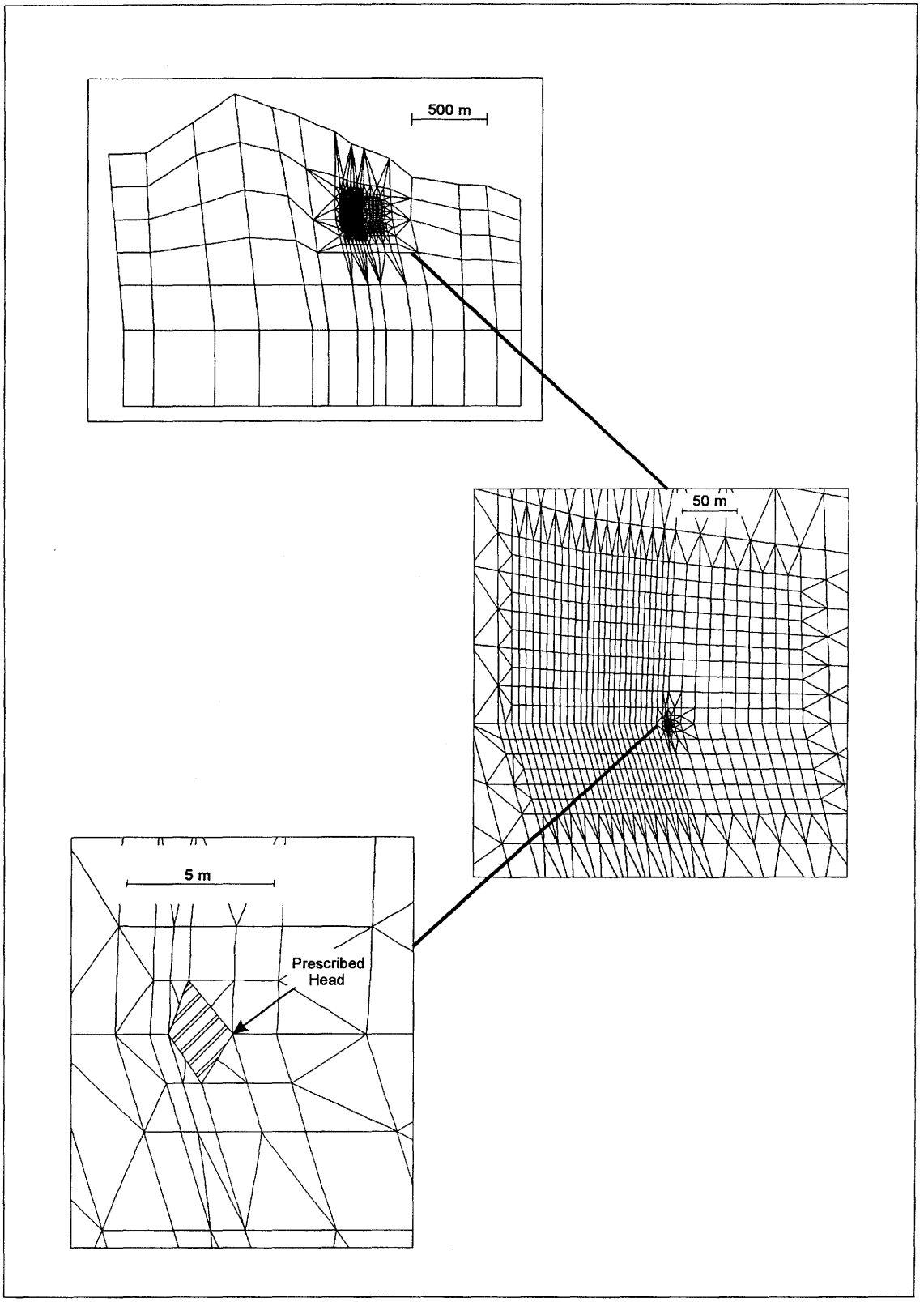

Figure 3.7 Grid of section cut33_5 with three different scales.

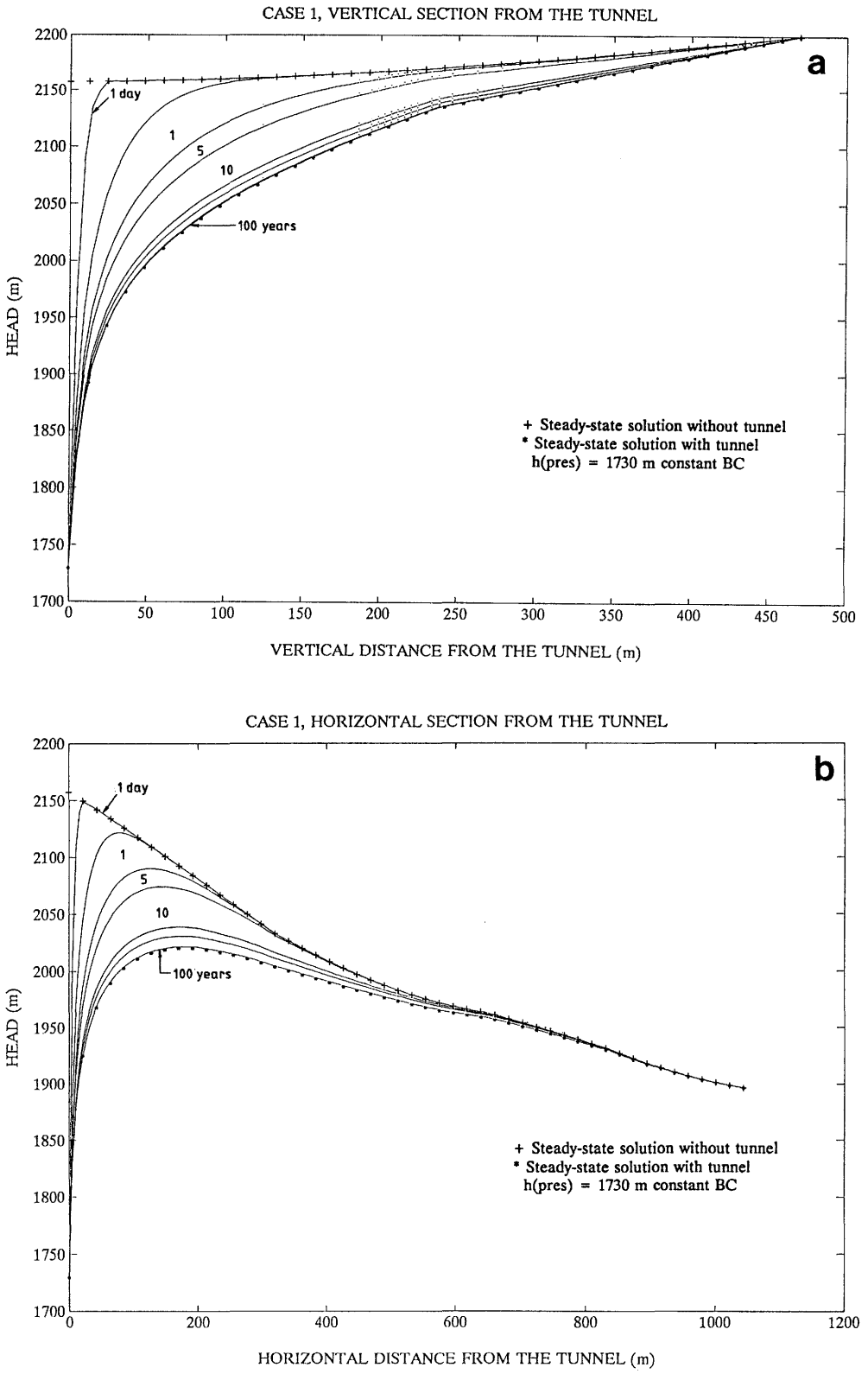

Figure 3.8 Results of simulations for case 1.

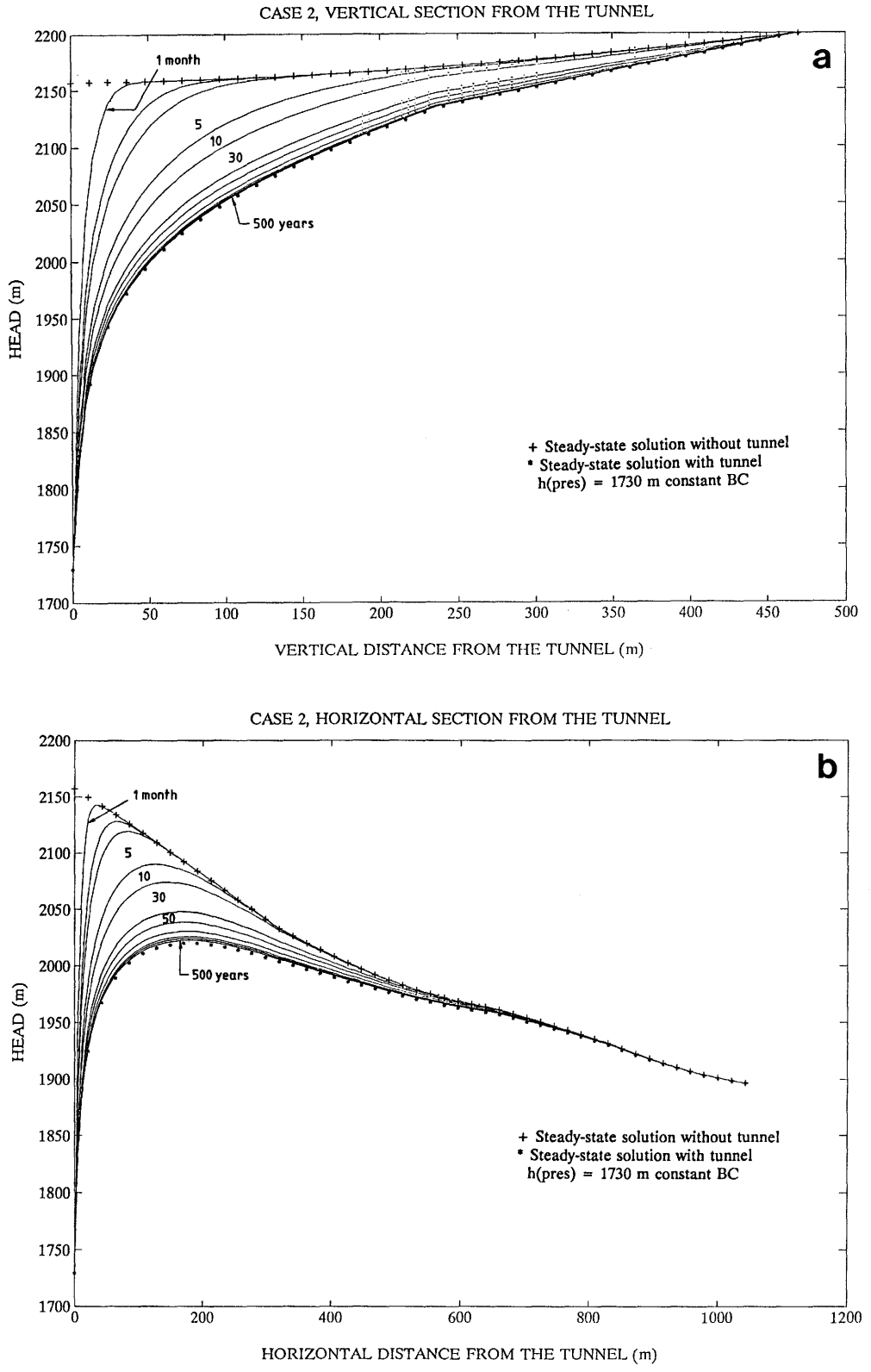

Figure 3.9 Results of simulations for case 2.

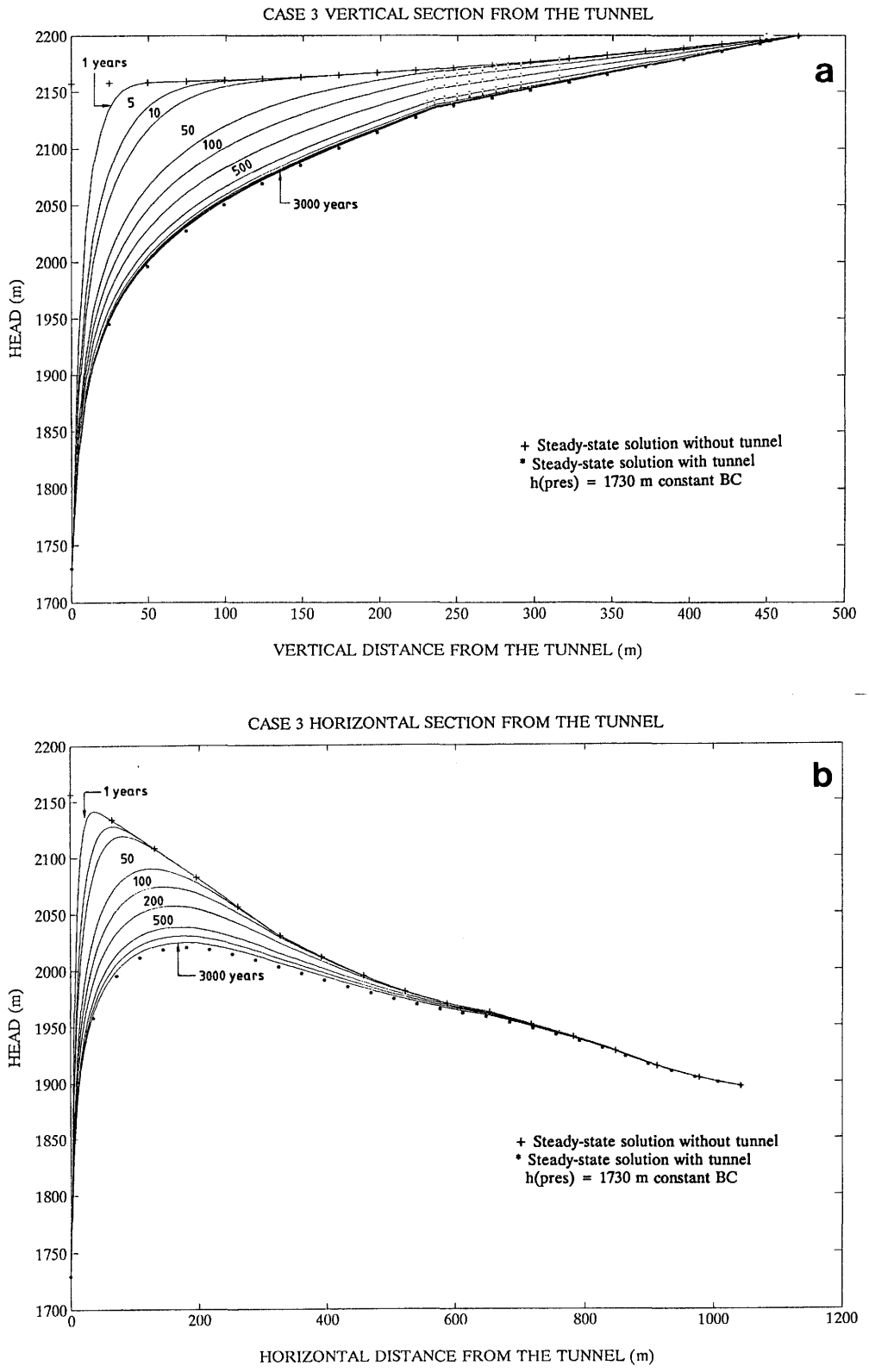

Figure 3.10 Results of simulations for case 3.

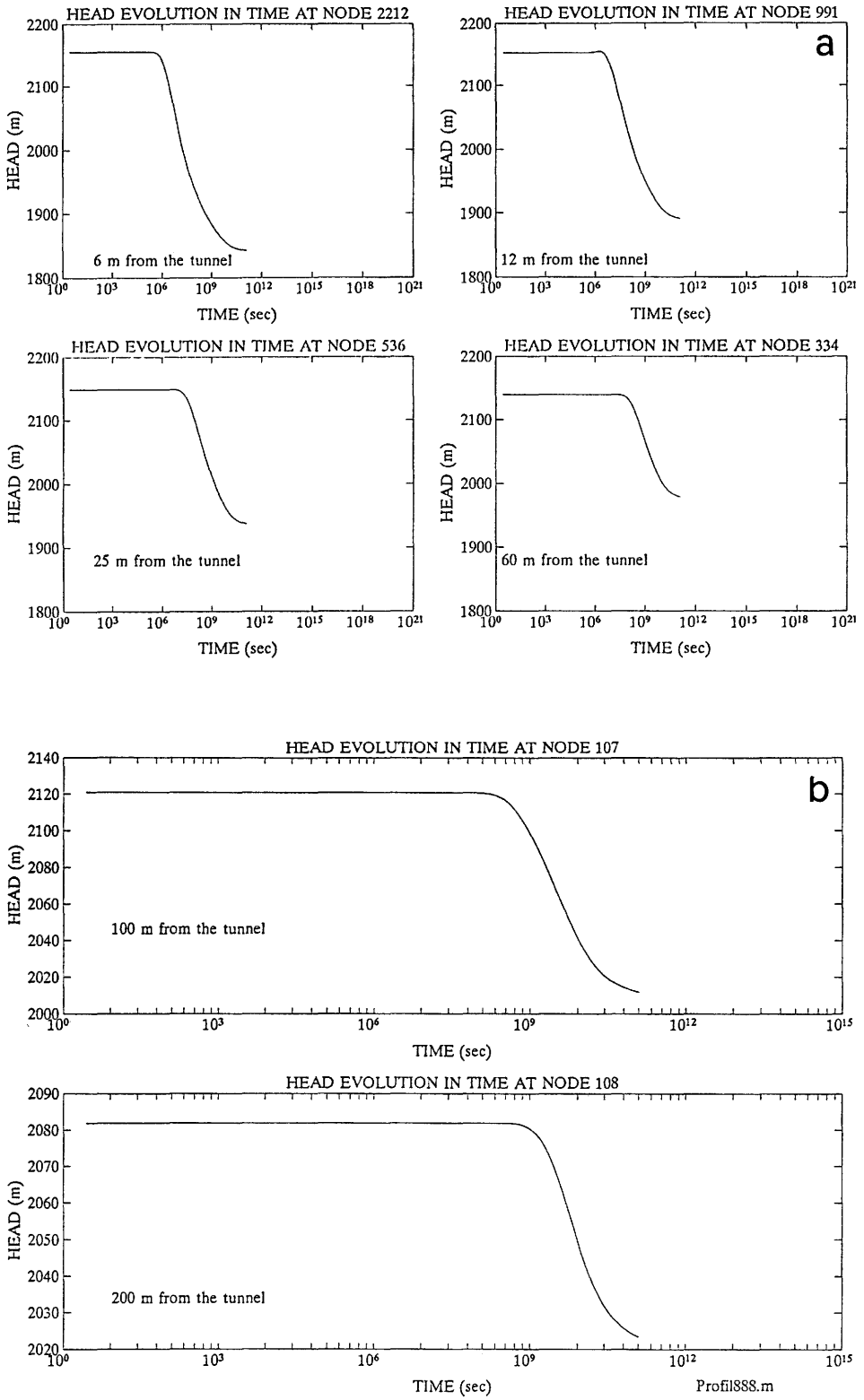

Figure 3.11 Head evolution with time at: (a) 6 m, 12 m, 25 m, and 60 m horizontal distance from the tunnel; and (b) 100 m and 200 m horizontal distance from the tunnel; (case 3).

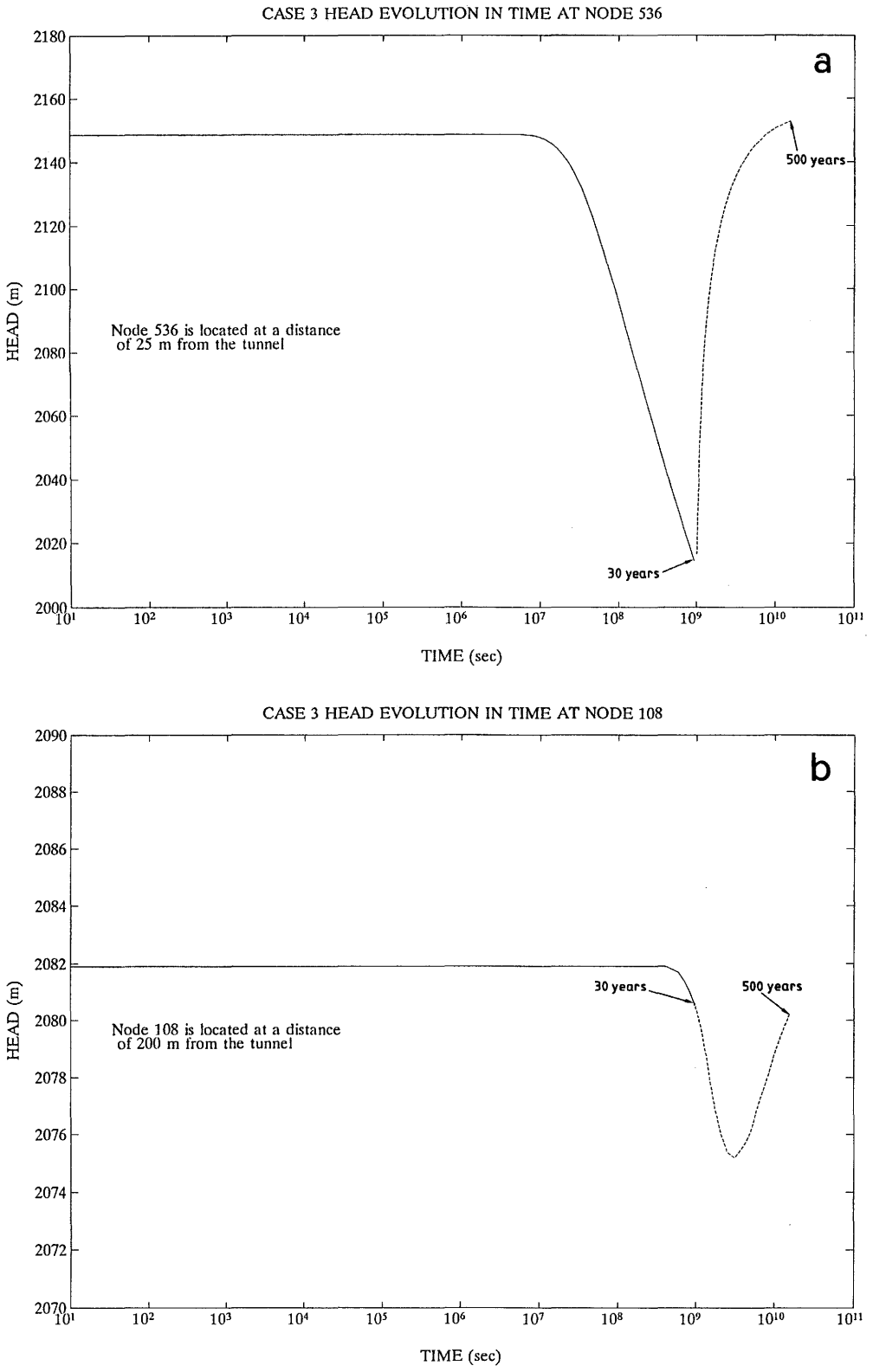

Figure 3.12 Head recovery after the sealing of the tunnel (30 years); (a) at 25 m and (b) at 200 m distance from the tunnel.

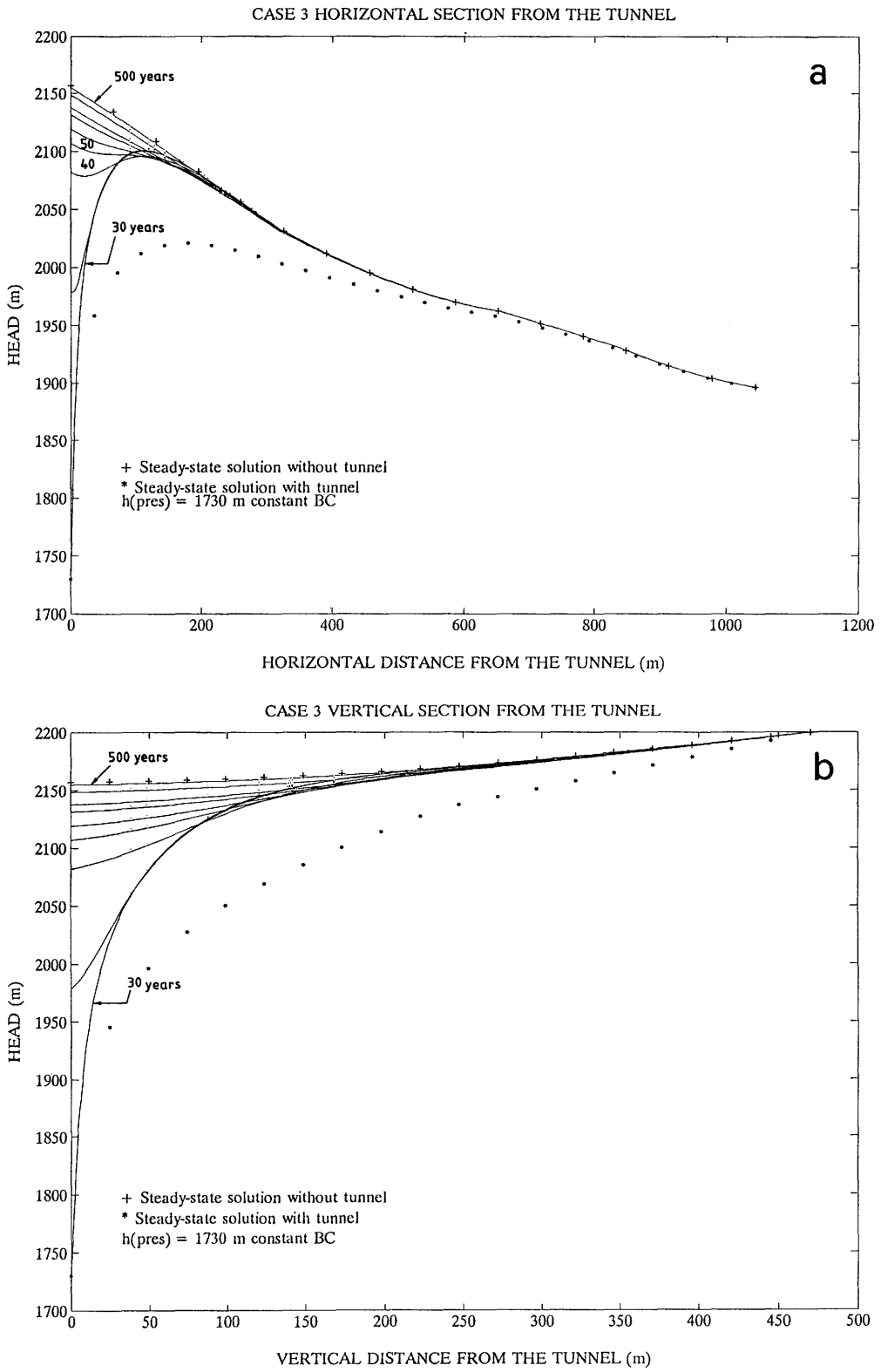

Figure 3.13 Head recovery after the sealing of the tunnel (30 years); (a) horizontal section and (b) vertical section from the tunnel.

3.2.2 Free-surface boundary conditions

Definition of the 2D problem

The same vertical NW-SE cross-section from the block model of the GTS (see Figure 3.5) was used to evaluate the effects of an infiltration-dependent boundary condition at the top of the model with a moving free surface. This numerical investigation also includes the effect of the presence of a tunnel, and it complements the results presented in section 3.2.1. The adopted cross section, referred to as cut33_5, has a space discretization containing 6 layers with 1054 quadratic elements and a total of 2817 nodes.

The same approach to simulating the influence of the tunnel presented in section 3.2.1 was kept for these simulations.

The code GW3D (TRÖSCH, 1990) was tested and used for these simulations. Since the simulations include a moving free-surface boundary condition, the calculations in transient are lengthy and more complex. Furthermore, new parameters must be included and an additional "variable", namely time, must be accounted for by a fine discretization. The approach used in GW3D, which does not deform the mesh, is an iterative procedure accounting for the unsaturated zone above the free surface using pressure-dependent permeabilities and a specific storage coefficient. Thus, with GW3D two types of specific storage coefficients must be assessed; one for the unsaturated zone (specific yield) which includes a saturation function and a pore space compressibility, and one for the saturated zone, which is mainly due to matrix compressibility and total porosity.

Initial and boundary conditions

The numerical simulations were done for the three cases presented in Table 3.4. For each case, the diffusivity ratio ($\kappa = K/S_s$) is different because of the three different storativity values used. For each case, the adopted initial and boundary conditions were:

- Boundary conditions:
  - — fixed lateral heads;
  - — no flow at the bottom; and
  - — free surface at the top.
- Initial conditions:
  - — steady-state solution with free surface; and
  - — no tunnel
- Transient conditions:
  - — fixed lateral boundaries;
  - — no flow at the bottom;

— opening, operation and sealing of the tunnel;
— moving free surface at the top;
— constant infiltration rate;
— simulation time: from 3000 to 30000 years depending on the case.

Parameter values

Table 3.4 presents the hydraulic parameter values used in the simulations for the three cases. In order to obtain a recharge rate (infiltration) for cut33_5 to be used with the moving free surface, a steady-state solution was first performed with fixed-head boundary conditions prescribed at the top. From these simulations, performed with and without the tunnel, a volumetric flux balance was evaluated and the results were adopted as the recharge rate input for the free-surface simulation. The steady-state water balance including the tunnel is as follows:

- Total flux flowing in: Qpos = 4.0119E-8 m^3/s
- Total flux flowing out: Qneg = -4.0119E-8 m^3/s
- Flux balance: Qsum = 6.24E-19 m^3/s

Considering a horizontal length of about 2000 m for cut33_5, the total flux flowing into the model accounts for 6.3E-4 m/y, that is, 0.63 mm/y. The tunnel itself drains about 34% of available inflowing flux. Figure 3.14 shows the distribution of fluxes at the top nodes, both with respect to model location (Figure 3.14a), as well as quantitatively for each node (Figure 3.14b). The results for the simulation without the tunnel indicated a recharge rate of about 0.53 mm/y.

The recharge rate finally adopted was 1 mm per year for all three cases. This value, which seems unrealistic, is very low indeed and corresponds to an extremely low percentage (~7 %) of the precipitation (P) in the region. It should be noted, however, that the amount of precipitation available for infiltration (probably 50 % of P) cannot infiltrate into the Grimsel massif due to the very low hydraulic conductivity of the uppermost layers (~10^{-10} m/s).

Results of the free-surface simulations

A series of six simulations were performed. These runs are summarized in Table 3.6.

The simulation concerning recovery after the sealing of the tunnel was not carried out. According to the fixed-head simulation case 3, the time for recovering (~500 years) is conservative. Thus, it is expected that with the free-surface boundary condition this effect would be even larger, i.e., it takes more time to recover.

Table 3.6: Description of the free-surface runs with cut33_5

RUN	CONDITION	REMARKS
3.1	Steady state without tunnel; with FH BC	FH= Fixed heads BC= Boundary conditions FS= Free surface
3.2	Steady state without tunnel; with FS BC	Comparison between 3.1 and 3.2
3.3	Steady state with tunnel; with FH and FS BC	Comparison of results between FH and FS BC
3.4	Transient with tunnel for case 1	for κ = 5E-4 m^2/s
3.5	Transient with tunnel for case 2	for κ = 5E-5 m^2/s
3.6	Transient with tunnel for case 3	for κ = 5E-6 m^2/s

Steady state without tunnel with FH and FS BC

This series of runs includes the two types of boundary conditions; one with fixed head prescribed at the top nodes, and one with free surface prescribed at the top nodes. The presence of the tunnel is not simulated in either of the two cases. The aim here is to compare the effect of these two types of boundary conditions on the model results.

Figure 3.15a presents the results for the free-surface simulation. The location of the free surface, in steady state, follows approximately the top surface of the model, as expected. In fact, one would expect to have complete saturation given the infiltration rate which represents the volume needed to keep the balance in equilibrium, as demonstrated with the fixed-head simulation. The position of the free surface at the highest node (node 5, Juchlistock) is about 36 m below the top. This difference is probably due to the rather coarse grid discretization at the top, preventing the numerical model from reaching convergence at that point. After several iterations the free surface does not move anymore.

Figure 3.15b is a plot of the differences in potentials (hydraulic heads) between the fixed-head and the free-surface simulations for the complete 2D vertical cut. The influence of the position of the free surface at the top node (node 5) on the simulated hydraulic heads, is clearly seen in this Figure; the differences are zero everywhere else.

Steady state with tunnel with FH and FS BC

The same comparison as in the previous case is presented here but this time with the inclusion of the tunnel. The simulation is again done in steady state and with the same infiltration rate as in the previous case.

Figure 3.16a presents the results for this free-surface simulation with the tunnel. The location of the free surface, in steady state, follows approximately the top surface of the model as in the previous case. The position of the free surface at the highest node (node 5, Juchlistock), is about 12 m below the top. This difference is probably due to the rather coarse grid discretization at the top, preventing the numerical model from reaching convergence at that point. After several iterations the free surface does not move anymore.

In Figure 3.16b the differences in potentials (hydraulic heads) between the fixed-head and the free-surface simulations are plotted for the complete 2D-vertical cut. The differences in this case are more important than in the case without tunnel (see Figure 3.15); the presence of the tunnel influences a larger area as can be seen in Figure 3.16b.

Transient simulations with tunnel with Free-surface BC

As mentioned before, the calculations in transient are lengthy and more complex. One of the most difficult parameters to evaluate is the time needed for the transient simulations. Depending on the diffusivity coefficient the simulation time may vary from a few hundred years to thousands of years. In order to avoid lengthy and expensive simulations, the number of time steps needed must be carefully assessed.

The maximum period of simulation time is also of great importance both for CPU time as well as for the post processing of the results. The discretization of the simulation phases (or time steps) should be fine enough, otherwise convergence will not be reached. Given the fact that this type of simulation includes two types of storativity values, it is very difficult to evaluate a priori the maximum time needed to achieve a steady-state condition after the building of the tunnel. Thus, an iterative procedure was used, starting from an initial guess of the maximum period of time, analyzing the results and if these are not yet in equilibrium, starting the simulation again from the last simulated conditions.

The conditions simulated in these runs correspond to cases 1, 2 and 3 (see Table 3.3). The conditions and control parameters for these transient simulations are given in Table 3.7

Table 3.7: Transient computations with free-surface conditions including the tunnel

PARAMETERS / CONDITIONS	Free-surface Boundary Conditions		
	Case 1	Case 2	Case 3
Model parameters:			
α [Pa^{-1}]	1E-11	1E-10	1E-9
S_s [m^{-1}]	1E-7	1E-6	1E-5
Hydraulic conductivity [m/s]	5E-11, 1E-11	5E-11, 1E-11	5E-11, 1E-11
Diffusivity ratio [m^2/s]	5E-4, 1E-4	5E-5, 1E-5	5E-6, 1E-6
Conditions and control parameters:			
— Convergence criteria (difference in calculated head)	1.0 m	1.2 m	1.3 m
— Maximum number of time steps	200	200	200
— Maximum no. of iterations per time step	100	30	30
— Maximum period of simulations	5'000 years	10'000 years	30'000 years
— Initial time step	1 sec	1 sec	10 sec
— Factor for time increase	1.2	1.2	1.2
— Output results	every 2 time steps	every 2 time steps	every 2 time steps
— Computer memory [Mb]	26	26	22
— Time to reach new steady state	≈ 3000 years	≈ 4000 years	≈30'000 years
— Total number of time steps	136	136	130

Figure 3.17a shows the results for case 1. It can be seen that about 3000 years after the tunnel boundary condition was prescribed, the transient effect is dissipated and reaches a new steady-state condition. More details of these simulations are given in RIVERA et al. (1993a).

Figure 3.17b shows the results for case 2. It can be seen that about 4000 years after the tunnel boundary condition was prescribed, the transient effect is dissipated and reaches a new steady-state condition.

Figure 3.18 shows the results for case 3. It can be seen that at about 30'000 years after the tunnel boundary condition was prescribed, the transient effect almost reaches a new steady-state condition.

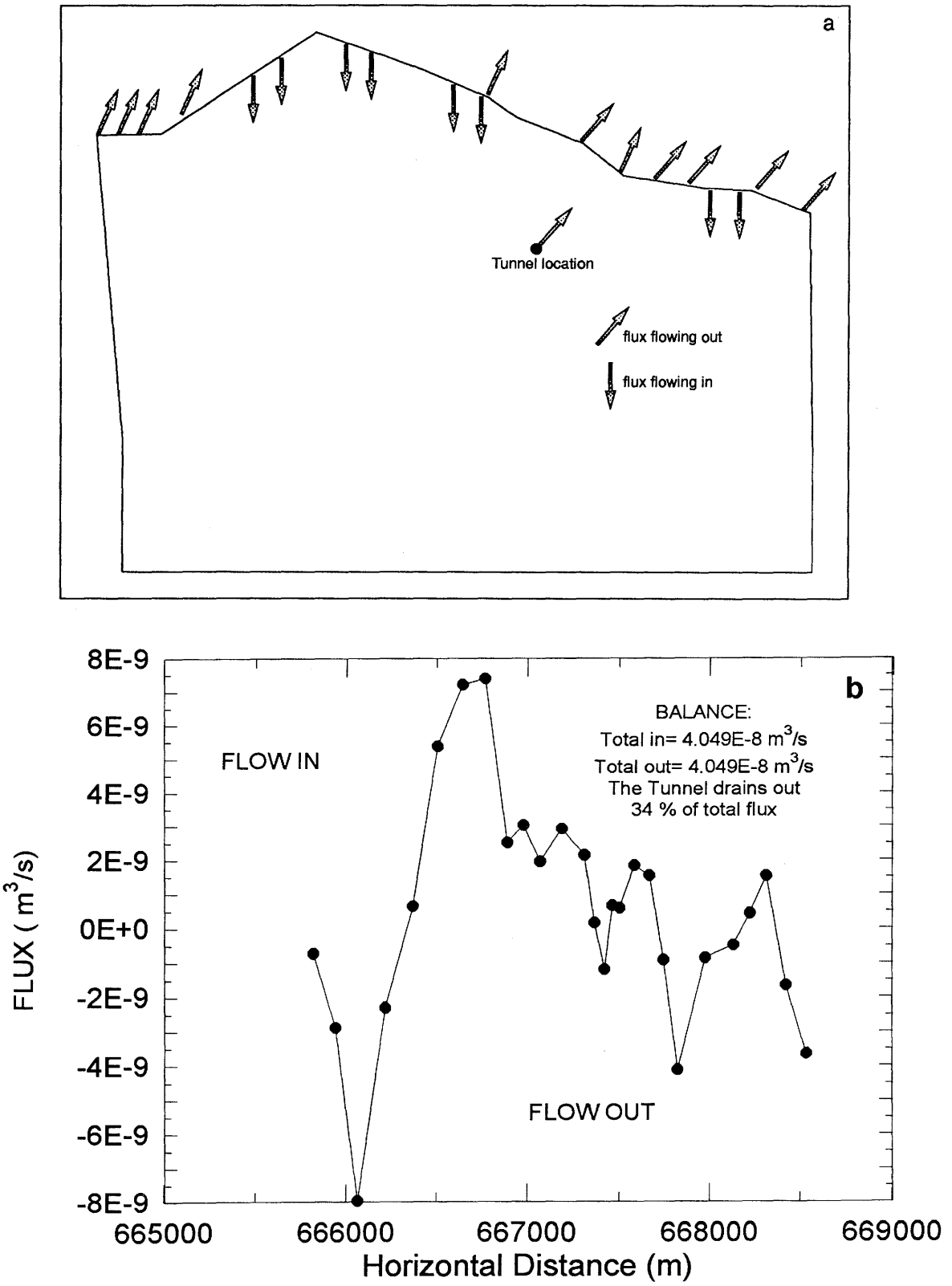

Figure 3.14 (a) Distribution of fluxes for cut33_5; and (b) Water balance.

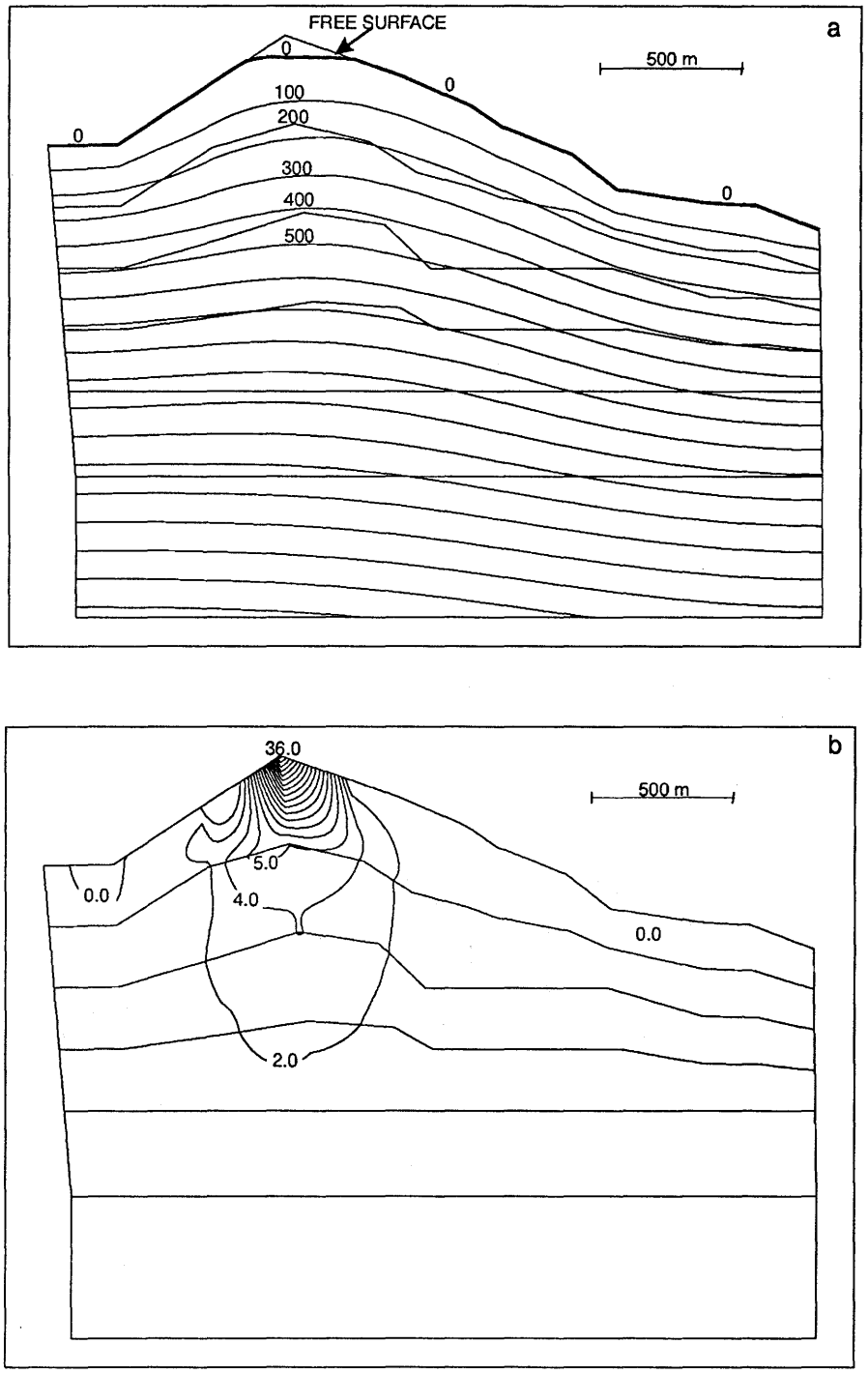

Figure 3.15 Steady-state results without tunnel: (a) free-surface simulations; (b) differences in hydraulic heads between the fixed-head and the free-surface simulations.

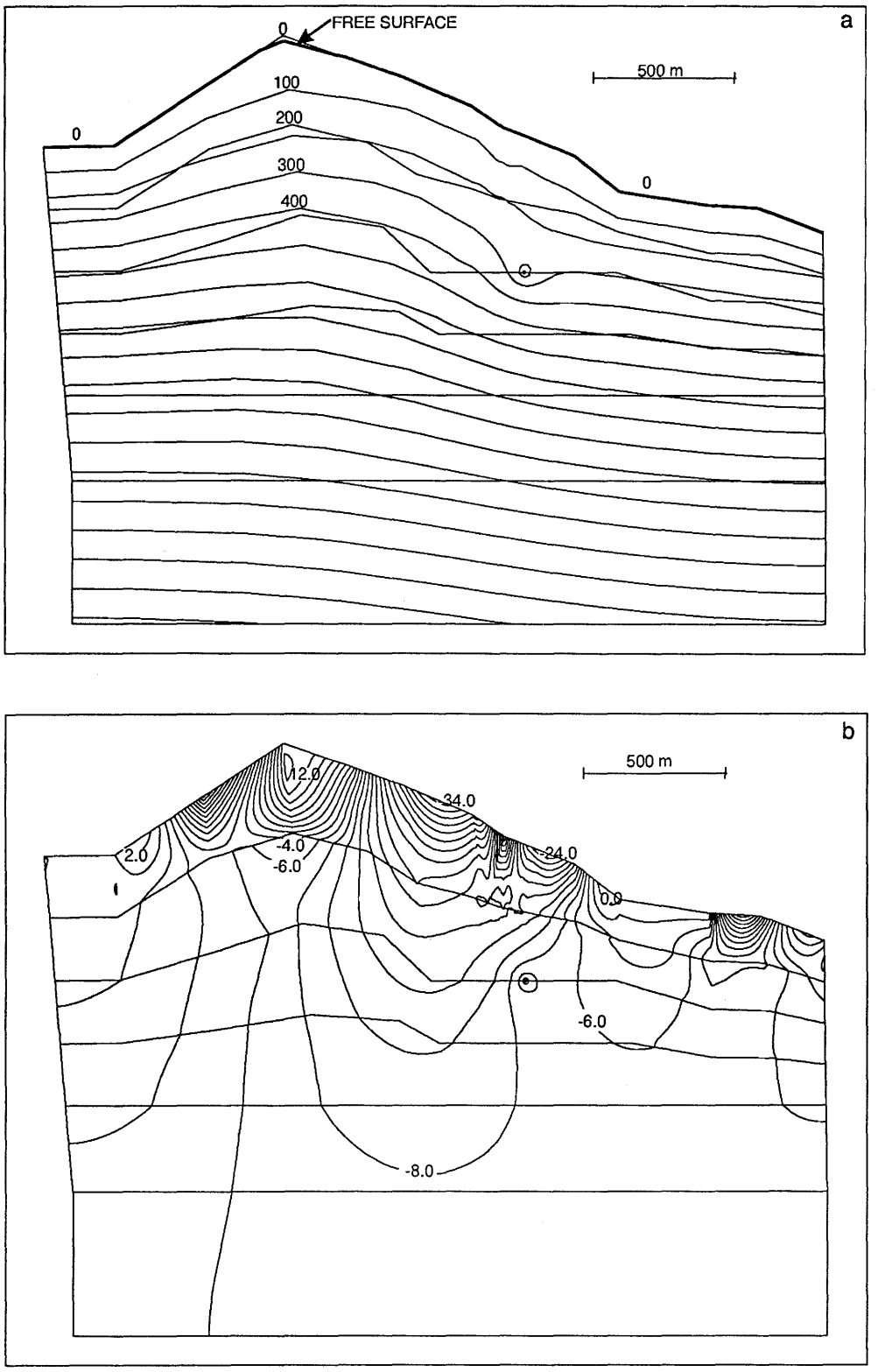

Figure 3.16 Steady-state results with tunnel: (a) free-surface simulation; (b) differences in hydraulic heads between the fixed-head and free-surface simulations.

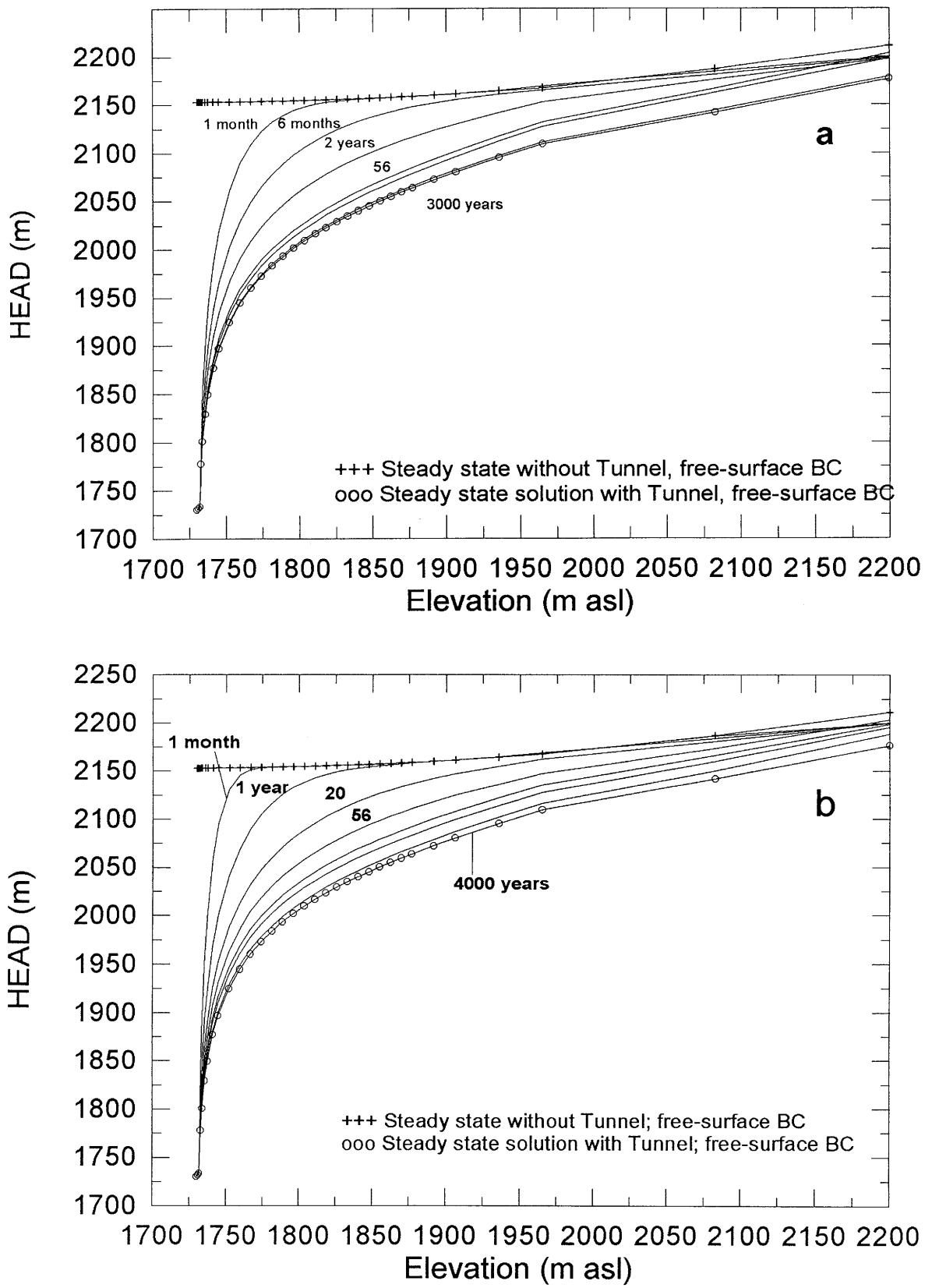

Figure 3.17 Free-surface transient simulation in a vertical section from the tunnel location to the top: (a) for case 1 (κ=5E-4 m^2/s); (b) for case 2 (κ=5E-5 m^2/s).

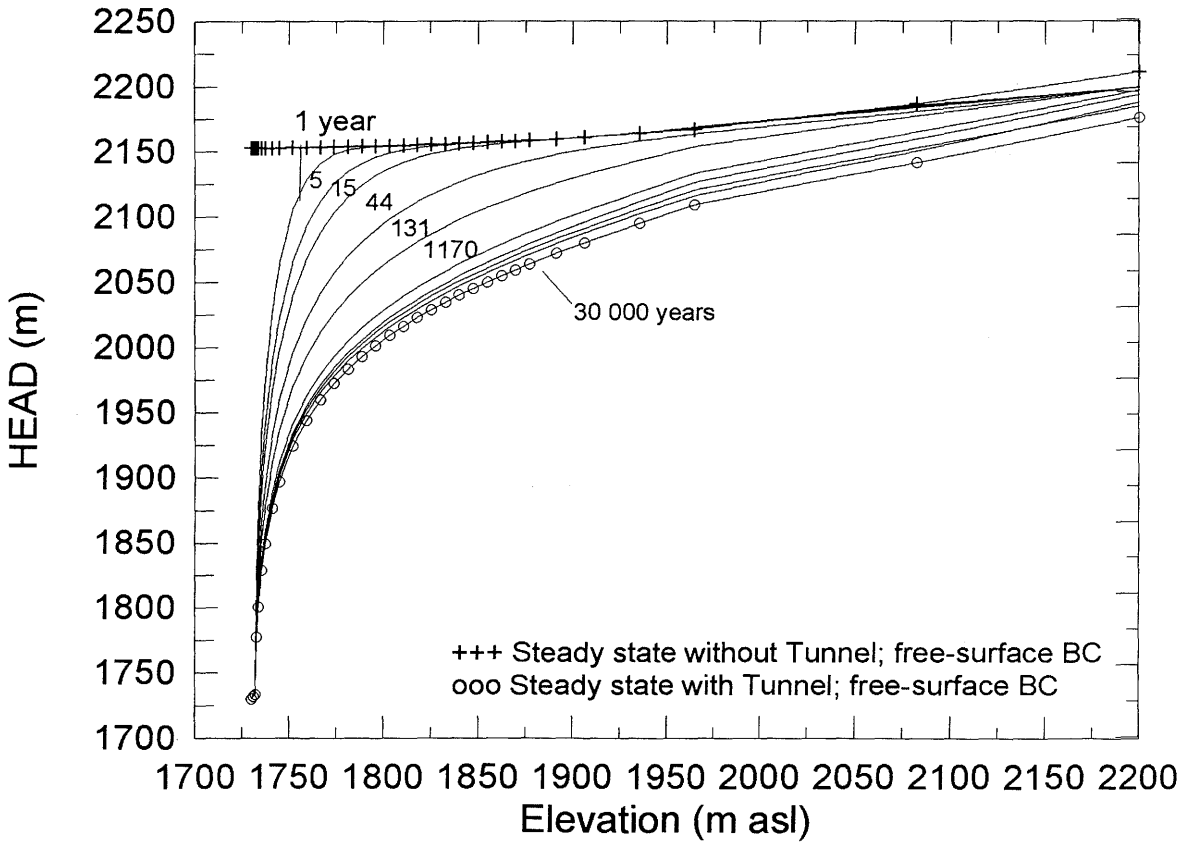

Figure 3.18 Free-surface transient simulation in a vertical section from the tunnel location to the top; case 3 (κ=5E-6 m^2/s).

3.3 Three-dimensional simulations at the sub-regional scale

3.3.1 Sub-regional model formulation

A "sub-regional Model" (SRM) was selected in order to provide a more manageable 3-D model for transient and coupled groundwater flow and heat transport simulations.

Infrastructure at the GTS

Since 1925, there has been a large amount of infrastructure construction in the region and the Grimsel area has undergone a vast change in hydraulic conditions with the construction of the dams and power stations in this area. The results of this report indicate that these changes in infrastructure may have a transient effect on the general groundwater regime around the GTS. The construction of a tunnel for access to a repository may cause perturbations through water drainage, changes in groundwater pressure in the rock formations, etc.

Table 3.8 shows the chronology for different construction projects in the Grimsel area since 1925.

Table 3.8: Chronology of the infrastructure construction in the Grimsel area

Construction Dates from - to	Infrastructure	Altitude / Water Level	Length / Volume
1925 - 1932	Grimsel Reservoir	1908.74 m	101.7 m^3
1925 - 1932	Connecting Tunnel between lake Grimsel and lake Gelmer	1908.74-1850.24 m	5222 m
1947 - 1950	Raeterichsboden Reservoir	1767.00 m	27.0 m^3
1950 - 1954	Grimsel I	1770.47 m	-
1950 - 1954	Lake Baechli	2161.70 m	-
1950 - 1954	Tunnel from lake Baechli to lake Grimsel	-	1360 m
June 1974 - June 1979	Grimsel II/KWO tunnel	-	-
30.05.1983 - Spring 1984	Grimsel Test Site	1730.00 m	-

The infrastructure at the GTS was built in the period from 30th May 1983 to spring 1984. On 20th June 1984, the GTS was officially opened. This infrastructure includes all tunnels built during this period (both by blasting and

by tunnel-boring machine), the central facilities, and the Fracture System Flow (Bohrlochkranz or BK) cavern. There have also been numerous boreholes drilled after the GTS opened on the 20th June 1984.

Measured hydraulic data

The KWO tunnel was constructed from the beginning of summer 1974, as access to the Grimsel II complex. In late 1980, Nagra drilled six exploratory boreholes at certain locations along this tunnel to check the suitability of the site for constructing an underground rock laboratory, which would be accessed by this tunnel. Initial results from these boreholes showed that this proposed location was ideal for Nagra's requirements. The data recorded during this time, from 1980 until 1983 (starting date of construction of GTS) included hydraulic head, water discharge, and temperature measurements from the boreholes at several positions along the KWO-tunnel.

From April 1983 to March 1987, the water discharge at numerous positions along the KWO tunnel was recorded, as was water temperature between April 1983 and January 1986. Until now this information was available only in the form of several graphs and tables of maximum/minimum values. To make this data available, all graphs were digitized, with one value taken for each calendar month (more or less frequently when appropriate). A complete explanation of the handling of these data is given in CHALMERS and CORREA (1993). Figure 3.19 shows the positions of the data taken along the KWO tunnel.

Of the hydraulic data reported in CHALMERS and CORREA (1993), only four data graphs are reproduced here in Figures 3.20 and 3.21 as examples. These are from the KWO tunnel at 709 m, 1698 m, 2171 m, and 2244 m. It can be seen from these Figures that, by the time the measurements were initiated (1983), the transient effects caused by the excavation of the main KWO access tunnel had already dissipated. The four-year measurements shown in Figures 3.20 and 3.21 seem to have almost reached hydrodynamic equilibrium (the seasonal/yearly variability is greater than the multiple-year variability).

3.3.2 Initial and boundary conditions

The GTS regional model (Chapter 2) used fixed-head boundary conditions at the upper model surface. The model surface was chosen to follow the topographic surface, with some smoothing of the relief to account for the possible existence of an unsaturated zone at the top of the mountain.

Due to the different permeability values in the rock matrix and the fracture zones, a highly variable water table is expected in the fractures. Because of the hydraulic dominance of the high-permeable fracture zones, the water table

in the model (i.e., the surface of the saturated flow model) was assumed to follow a line connecting the water tables in the fracture zones, thus neglecting the local flow systems in the uppermost parts of the rock matrix.

This approach was guided by the following reasoning (VOBORNY et al., 1991):

1. The main purpose of the regional model was to supply the local model around the GTS tunnel system with hydraulic head boundary conditions. These head values at the "local box" boundaries were expected to be only slightly influenced by the position of the water table below the tops of the mountains.
2. The amount of work to be invested in the regional model should not exceed a given limit, which resulted in the selection of a simple modeling approach.
3. The lack of information concerning the fracture zones (permeabilities, extent, connectivity with top surface, etc.) would have resulted in additional uncertainties if a more detailed modeling approach had been chosen.

In section 3.2.2, the resulting infiltration rates into the model surface were compared with the natural precipitation rates, as a check for the selected water-table position. With the adopted conductivity values for the rock matrix and the fracture zones (10^{-10} m/s and 10^{-7} m/s, respectively), infiltration rates of 3 mm/y in the matrix and up to 3 m/y in the fractures were calculated to saturate the model.

The needed infiltration rates for the fracture zones are in the same order of magnitude of the measured precipitation rate. Because of a possible sampling effect of the surface runoff to the draining fractures, and the strong dependence of the infiltration rate on the fracture transmissivities, it was decided to keep the selected model surface.

The issue of the phreatic boundary condition was discussed in consideration of the general scope of the modeling efforts of project MOD. The application of an algorithm described in FORSTER and SMITH (1988) was proposed. Because this algorithm is not applicable, without major adaptations, to a regional 3D-model (see section 3.2.2), it was decided to use the method of successive estimation and correction of the water-table position in an iterative procedure (e.g., NEUMANN and WITHERSPOON, 1970). The mesh-deformer algorithm MOVEMESH for the finite-element codes FEM301 and NAMMU was developed and applied to a test case (HÜRLIMANN et al., 1992). Another approach to this issue was implemented in the GW3D code and tested as reported in Rivera et al. (1993a).

These algorithms allowed the study of the influence of the phreatic boundary conditions in the regional model on the boundary conditions of the embedded models. Therefore, in a first step, a pre-processing algorithm was developed

and tested to allow the study of uncertainty/sensitivity of both boundary conditions (top and bottom) of the embedded sub-regional and local models.

Top boundary conditions

In order to provide boundary conditions for the surface of the SRM, a series of free-surface calculations for the regional GTS model were performed and are documented in RIVERA et al. (1993a); these include:

- a description of two different approaches (GW3D and FEM301/MOVEMESH);
- a comparison of results; and
- a parameter study (infiltration rate).

The free-surface calculations performed for the regional model pursued the following goals:

a) Create an operational tool for the treatment of free-surface problems which can also be used at other sites (e.g. Wellenberg model).
b) Check the selected approaches of GW3D and FEM301/MOVEMESH.
c) Check the assumption of full saturation up to the topographic surface of the model made in previous works.
d) Supply a quantitative basis for the selection of a 3-dimensional submodel which can be used for the more time-consuming (transient and/or coupled) simulations with NAMMU and/or GW3D.

Further details on the infiltration rate issue, computed with GW3D and MOVEMESH, are discussed in RIVERA et al. (1993a). These authors performed a detailed numerical investigation of fixed-head and free-surface boundary conditions at the top of the three-dimensional regional and sub-regional models, with and without the KWO tunnel. Their most relevant findings are:

- A discrete infiltration rate range of 10 to 15 mm/y for the case of Grimsel would be adequate to saturate the massif including fractures.
- Due to the presence of high-permeable fractures and/or drains, even small differences in head at the top surface (~20 m) are propagated down to the tunnel at some locations.
- It is concluded that, due to the very low matrix permeability in the case of the GTS, a fixed-head boundary condition prescribed at the top (full saturation) is sufficient.
- For other sites, where the rock matrix has a higher permeability (2 to 3 orders of magnitude), the infiltration rate becomes the limiting

factor for saturation, and not the matrix permeability. In those cases the free-surface approach may be necessary.

Lateral boundary conditions

The lateral boundary conditions for the SRM are those calculated from the regional GTS model using the selection criteria explained in the next section.

3.3.3 Selection of the SRM based on groundwater flow statistics

Selection criteria

The selection criteria to define the SRM is based in the following considerations (see Figure 3.22):

1. The SRM must contain the Test Site area (GTS site).
2. The SRM should consist of considerably less elements than the regional model.
3. The boundaries of the SRM should be selected at locations where the variability of the model results due to the model structure (with and without tunnels), and on the prescribed infiltration rate, is at a minimum.

For the different runs to be performed with the selected SRM, the boundary conditions at the lateral boundaries (prescribed heads or prescribed fluxes) will be maintained as for the regional model. With the third selection criterion it can be ensured that lateral boundaries of the SRM are less dependent on the unknown position of the groundwater table and on the presence of the 2D fractures in the model.

Variance of fluxes across the submodel boundaries

The free-surface calculations were performed for the regional GTS model with the conditions as listed in Table 3.9. The characters A, B, C denote the model runs with different infiltration rates given as follows:

Run	Infiltration rate q_0 [mm/y]
A	0.3
B	0.6
C	3.0

Table 3.9: Description of the regional GTS model runs

	INTERIOR BOUNDARIES (*)	
MODEL STRUCTURE	Without tunnels (i.e. no interior sinks)	With tunnels (atmospheric conditions at selected interior points)
Complete regional model (2D and 3D)	**v11A, v11B, v11C**	**v08A, v08B, v08C**

(*) The lateral boundaries are the same as presented in VOBORNY et al. (1991).

The variations in the regional model results for the 6 runs shown in Table 3.9 were monitored in the following way.

For each of the 6 runs the Darcy flow velocity at all nodes of the model is calculated. From previous results, the mean value and standard deviation of the flux are derived for all nodes for a given ensemble of model runs.

The mean values are given by component-wise averaging of the velocity vectors:

$$
\begin{aligned}
q_x^{mean}(i) &= \frac{1}{NR}\sum_{k=1}^{NR} q_x^k(i) \\
q_y^{mean}(i) &= \frac{1}{NR}\sum_{k=1}^{NR} q_y^k(i) \\
q_z^{mean}(i) &= \frac{1}{NR}\sum_{k=1}^{NR} q_z^k(i) \\
q^{mean}(i) &= \sqrt{[q_x^{mean}(i)]^2 + [q_y^{mean}(i)]^2 + [q_z^{mean}(i)]^2}
\end{aligned}
\qquad (3.6)
$$

where the index k runs over the selected model runs and i runs over all nodes.

The standard deviations are:

$$\sigma^2_{qx}(i) = \frac{1}{NR}\sum_{k=1}^{NR}[q_x^k(i) - q_x^{mean}(i)]^2$$
$$\sigma^2_{qy}(i) = \frac{1}{NR}\sum_{k=1}^{NR}[q_y^k(i) - q_y^{mean}(i)]^2 \qquad (3.7)$$
$$\sigma^2_{qz}(i) = \frac{1}{NR}\sum_{k=1}^{NR}[q_z^k(i) - q_z^{mean}(i)]^2$$
$$\sigma_q(i) = \sqrt{\sigma^2_{qx}(i) + \sigma^2_{qy}(i) + \sigma^2_{qz}(i)}$$

As a measure for the flux variation at the nodes the normalized standard deviation is used,

$$V_q(i) = \frac{\sigma_q(i)}{q^{mean}(i)}\ , \qquad (3.8)$$

where the normalization makes the variation $V_q(i)$ independent of the absolute value of the flux at node i.

The variation measure $V_q(i)$ has been investigated for the full model run-ensemble (Table 3.9).

E1: v11A, v11B, v11C, v08A, v08B, v08C

Figure 3.23 shows the spatial distribution of the normalized variance of the flux in the case of ensemble E1. Due to the large conductivity contrasts in the full model, the mean value of the flux varies over several orders of magnitude, whereas the normalized variance has values between 0.1 and 10.

The Figure shows iso-surfaces for flux variances: <37 %=blue; 37 %=green; >37 %=black; the yellow line crossing the model in a NNW-SSE direction represents the Bächlisbach shear zone; the red color represents the topography. As expected, the variances are smaller at the lower parts of the model and larger in regions where the groundwater table movements are of influence (top of the model).

From Figure 3.23 it can be concluded that zones with minimum normalized variance of the flux are present (zones in light blue). A sub-region then exists containing the GTS, which can be limited by following the zones of minimum variation of normalized variance of the flux. Applying this criterion, a sub-regional model was selected as displayed in Figure 3.24. The limits of the SRM are: the Bächlisbach shear zone to the north, The Räterichsboden to the east, the Grimsel lake to the south, and a natural water divide zone to the west (the two latter are the same as in the regional model, see Figure 2.1). The various colours in Figure 3.24 represent the different layers of the model.

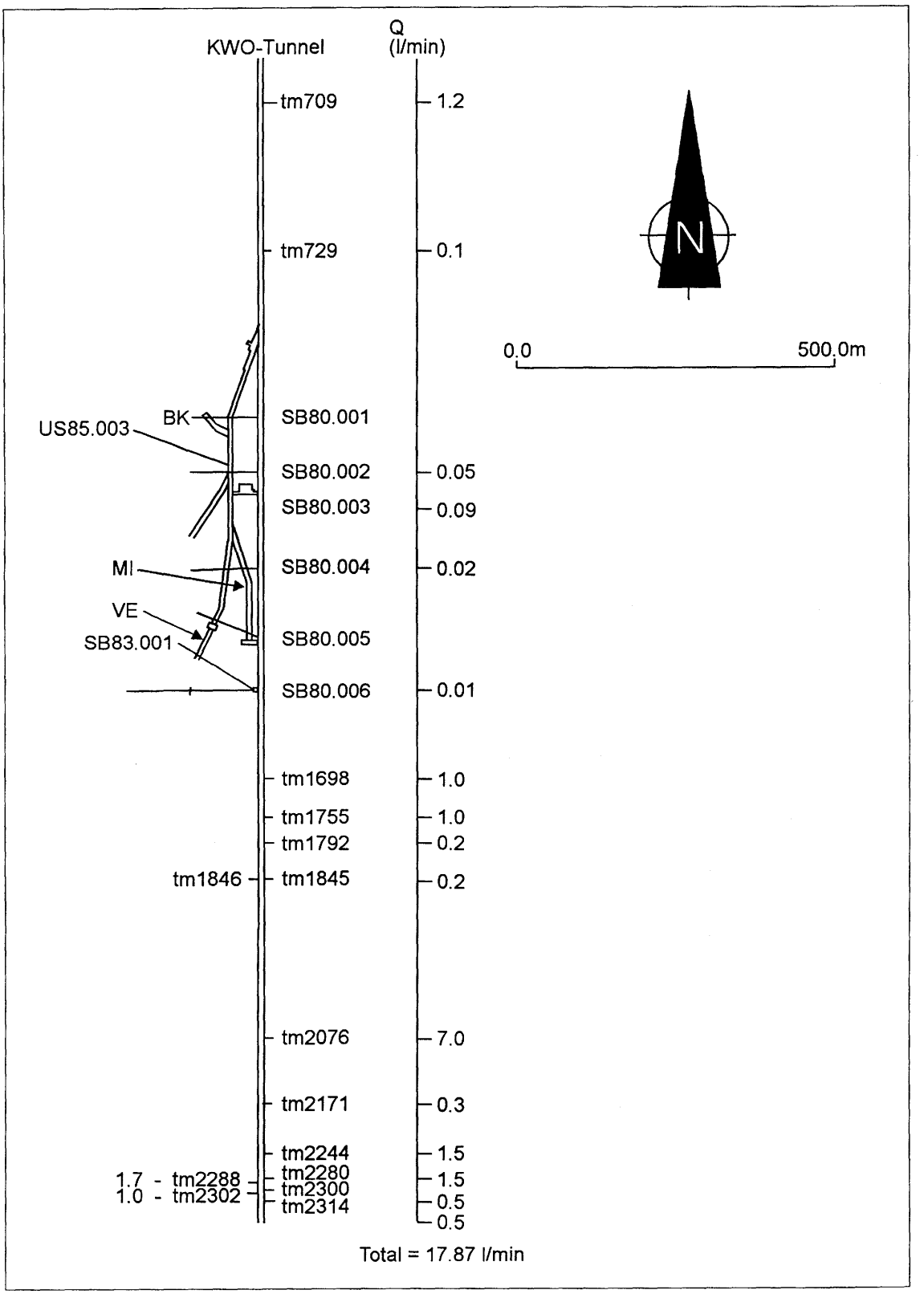

Figure 3.19 Fluxes measured along the KWO tunnel for the period of 1983-1987; modified from CHALMERS and CORREA (1993).

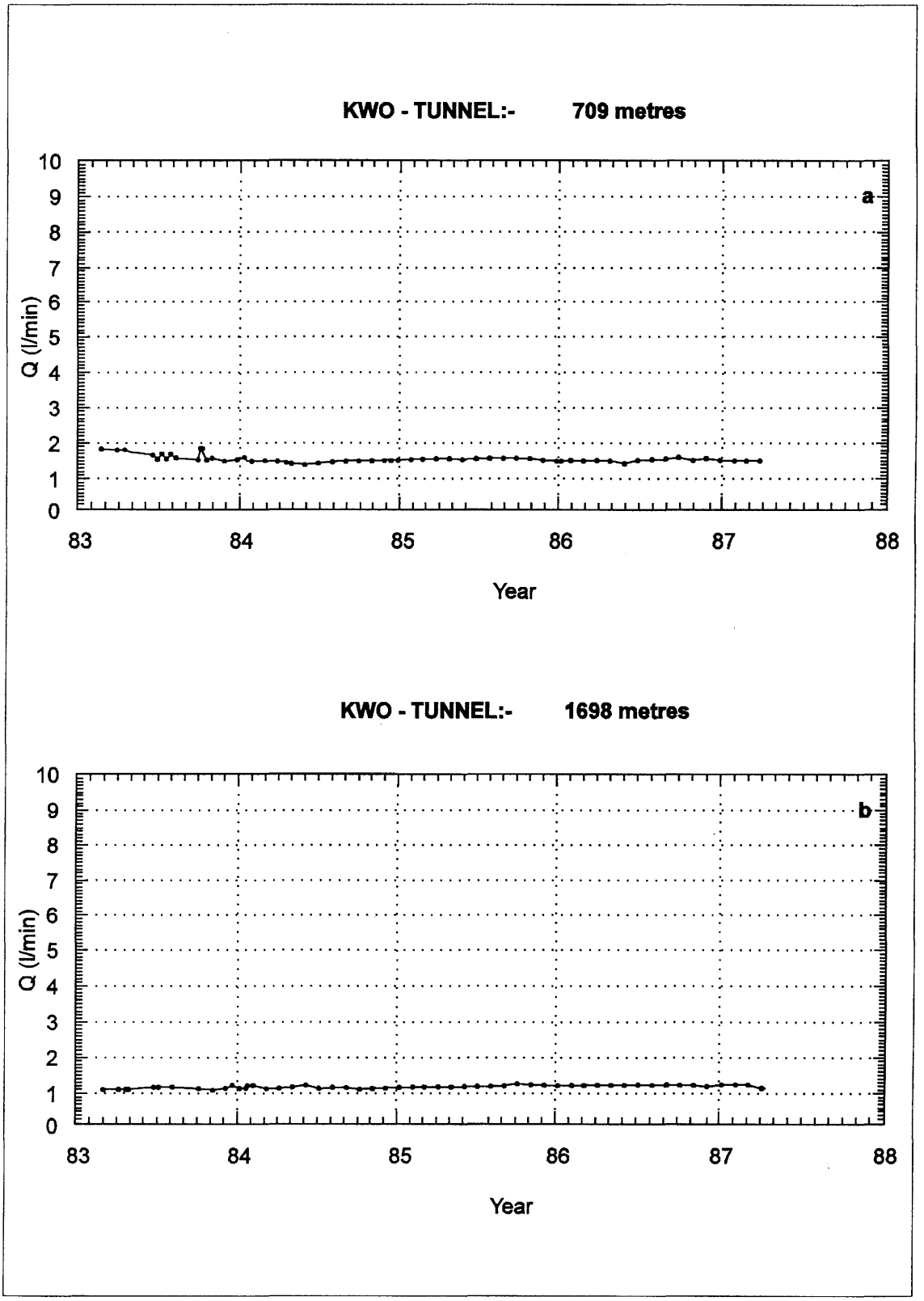

Figure 3.20 Fluxes drained by the KWO tunnel, measured at: (a) tm709; and (b) tm1698 (see Figure 3.19 for location); from CHALMERS and CORREA (1993).

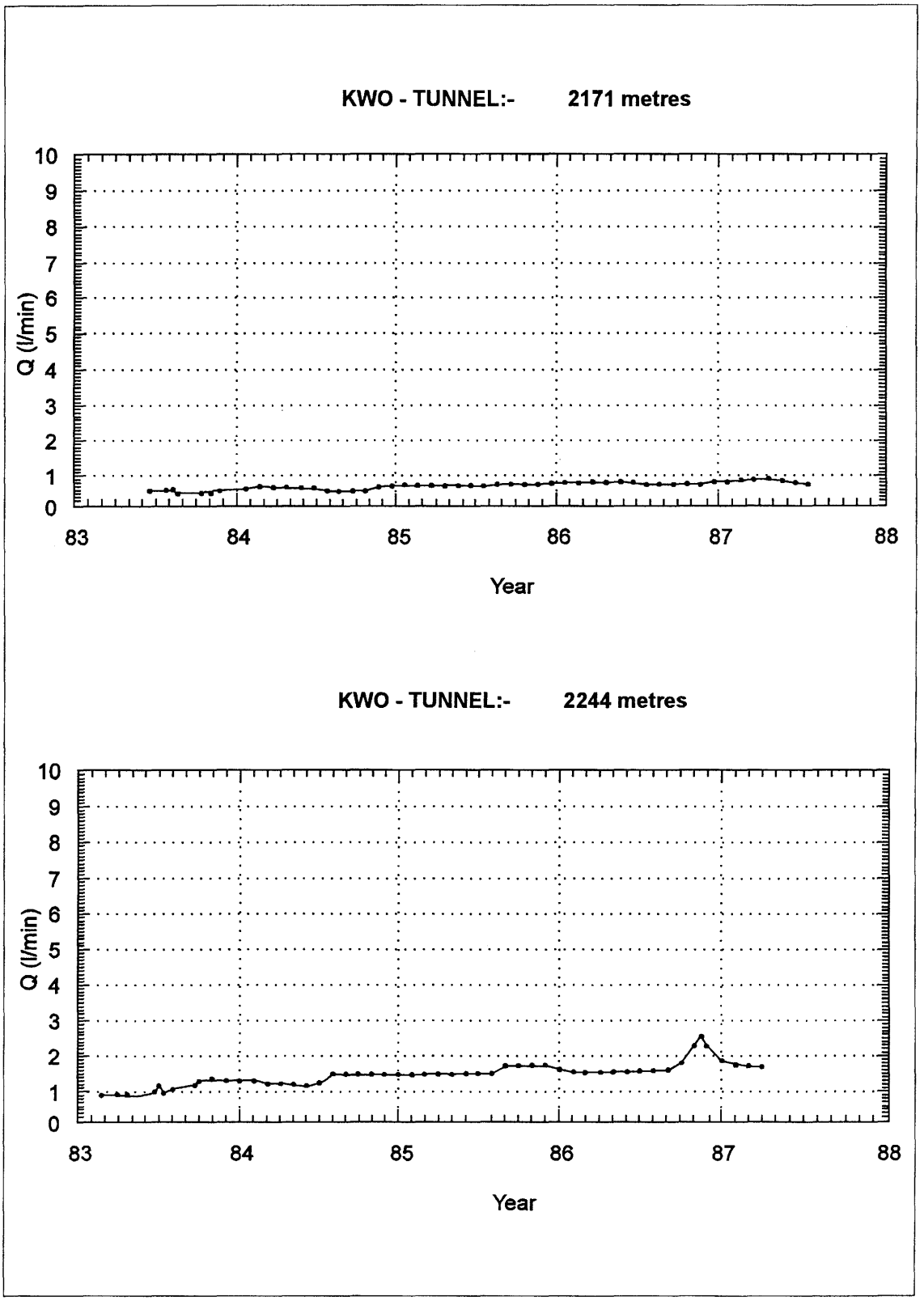

Figure 3.21 Fluxes drained by the KWO tunnel, measured at: (a) tm2171; and (b) tm2244 (see Figure 3.19 for location); from CHALMERS and CORREA (1993).

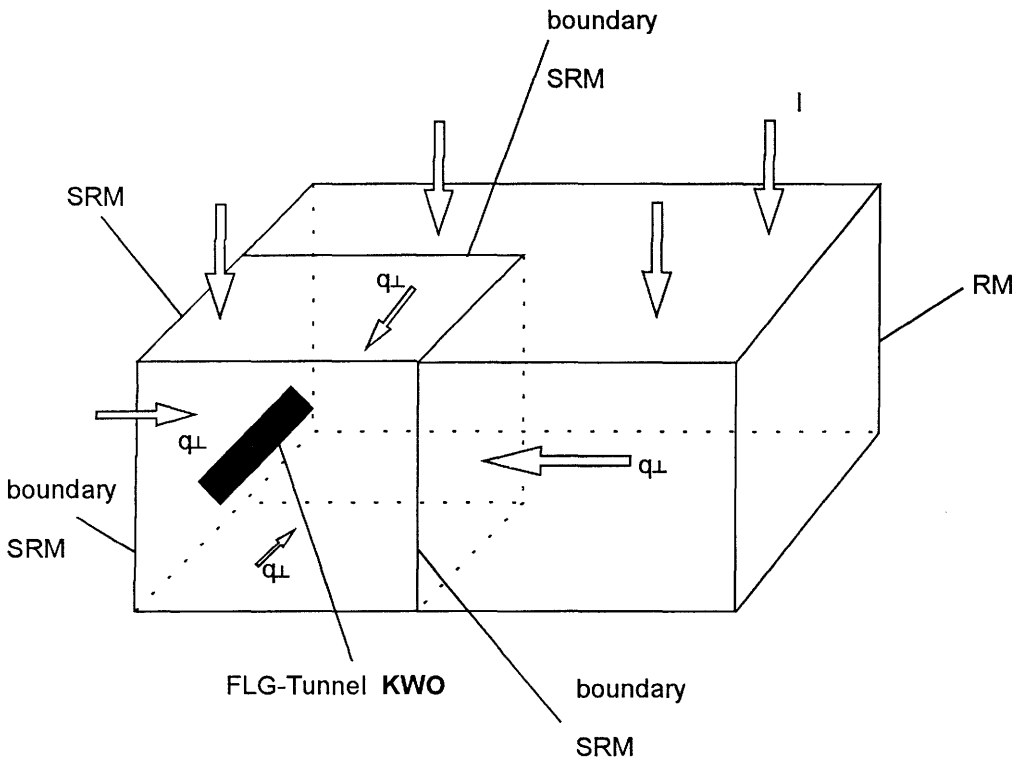

q⊥: Flow perpendicular to the element

RM: Regional model

SRM: Sub-regional model

I: Infiltration

Figure 3.22 Schematic diagram for selecting the sub-regional model.

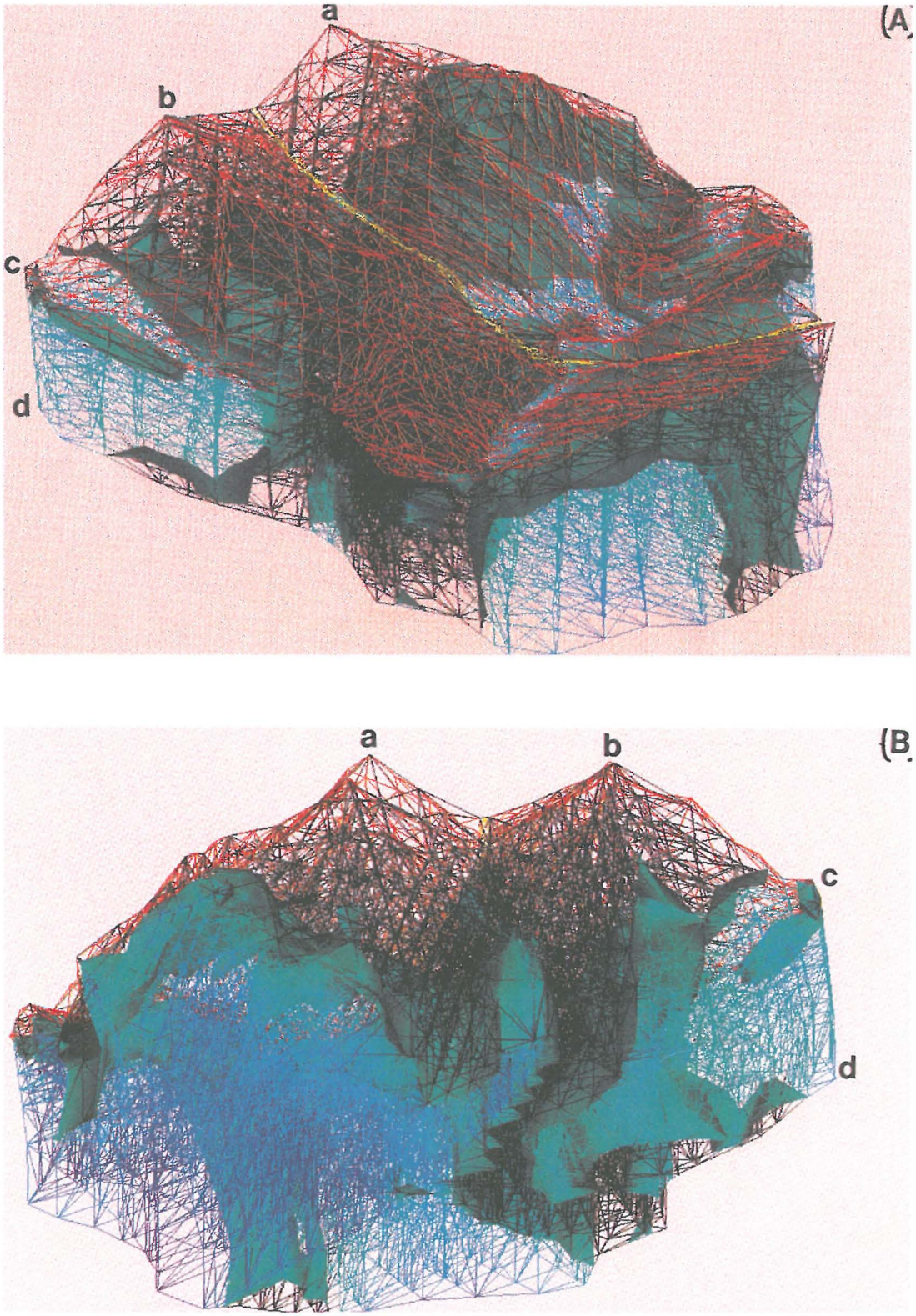

Figure 3.23 Iso-surfaces for normalized flux variances up to 37 % (blue to green) for the ensemble E1: (A) view is from SSW; (B) view is from NNW (seen from bottom up). Red color represents the topography.

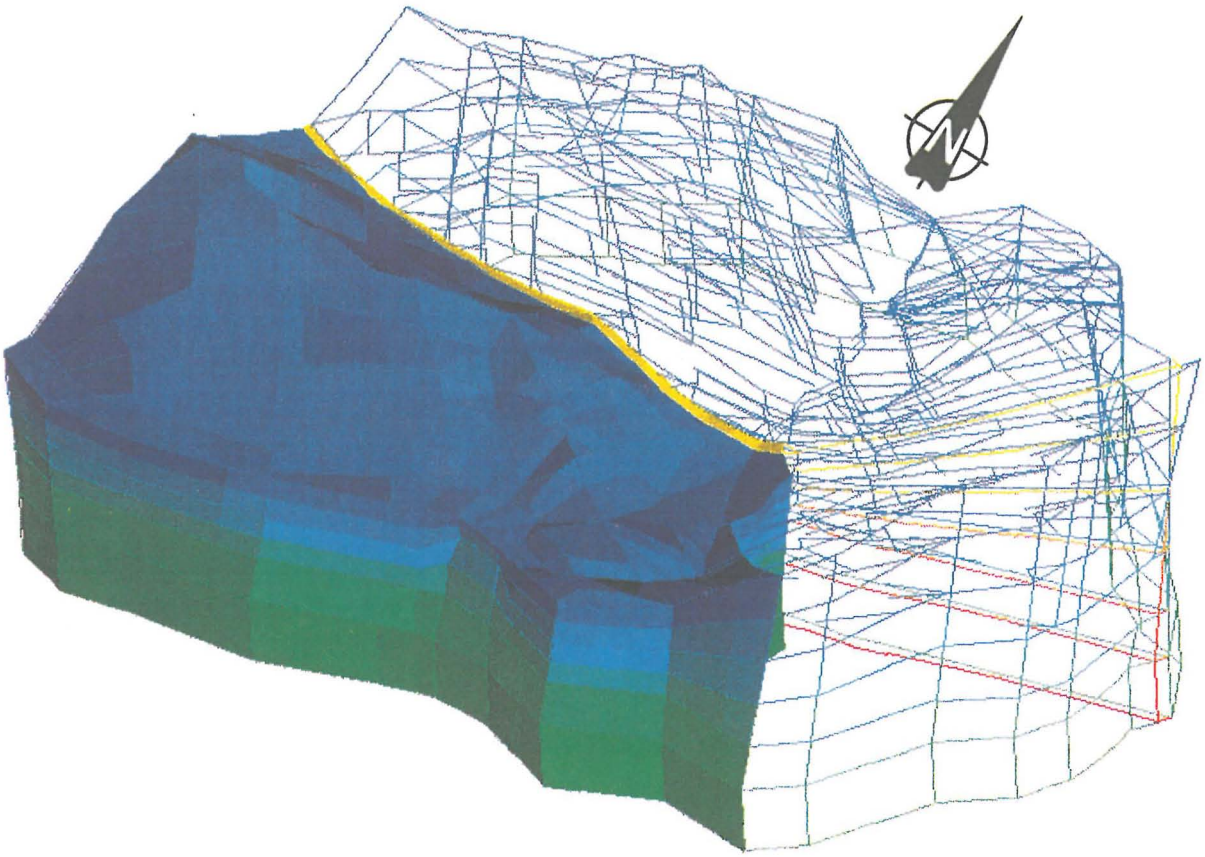

Figure 3.24 Sub-regional model (SRM) as a part of the regional model (RM). The yellow part is the Bächlisbach 3D shear zone, the view is from SSW. The various colours represent the different layers.

3.3.4 3D discretization of the KWO tunnel

Modeled area and grid refinement

The south and west boundaries of the SRM are the same as in the regional model. The Baechlisbach shear zone (north boundary) and the Raeterichsboden act as water divides and were therefore considered as natural boundaries between the SRM and the complete model (Figure 3.25). The criteria for the selection of these boundaries are explained in the previous section. Considering only a part of the complete model has the advantage of having less nodes and elements to be handled in the programs.

A comparison of the sizes of the three grids used in the three models, i.e., regional (RM), sub-regional (SRM) and refined sub-regional (SRM2) models, is given in Table 3.10.

Table 3.10 : Sizes of the grids used in the three models

MODEL	TOTAL No. OF ELEMENTS	TOTAL No. OF NODES	COMMENTS
RM	6576	13'239	With 1D & 2D vertical features
SRM	1710 3660	6765 6765	Only 3D elements With 1D & 2D vertical features
SRM2	7852	18'279	With 1D & 2D vertical features. Including the KWO tunnel refined in 3D

The SRM has the following hydraulic units:

— Rock matrix: represented in the numerical model by 3D elements divided into six layers;
— Fractures: represented in the numerical model with vertical 2D features; and
— Drains: represented in the numerical model with 1D vertical elements.

The boundary conditions for the Baechlisbach shear zone were derived from the results of the regional model.

KWO tunnel discretization

The location of the KWO tunnel is shown in Figure 3.25a. The KWO tunnel is oriented more or less from north (main entrance) to south (Grimsel lake). In reality the KWO tunnel is not completly straight but has some deviations (less than 2 m). In order to accommodate the KWO tunnel, and for the sake of

simplicity, the tunnel was aligned into a straight line in the SRM model between A and B as shown in Figure 3.25a. The alignment of the nodes between A and B was done with the program *FED*. This small modification has no significant effect on the results. In the SRM2 the tunnel has a quadratic shape of 4.5•4.5 m. The tunnel was constructed with 3D elements, mostly bricks. The top of the tunnel corresponds to the boundary between layer 2 and 3, i.e., the tunnel lies in layer 3.

Refinement

The refinement of the SRM mesh around the KWO tunnel was a challenging task. It could be accomplished using existing and new FE discretization and visualization tools, developped by the Hydrodynamic modeling group at COLENCO. The procedure and details of this issue are given in RIVERA et al., (1993b). Here we will present only the most relevant information, findings and results.

The refinement of the grid was more or less empirical. At the beginning, some ideas of grid refinement for transient simulations were taken from the experience with two-dimensional meshes, as presented in section 3.2. Therefore it was expected that the initial spatial discretization would not fit the problem and further refinement of the grid would be necessary. To avoid manual work and errors, and to reach a high level of quality assurance for the mesh refinement, all programs and file manipulations used in the refinement were implemented in shell files. This gives a totally automatic refinement. Creating a mesh with a different, coarse, spatial discretization is possible by changing only a few parameters in the shell files.

According to the results of the 2D discretization for transient simulations, it is known that reasonable results can be achieved if the distance between the nodes is doubled, starting at the location of the main perturbed zone (i.e. the tunnel). The grid discretization around the tunnel, in horizontal and vertical directions, was selected as 6, 12, 25, 50 m; that is, the first row of nodes around it should not be at a distance of more than 6 m. Figure 3.25b shows a schematic representation of this spatial discretization.

Because the refinement is necessary only in the region of the tunnel, a smaller part of the SRM was used. After the refinement was completed, this part was restored in the SRM model. The part of the model selected for the 3D discretization of the tunnel and refinement of the surrounding elements is shown with a shaded region in Figure 3.25a. Figure 3.26a also shows this refined part included back into the SRM; the zone is colored red, yellow and green, and is shown between layers 2 and 3 (in blue).

The horizontal refinement was carried out with the program *SUBELM.* The program *SUBELM* divides a layer horizontally into two parts. The geometric characteristic of the new layer can then be manipulated.

In the SRM, layer 2 was refined 3 times (cr_layer1a) and layer 3 five times (cr-layer2a), which leads to 8 new layers in the refined part of the model.

The vertical refinement was performed with the program *FRACMESH*. This program is able to refine an existing 3D mesh (HÜRLIMANN, 1993). In order to use *FRACMESH*, it was necessary to align all the 2-D vertical fractures located in the selected region into straight planes (a limitation of *FRACMESH*). This modification changed the original orientation of the 2D features in the numerical model (i.e., azimuth and dip). In the rest of the SRM, the 2D features were kept with their original orientation.

Figure 3.26b is a three-dimensional view of the SRM; layer 1 was taken out in order to show the 2D features embedded in the rock matrix; the colours represent the different layers. Figure 3.27a shows the discretized tunnel together with the 2D features in layers 2 and 3. Fourteen two-dimensional fractures cross the discretized 3-D tunnel, as shown in Figure 3.27b; the position of these and all the 2D features was respected and only their inclination was modified.

The refinement was carried out by including active "fractures" parallel to the tunnel. The selected distances from the tunnel were 6, 12, 25 and 50 meters. The use of *FRACMESH* markedly increased the number of elements (see Table 3.10).

Concluding remarks

Given the present limitations of the available numerical tools for refining existing grids, the SRM grid refinement had to be done first horizontally, and in a second step, vertically. For large 3D models of complex geology such as the SRM, one must always be aware of the increasing size (nodes and elements) of the grid that is being refined. A very important tool for avoiding a prohibitively large number of nodes and elements is the program *SHRINK*. Shrinking the newly refined elements has the advantage of keeping the element topology such that parts of a large model can be refined separately, and later reinserted into the whole model. However, in order to follow this procedure the modula 2000 characteristic must be used.

The vertical refinement was carried out with the program *FREMFAC* which is a shell file that calls the program *FRACMESH*. *FRACMESH* was originally developed as a mesh generator, but some modifications allow the inclusion of fractures in an existing mesh. However, to avoid numerical problems when applying this program, the coordinates have to be transformed (small values). In complex mesh geometries some additional problems due to the shape and size of the elements may occur. After the application of *FRACMESH*, the resulting refined elements had inconvenient shapes. Many of them had fancy "pinched" shapes that neither *NAMMU* nor the *FEM301-NAMMU* interface could possiblly handle. A special program *PINCH* (to unpinch elements) was

specially developed to convert these elements into a format that *NAMMU* could read. This task was very time consuming because it had to be done by choosing separately each of the different element shapes.

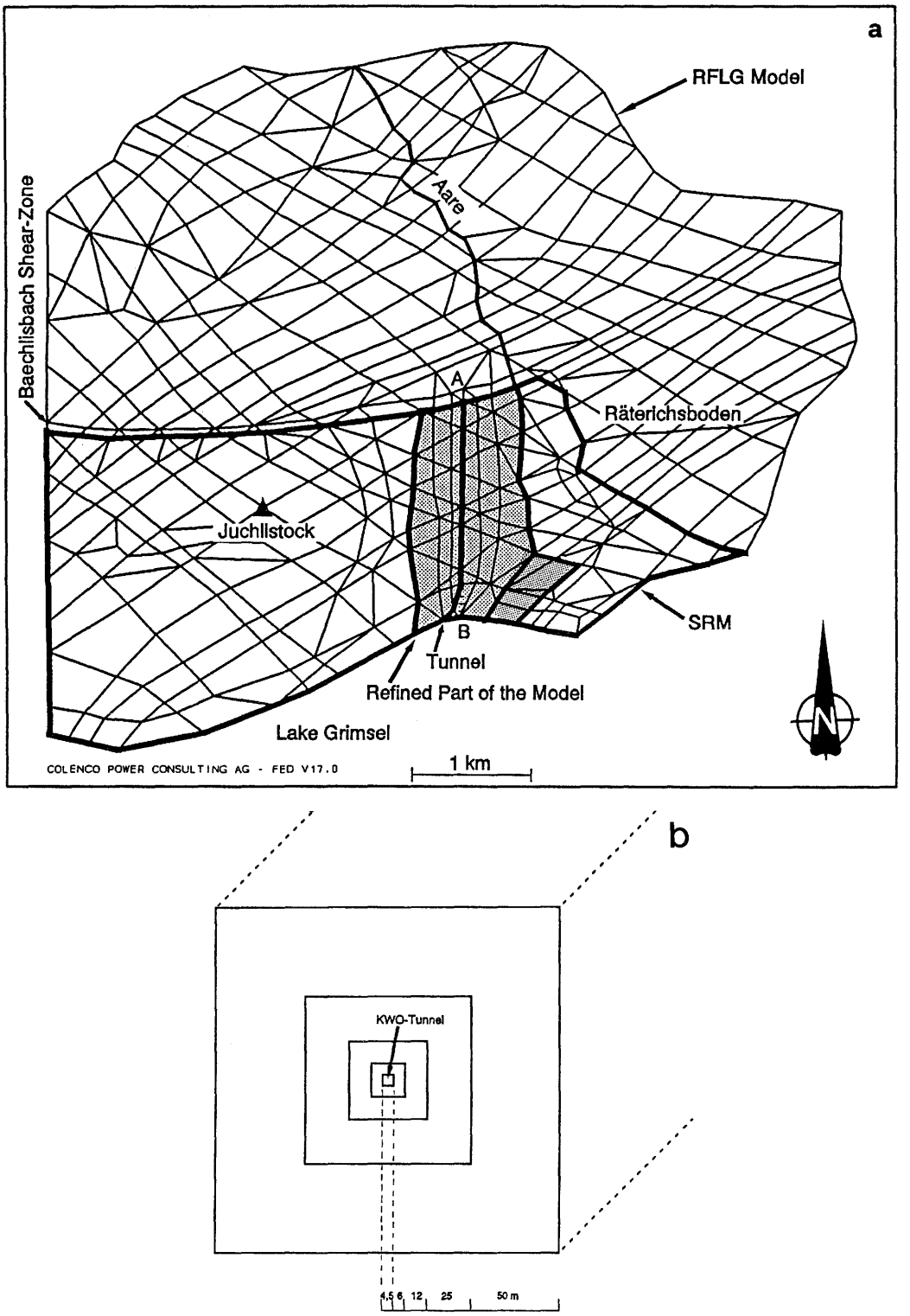

Figure 3.25 (a) Location of the sub-regional model with the Baechlisbach shear zone in the regional model. (b) Schematic representation of the spatial discretization around the tunnel (2d cut).

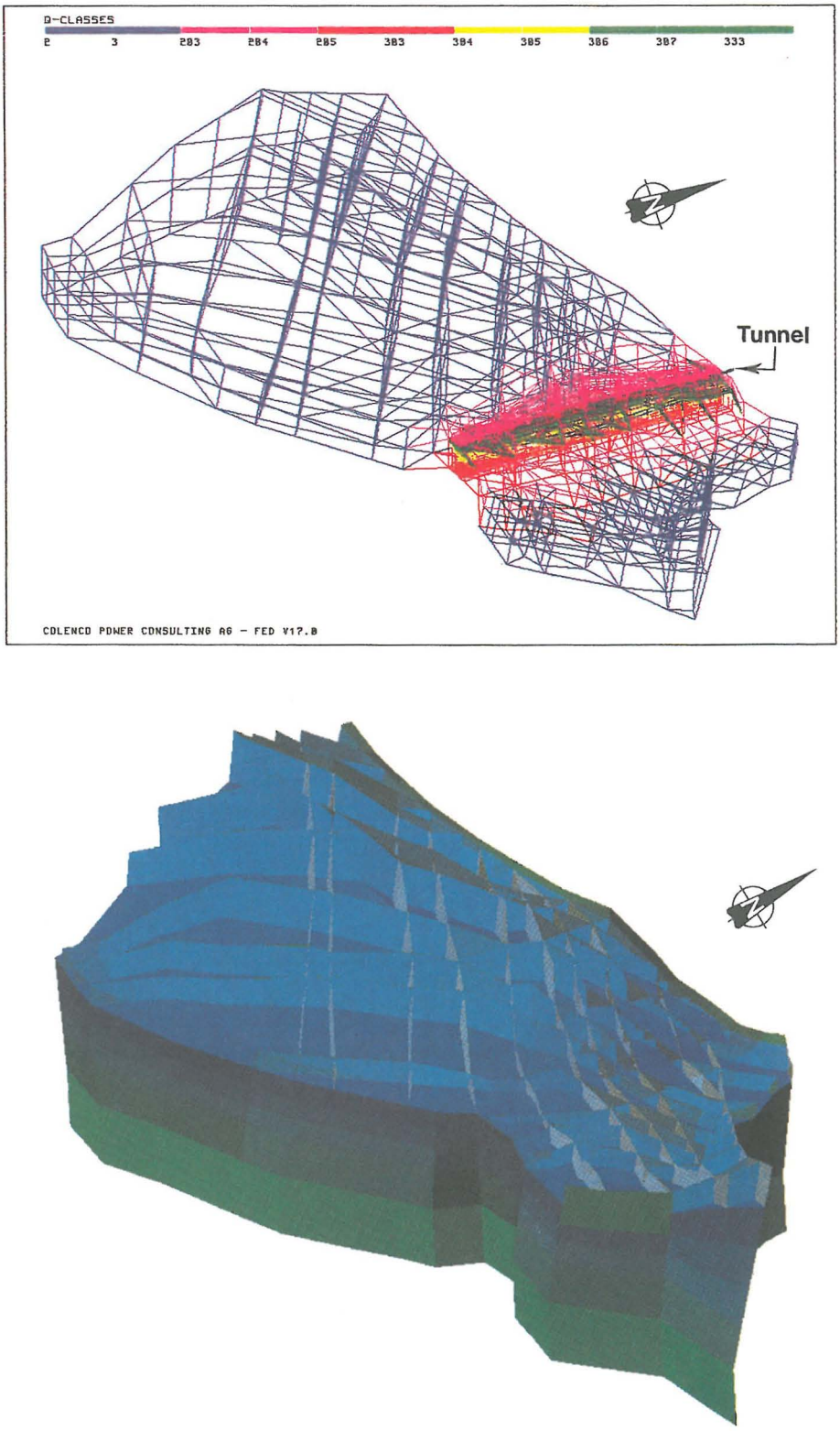

Figure 3.26 (a) Refined part of the SRM between layers 2 and 3. The red, yellow and green colors represent this area; the rest of the mesh (in blue) was not further refined. (b) 3D view of the SRM without layer 1 to show the 2D features.

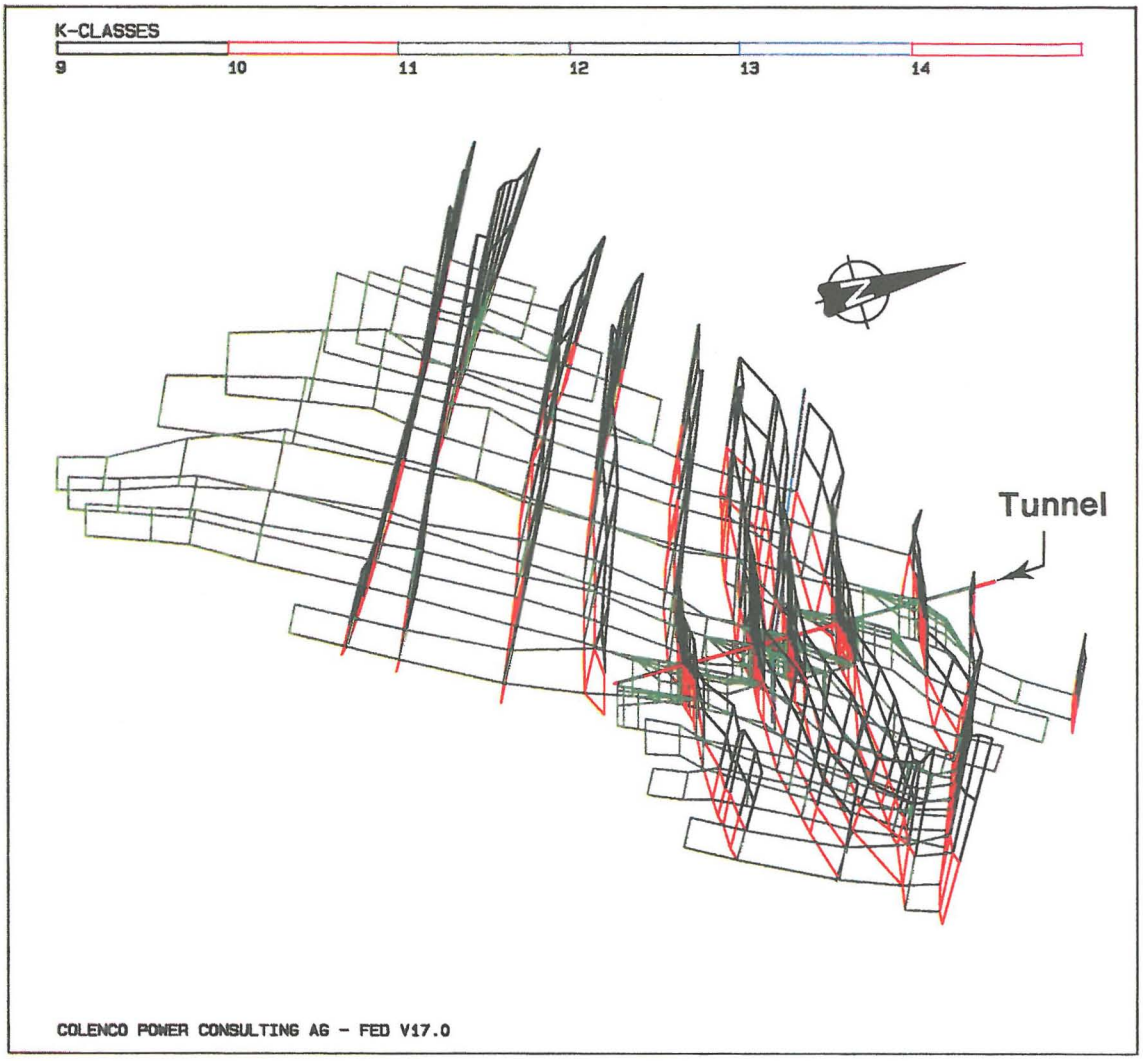

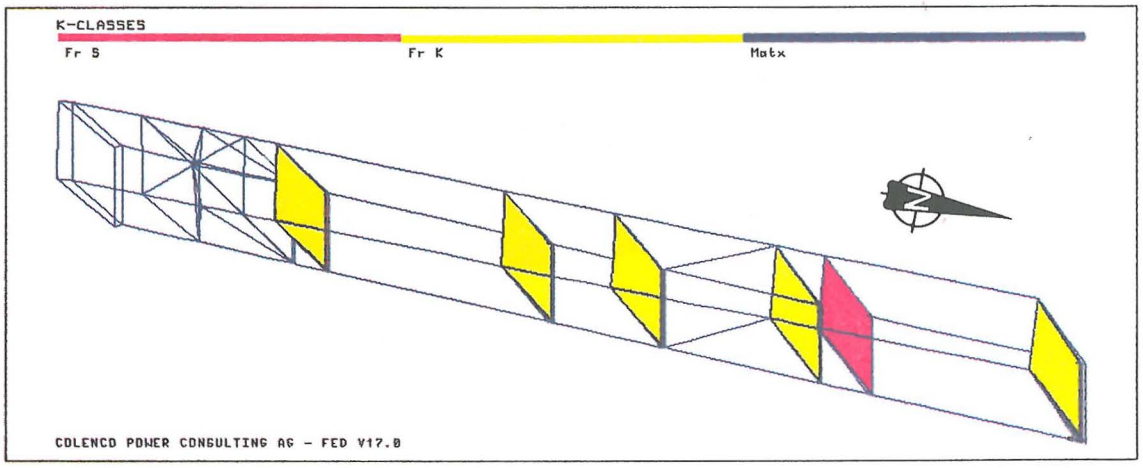

Figure 3.27 (a) Location of the discretized 3D KWO tunnel, shown with the 2D features between layers 2 and 3. (b) Magnified part of the 3D tunnel showing the intersecting 2D fracture system.

3.3.5 Steady-state simulations

This section presents the results of numerical simulations performed under steady-state conditions with the new discretized SRM2, both with the tunnel activated through the adequate boundary conditions as well as when the tunnel is turned off.

Reproduction of previous 3D SRM results with the new grid

Of particular importance was the generation of the previous results in three dimensions (RIVERA et al., 1993b) with the sub-regional model, as a means of verifying the newly refined grid. As a first step, it was intended to reproduce steady-state results without the tunnel. In the present case, the tunnel was created as a three-dimensional feature, (§ 3.3.4), but for this simulation the boundary conditions at the tunnel location were not activated.

The adopted boundary conditions in this case are:

- fixed heads at the surface (saturated conditions, h=elevation);
- fixed lateral heads (these were obtained from the RM and interpolated for the newly refined grid, see section 3.3.3) along the Baechlisbach shear zone to the north;
- fixed heads at the Räterichsboden lake to the northeast;
- no flow at the bottom; and
- the presence of the tunnel is not simulated.

The parameter values used in this simulation, e.g., permeabilities, are the same as the ones used in the previous SRM simulation presented in RIVERA et al., 1993a; they represent the base-case conditions and are reproduced in Table 3.11 for convenience.

Table 3.11 : Hydraulic properties assigned for the base case

LAYER No.	MATRIX **K** (m/s)	2D FRACTURE SYSTEMS **T** [m^2/s]		1D VERTICAL DRAINS (Intersections) **K** (m/s)
		K	S	
1	1E-10	1E-7	1E-8	1E-6
2	5E-11	1E-7	1E-8	1E-6
3	1E-11	5E-8	5E-9	5E-7
4	5E-12	1E-8	1E-9	1E-7
5	1E-12	1E-8	1E-9	1E-7
6	1E-12	1E-8	1E-9	1E-7

Figure 3.28 presents the results of this simulation displayed in a horizontal section at the GTS level (top of layer 3, elevation 1730 m a.s.l.), and in a vertical section parallel to the main tunnel. Figure 3.29 presents the results, for the same conditions and the same sections, but with the former SRM grid; this Figure is reproduced directly from RIVERA et al. (1993a; Figure 7.2) and is presented here only for comparison purposes. The titles in Figure 3.28 are: *SRM2* for "refined sub-regional model," and *sso.res* for "steady-state results without tunnel".

Because the total number of nodes is not the same in both grids, a direct, quantitative comparison is not possible; this can only be done qualitatively. From these Figures it can be seen that the calculation with the refined grid did not exactly reproduce the previous results. The differences between the two simulations are about 40 meter in the northeastern and southwestern parts of the model. On the other hand, two-thirds of the model, in the western part, reproduced the previous results, as can be seen in Figure 3.28a compared with Figure 3.29a. The 40-meter difference almost certainly comes from the fact that the newly refined SRM2 had to align, into vertical columns (as discussed in section 3.3.4), the otherwise inclined system of fractures around the tunnel area. The difference in the inclination of the 2D vertical fractures is clearly seen in Figures 3.28b and 3.29b.

Steady-state calculations including the tunnel

A steady-state calculation was performed with the same boundary conditions; in this case the tunnel is simulated by activating the internal boundary condition, i.e., prescribing atmospheric pressure at all the nodes located at the walls of the tunnel. This is done by simply prescribing a fixed head equal to the node elevation and giving a high value for permeability to all the elements inside the tunnel, i.e., K= 1.0 m/s.

Figure 3.30 presents the results of this simulation displayed in a horizontal section at the GTS level and in a vertical section parallel to the main tunnel. Figures 3.32(a,b,c) show vertical profiles of the hydraulic head from the top to the bottom of the model, for the three selected vertical sections shown in Figure 3.31, both for the simulations when the tunnel is activated and when it is not.

Effects of the 3D discretization of the KWO tunnel

A steady-state calculation with the tunnel was also done with the newly refined grid, SRM2, but simulating the tunnel in one dimension. A fixed head (atmospheric pressure) was prescribed at the nodes on a line of one-dimensional elements corresponding to the tunnel elevation, as in the original SRM.

Figure 3.33 shows the results of this simulation displayed in a horizontal section at the GTS level (top of layer 3) and in a vertical section parallel to the main tunnel.

Figure 3.34 presents the results, for the same conditions and the same sections, but with the former SRM grid. This Figure is reproduced directly from RIVERA et al. (1993a; Fig. 7.3) and is presented here only for comparison purposes.

Finally, Figure 3.35 is a plot of the differences in hydraulic heads between the simulations with the three-dimensional tunnel and the one in which the tunnel is simulated in one dimension.

Conclusions

The refinement of the SRM to accommodate the KWO tunnel in three dimensions (new grid SRM2) increased the total number of elements by more than a factor of two and the total number of nodes by almost a factor of three (Table 3.10). A first concern was that the number of operations required to solve the equations increases very rapidly with the size of the model.

Additionally, because the RM and the SRM have large contrasts in the permeability with irregular meshes, care was taken to minimize the large three-dimensional groundwater flow problem at the GTS without having to sacrifice the accuracy of the numerical solution. Because the objectives of this work were to perform transient calculations, a compromise had to be found between computational costs and computer space availability, with the most realistic conditions possible given such a complex numerical model.

In order to refine the KWO tunnel in three dimensions, and to find the optimum refinement of the elements around it for later transient calculations, the topology of the two-dimensional fractures had to be modified, given the limitations of the available discretization tools (see section 3.3.4). This translated in the modification of the piezometry in steady state in about 40 meters, mostly to the east and below the discretized KWO tunnel (Figures 3.28 to 3.30). On the other hand, a quantitative comparison between a 3D tunnel and a 1D tunnel steady-state simulations showed differences in the hydraulic heads of up to -100 m (Figure 3.35). These results show the importance of the model topology and the appropriate treatment of this internal boundary.

We conclude that, in future 3D models with similar complexity, the discretized 3-D tunnel should be included from the very beginning, when the grid is created following the original geology. Otherwise, it becomes very difficult, if not impossible, to include such a 3D feature in an existing grid such as the one in the SRM, without having to modify the original model topology.

Nevertheless, we believe that the numerical results with the new refined model

SRM2 still give a good indication of the 3D groundwater flow at the GTS site. The effects of the hydrodynamic transient behaviour when the tunnel is activated also gave plausible results with the SRM2 grid, as will be shown in the remaining sections of this Chapter.

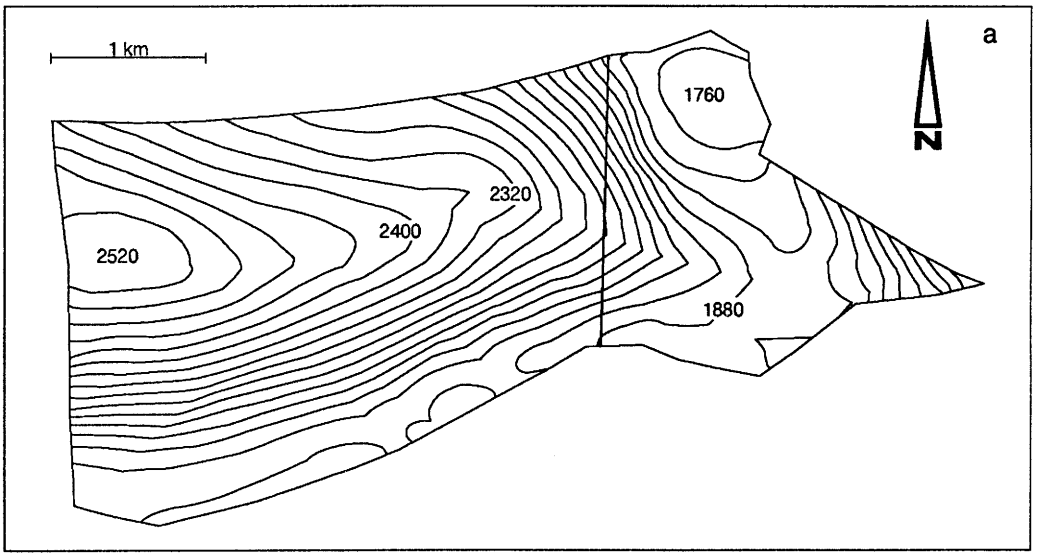

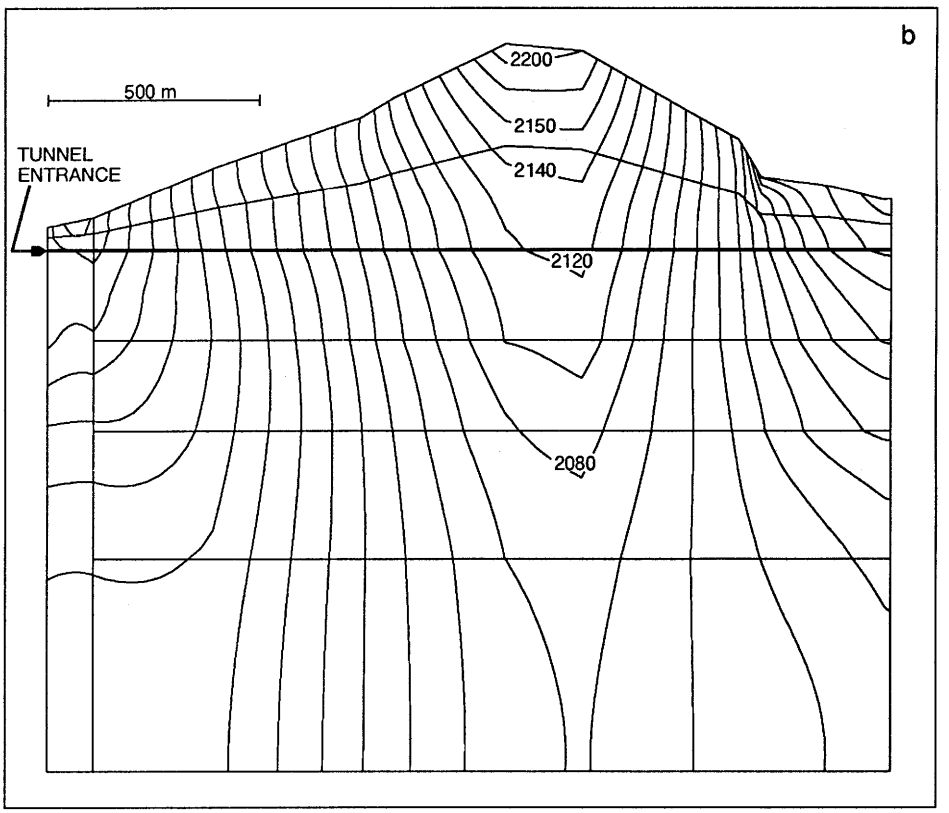

Figure 3.28 Steady-state results without tunnel for: (a) a horizontal section (top of layer 3); and (b) a vertical section parallel to the tunnel.

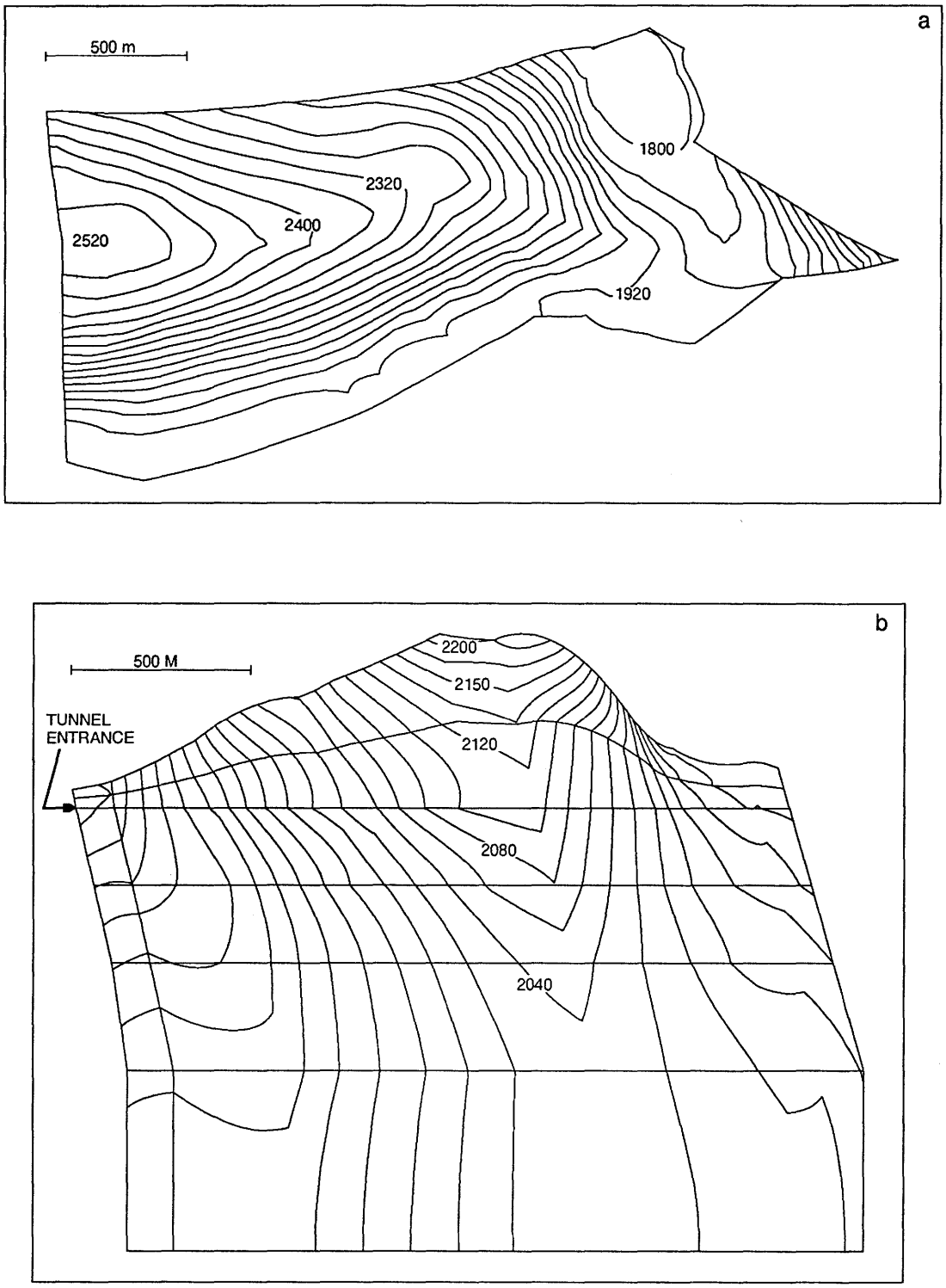

Figure 3.29 Steady-state results without tunnel: (a) a horizontal section (top of layer 3); and (b) a vertical section parallel to the tunnel (from RIVERA et al., 1993a).

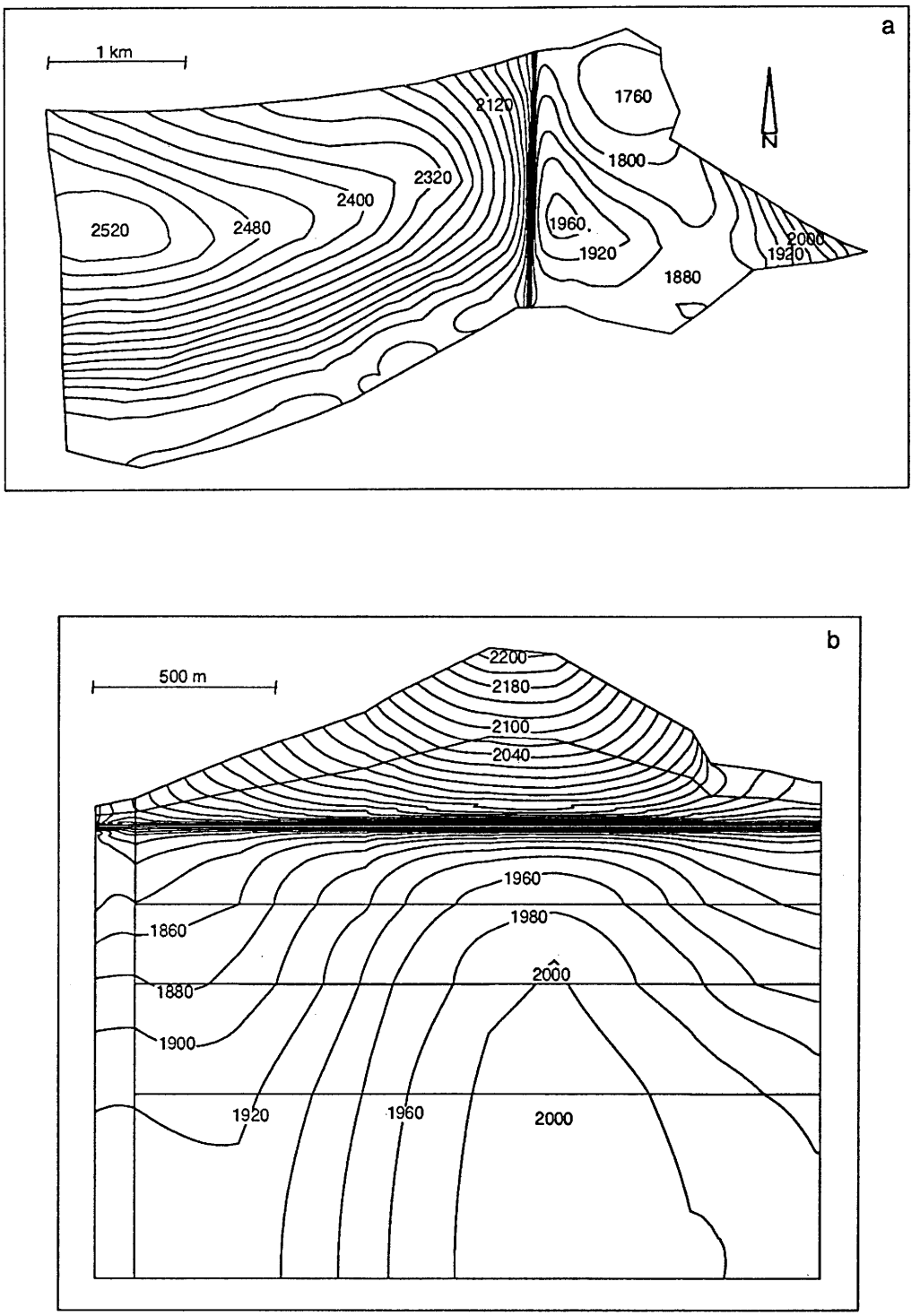

Figure 3.30 Steady-state results with tunnel: (a) a horizontal section (top of layer 3); and (b) a vertical section parallel to the tunnel.

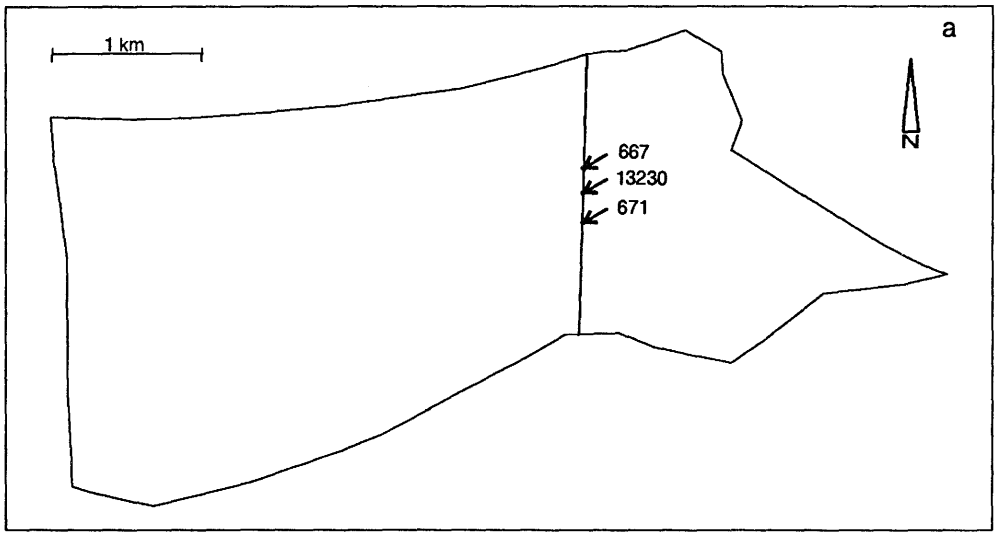

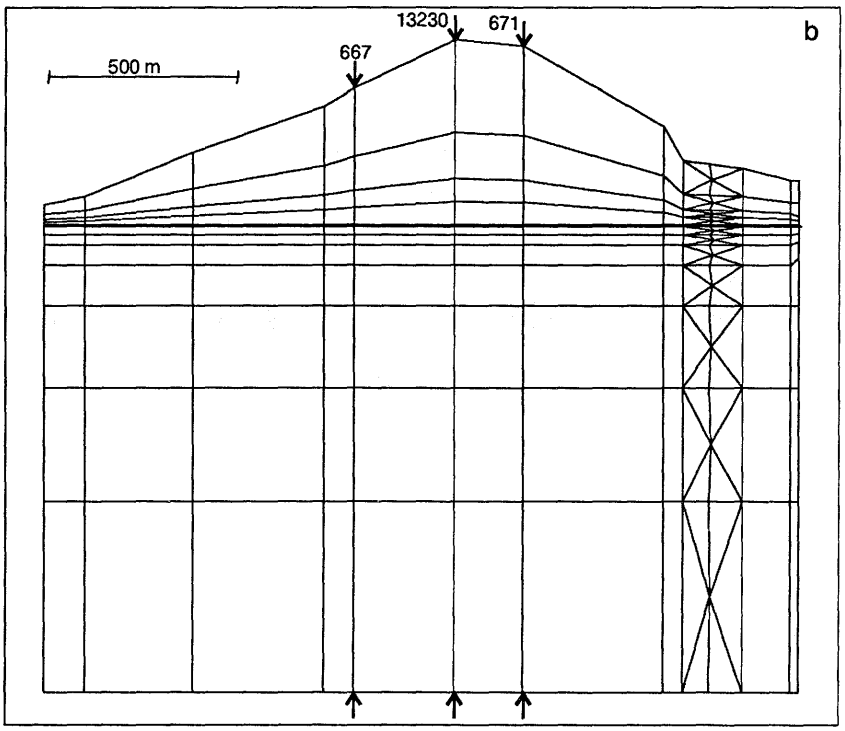

Figure 3.31 Selected vertical profiles for plotting results with and without tunnel: (a) top of layer 3; (b) vertical section parallel to the tunnel.

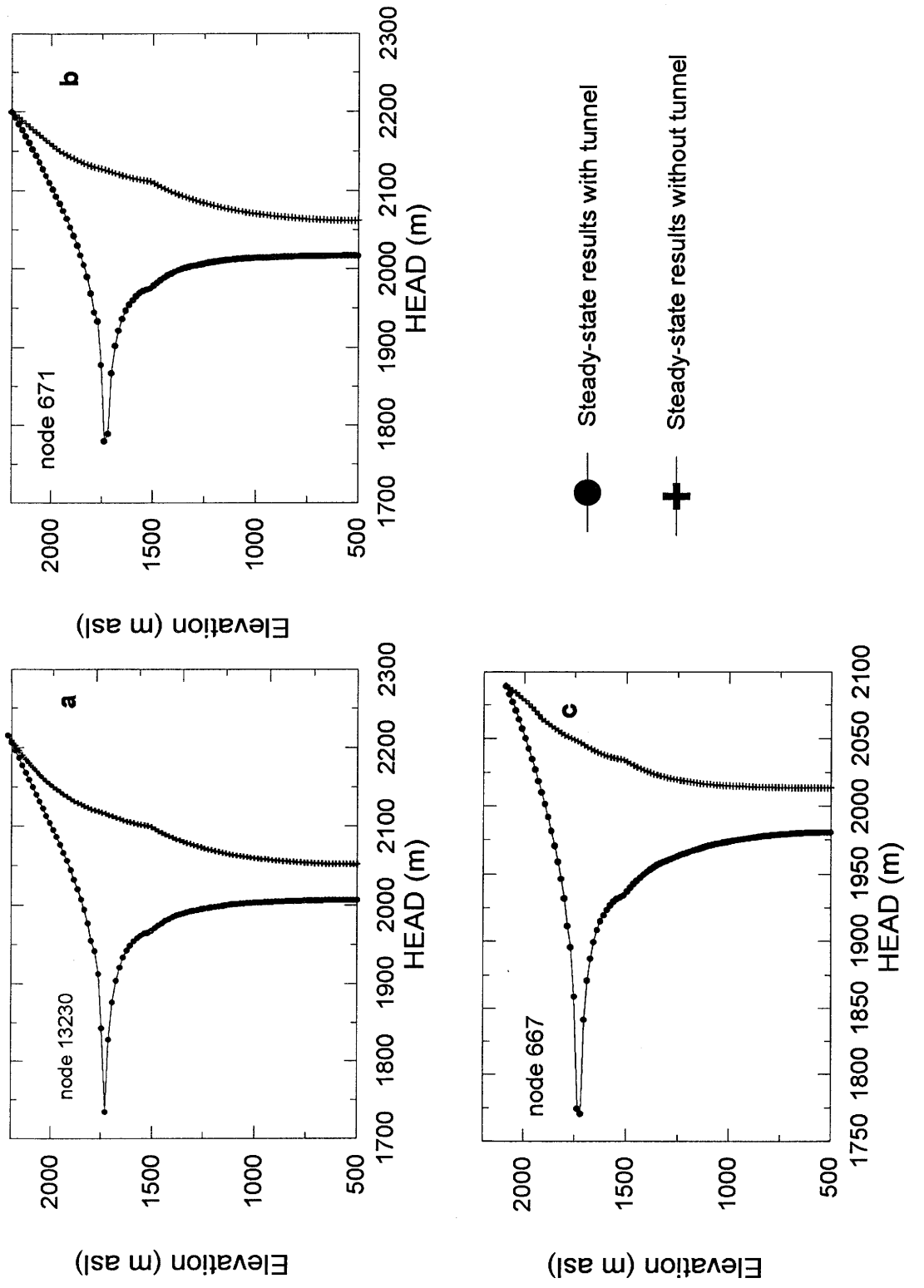

Figure 3.32 Hydraulic head profiles at: (a) node 13230; (b) node 671; and (c) node 667.

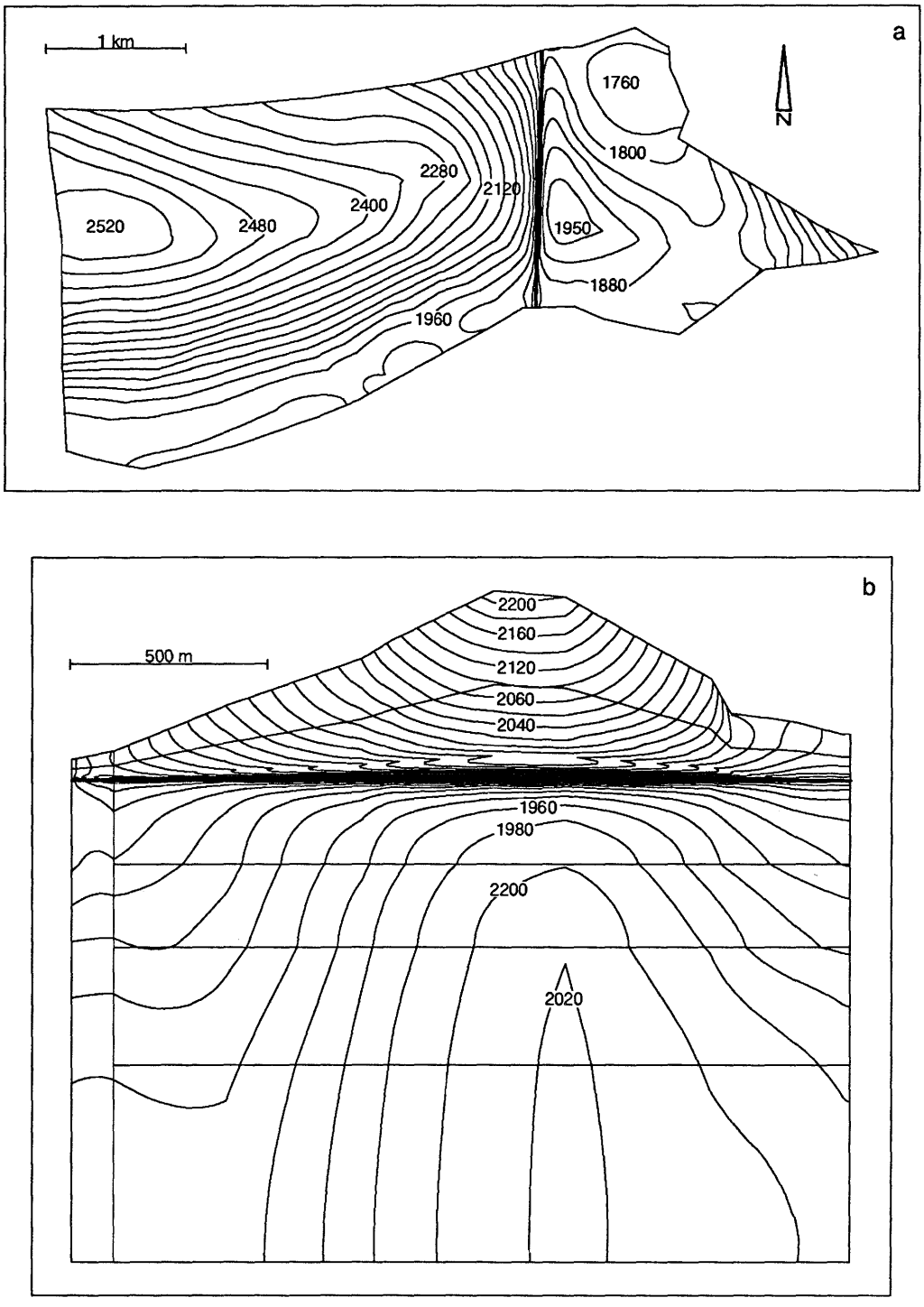

Figure 3.33 Steady-state results with tunnel in 1D for: (a) a horizontal section (top of layer 3); and (b) a vertical section parallel to the tunnel.

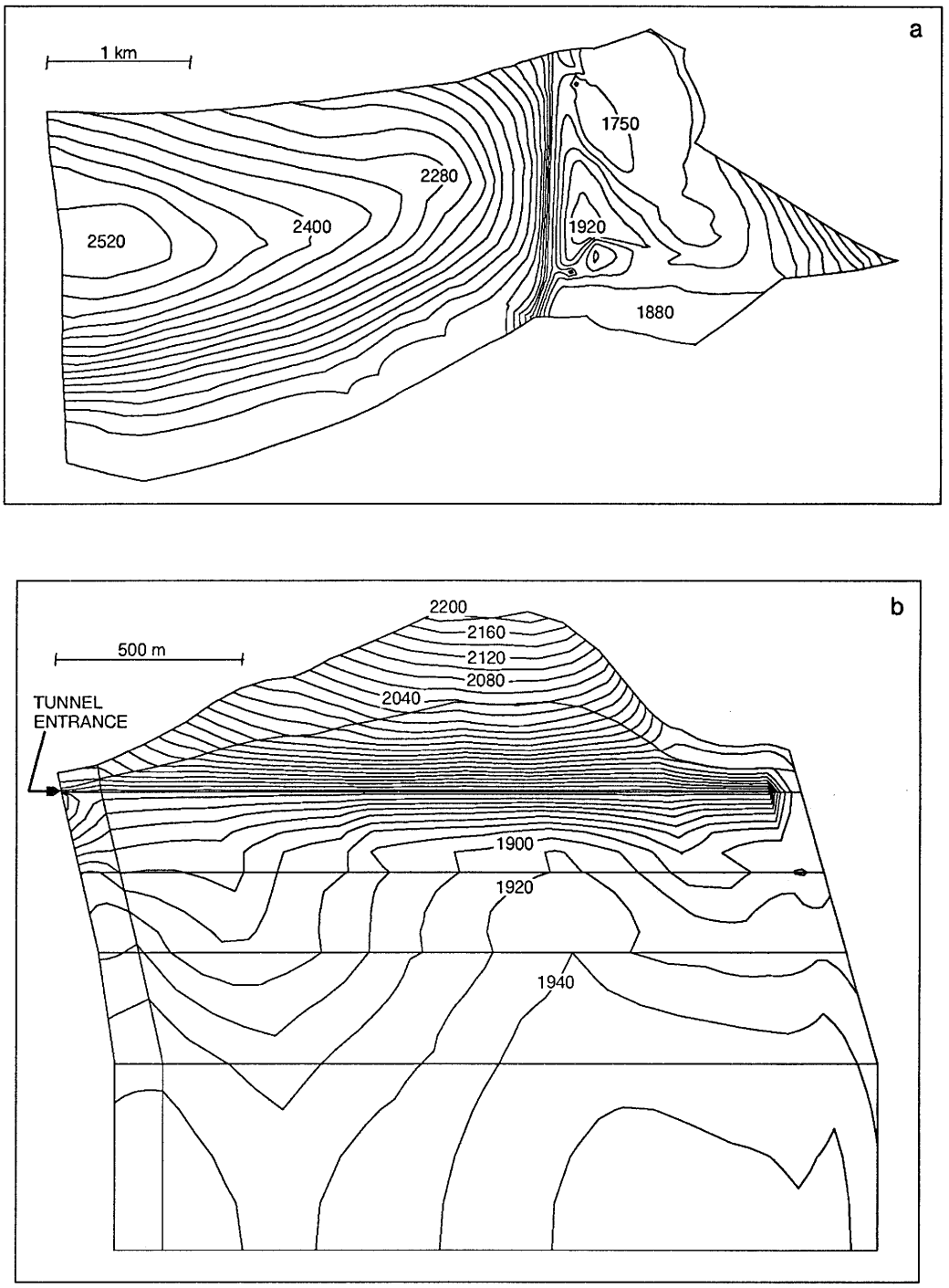

Figure 3.34 Steady-state results with tunnel in 1D for the non-refined SRM for: (a) a horizontal section; and (b) a vertical section parallel to the tunnel (from RIVERA et al., 1993a).

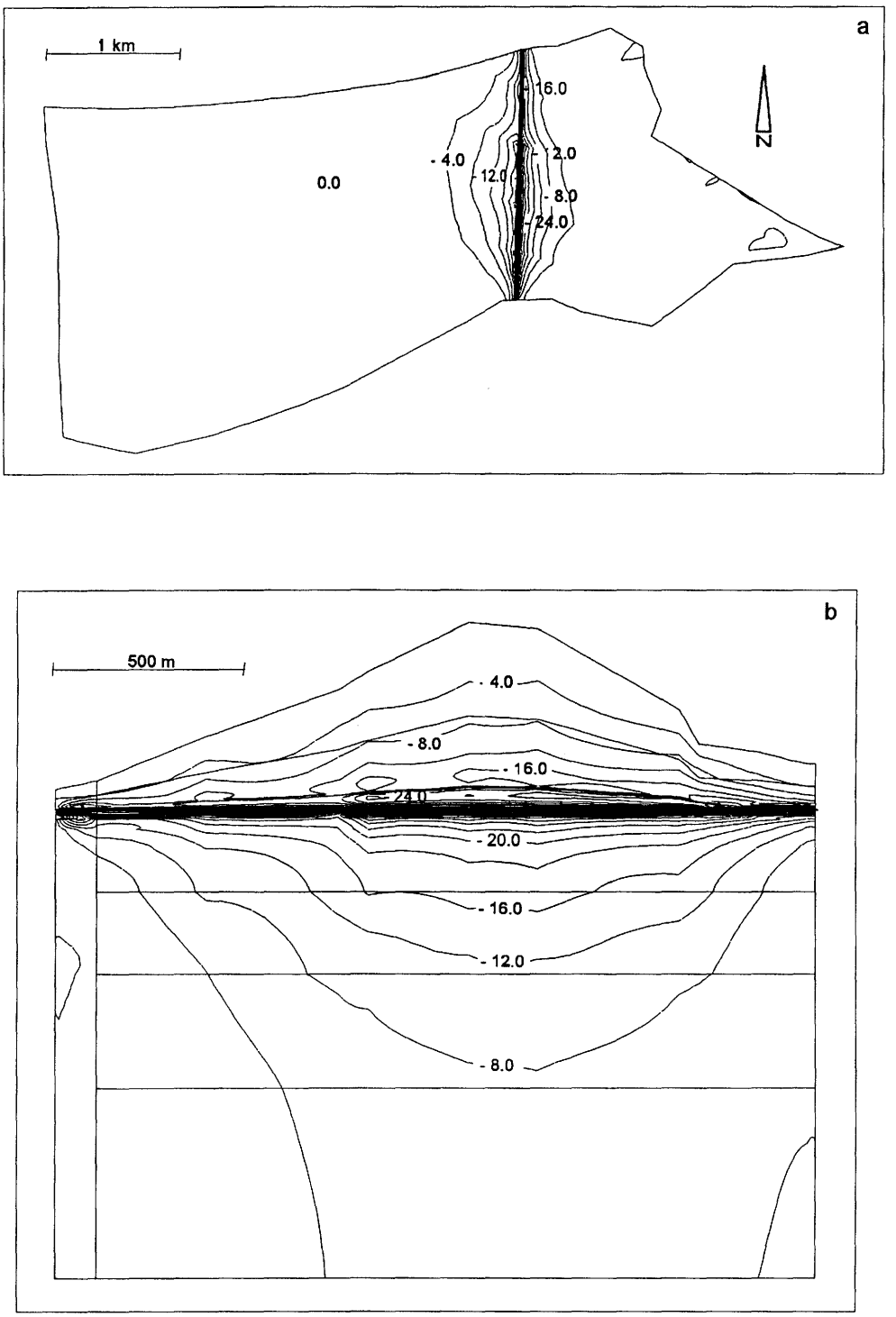

Figure 3.35 Differences in hydraulic heads between the 3D and the 1D tunnel simulations.

3.3.6 Transient simulations with the KWO tunnel

The simulations presented in this Chapter correspond to the base-case conditions, that is, the parameter values and boundary conditions are those of the GTS base case of the SRM which is believed to be the most representative numerical model of this site. All the transient simulations were performed with the numerical code NAMMU.

Parameter values, boundary and initial conditions

The adopted boundary conditions are the ones described in the preceding Chapter; the presence of the tunnel is simulated by prescribing atmospheric pressure at all the nodes located at the walls of the three-dimensional tunnel. Fourteen permeability classes were adapted to the six different layers representing the rock matrix as well as the 2D fracture systems and 1D vertical drains. Table 3.12 presents the conductivity classes with values and associated material units.

Table 3.12: Conductivity classes and hydrogelogical units for the GTS base case

K-Class No.	Hydraulic Conductance		Hydrogeological Unit	Dimension of FE
	K (m/s)	T (m^2/s)		
1	1E-10		Granite matrix-layer 1	3-D
2	5E-11		Granite matrix-layer 2	3-D
3	1E-11		Granite matrix-layer 3	3-D
4	5E-12		Granite matrix-layer 4	3-D
5	1E-12		Granite matrix-layer 5	3-D
6	1E-12		Granite matrix-layer 6	3-D
7	1E-8		Baechlisbach shear zone-layer 1	3-D
8	1E-9		Baechlisbach shear zone-layers 2,3,4,5,6	3-D
9		1E-7	K-system factures	2-D
10		5E-8	K-system fractures	2-D
11		5E-9	S-system fractures	2-D
12	1E-6		Vertical drains	1-D
13	5E-7		Vertical drains	1-D
14	1.0		TUNNEL	2D & 3D

The sections of the 2D fractures crossing the tunnel are attributed a K-class of 14.

In order to be consistent with the NAMMU formulation, the hydraulic conductivities (K) were transformed into rock permeabilities, or *intrinsic permeability* (k), by using the relation $k=K \cdot 10^{-7}$. The permeabilty tensor was considered isotropic and the values presented in Table 3.11 are therefore the same for the three dimensions.

Table 3.13 presents the porosities (ϕ), compressibilities (α), specific storativity coefficients (S_s), and diffusivity ratios (κ) associated with the hydrogeological units of the SRM2.

Table 3.13: Diffusivity values for the GTS base case

UNIT	ϕ	α (Pa^{-1})	S_s (m^{-1})	κ (m^2/s)
Granite matrix-layer 1	0.01	2.3E-11	2.3E-7	4.3E-4
Granite matrix-layer 2	0.01	2.3E-11	2.3E-7	2.1E-4
Granite matrix-layer 3	0.01	2.3E-11	2.3E-7	4.3E-5
Granite matrix-layer 4	0.01	2.3E-11	2.3E-7	2.1E-5
Granite matrix-layer 5	0.01	2.3E-11	2.3E-7	4.3E-6
Granite matrix-layer 6	0.01	2.3E-11	2.3E-7	4.3E-6
Baechlisbach shear zone- layer 1	0.01	2.3E-11	2.3E-7	4.3E-2
Baechlisbach Shear zone- layer 2,3,4,5,6	0.01	2.3E-11	2.3E-7	4.3E-3
K-system fractures	0.01	2.4E-11	2.4E-7	0.41
K-system fractures	0.01	2.4E-11	2.4E-7	0.21
S-system fractures	0.01	2.4E-11	2.4E-7	2.1E-2
Vertical drains	0.01	2E-11	2E-7	5.0
Vertical drains	0.01	2E-11	2E-7	2.5
TUNNEL	1.0	1E-4	1.0	1.0

The initial conditions are those of the three-dimensional steady-state simulation without the tunnel, as presented in section 3.3.5 (Figure 3.28). At time=0, the tunnel is activated in the numerical model and the transient calculation begins.

The transient calculation with NAMMU was done with the Gears' method, using several Newton-Raphson iterations for each time step. The initial control parameters for the numerical simulation were defined as follows:

—Newton-Raphson iterations	3
—Factor for time step increase	1.2
—Initial step size	1E+05 sec
—Final time step	200
—Final time	2.6E+06 sec [30 days]
—Convergence criterion	0.1

Because the duration of the simulations is very large (in the order of 35 to 50 hours), these were carried out by phases in order to provide intermediate results. Therefore, the calculations were separated into five phases as follows:

Phase 1 = 0 - 1 month
phase 2 = 1 month - 1 year
phase 3 = 1 year - 10 years
phase 4 = 10 years - 30 years
phase 5 = 30 years - 630 years

For each phase, the initial time of the simulation was the final time of the preceding phase. All the other transient parameters for the numerical simulations were kept the same. This same procedure is used in all the other simulated cases presented in the following sections.

The initial step size of about one day (1E+5 sec) was selected on the basis of a simple transient analytical calculation as a function of element lengths. A smaller initial time step would only have been realistic if a true time-varying boundary condition (boundary condition of the tunnel) had been adopted.

The time required to dissipate an instantaneous perturbation (change in head) in a groundwater system in one dimension is,

$$t = S_s \cdot x^2 / K \qquad (3.9)$$

where x is the size of the dimension in which the perturbation propagates. A simple calculation with (3.9) in the vertical dimension from the tunnel up, using values from the base case (Tables 3.12 and 3.13), and with a 6 m element length, gives:

$$t = 2.3E\text{-}7 \cdot 36 / 5E\text{-}11 = 1.6E+5 \text{ sec}$$

Thus, for an element length of that size, an initial time step of less than 1.6E+5 sec seems to be adequate.

Since the interest was focused more on the medium- to long-term results, and considering the very costly simulations when very short time steps are used, the time step ranges adopted in all the transient simulations were such that the numerical calculations provided results equilibrated in terms of months rather than days or seconds in the initial phases. Except for the first phase (1 month), all of the transient phases simulated readily converged at the first iteration per time step.

Simulated times, CPU time, disk space, RAM

The transient simulation was designed to last until a new equilibrium (new steady state) condition is reached with the presence of the tunnel. The five different phases, described above covered a total simulated time of 630 years.

The CPU time needed for each phase, the in-core (RAM) and hard disk space, as well as the time steps needed per simulated phase, are given in Table 3.14.

Table 3.14: Summary of computer load for the GTS base case

Simulated time (phases)	CPU time (hrs)	Disk space (Bytes)	RAM size (Mbytes)	Time steps per simulated phase
0 - 1 month 1 m - 1 year 1 y - 10 y 10 y - 30 y 30 y - 630 y	12.95 6.88 5.46 4.26 7.34 Total= 29.07	FOR003= 85'681'024 FOR004= 1'380'464 FOR011= 45'465'600 FOR024= 2'113'933 OUTPUT file= 14'148'270 (5 files) Results FEM301 format= 12'295'590 (17 files) Global freedoms = 8'297'856 (5 files) TOTAL = 169'382'737	47	18 10 9 7 12 Total= 56

Hydraulic heads

Figures 3.36 and 3.37 illustrate the hydraulic head distributions in meters above sea level displayed for horizontal sections at the GTS level (top of layer 3), and for vertical section parallel to the KWO tunnel. In these Figures, the results for the time periods of 1 and 500 years, respectively are plotted.

The heading in each Figure means:

—GTS BASE CASE = describes the present case
—lay3_surf.xyz = describes the coordinate file for the top of layer 3
—lay3_surf.el = describes the element file for the top of layer 3

—cut_vert.xyz =	describes the coordinate file for the vertical cut parallel to the tunnel
—cut_vert.el =	describes the element file for the vertical cut parallel to the tunnel
—1y.res =	describes the time for which the results are plotted

The time needed to re-equilibrate to a new steady-state condition after the pressure field has been disturbed by the presence of the the tunnel was variable. It took from 5 to 10 years for the hydraulic heads to reach a steady-state condition between the tunnel elevation and the top surface, at the level parallel to the location of the tunnel. The westernmost part of the model was actually not very much affected by the presence of the tunnel, given the very high topographic relief which conditioned the infiltration (Juchlistock massif). The effect of the tunnel in that region was "felt" by the pressure field only approximately 1 km west of the tunnel. The eastern part of the tunnel was more affected and it took about 10 to 20 years to reach a steady-state condition.

On the other hand, the vertical head distribution showed that the hydraulic head below the tunnel needs a much longer time to reach a new steady-state condition, i.e., in the order of 300 years or more.

Figures 3.38 and 3.39a show the results through vertical profiles from the top to the bottom of the model for the three selected vertical sections as shown in Figure 3.31 From these, it can be seen that the heads below the tunnel elevation take longer to re-equilibrate to the steady-state condition with the tunnel.

Finally, Figures 3.38b to 3.40b show the span of the simulated time at single points, with the head evolution plotted against time at approximately 25 m, 75 m, and 150 m distances from the tunnel. The selected points are located around the tunnel, above, below, east, and west at the distances shown in the Figures. These Figures show that it takes about 20 years for the 25 m-distant nodes to reach equilibrium, about 30 years for the 75 m-distant nodes and 25 to 70 years for the 150 m-distant nodes.

Simulated volumetric fluxes

An important part of this modeling work was the calculation of volumetric fluxes drained by the tunnel as a function of time.

The present sub-regional model calculations aimed more at understanding and establishing know-how in terms of the general hydraulic behaviour under transient conditions with the presence of a tunnel in a three-dimensional complex model. Therefore, no attempt was made here to calibrate the model with measured inflows into the tunnel. Thus, the calculated volumetric fluxes as

shown here come directly from the first results of the model without any changes.

In Figure 3.41 the total calculated fluxes drained by the tunnel through the rock matrix and fractures are plotted. As expected, most of the fluxes come from the fractures, i.e., 88 %. After the first year, the total flux decreases from 3.23 l/min to about 2.4 l/min; at 10 years it is 2.25 l/min. It continues decreasing at a very low rate up to 100 years when it reaches 2.2 l/min. After that time the total flux remains almost unchanged - it has reached a steady-state condition, given the boundaries and the hydraulic parameters of the model.

Comparison with measurements

The magnitude of the volumetric fluxes actually drained by the tunnel, and their evolution with time, are given in CHALMERS and CORREA (1993). In Figure 3.19 (§ 3.3.1.2), modified from these authors, the partial fluxes measured along the KWO tunnel are given. According to the authors, these measurements were taken along the main KWO tunnel and are presented in the Figure for the year 1987.

The measured total fluxes along the KWO tunnel accounted for about 18 l/min in 1987, that is approximately 13 years after the construction of the KWO tunnel began in 1974. Quantitatively, the present calculations are out by a factor of 6. However, qualitatively, the 3D transient simulation showed that the area with the highest flux drained is located at approximately the same location as where the highest fluxes were measured, i.e., approximately 1600 m south of the main access to the tunnel, (described as "tm2076" in CHALMERS and CORREA (1993); see Figure 3.19).

The transient numerical calculation suggests that the sum of the observed fluxes in the KWO tunnel, as for 1987, was about 70 % of the maximum initial condition. This means that if the same conditions prevail for a very long period of time, the fluxes will continue dropping at a very low rate for 80 more years until they reached equilibrium. Of course this statement is based on the assumptions under which the model was constructed (boundary conditions and hydraulic parameters adopted).

The present sub-regional numerical model is suitable for calibration, i.e., the sum of the measured fluxes could be reproduced with additional runs of model calibration. Chapter 5 presents an inverse modeling approach to calibrating the SRM with fluxes from the KWO tunnel.

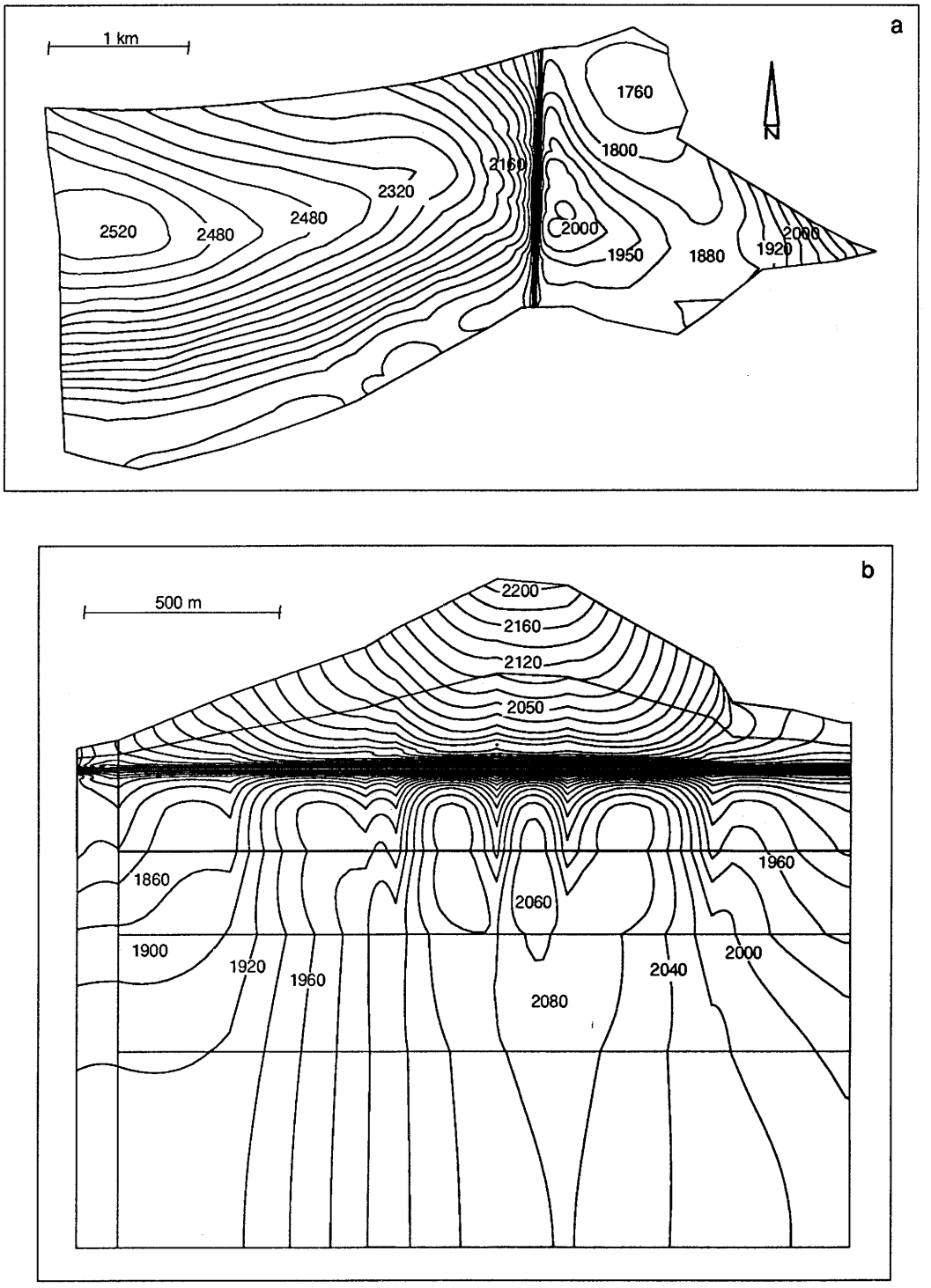

Figure 3.36 Transient results with tunnel at t= 1 year for: (a) a horizontal section; and (b) a vertical section parallel to the tunnel. GTS base case.

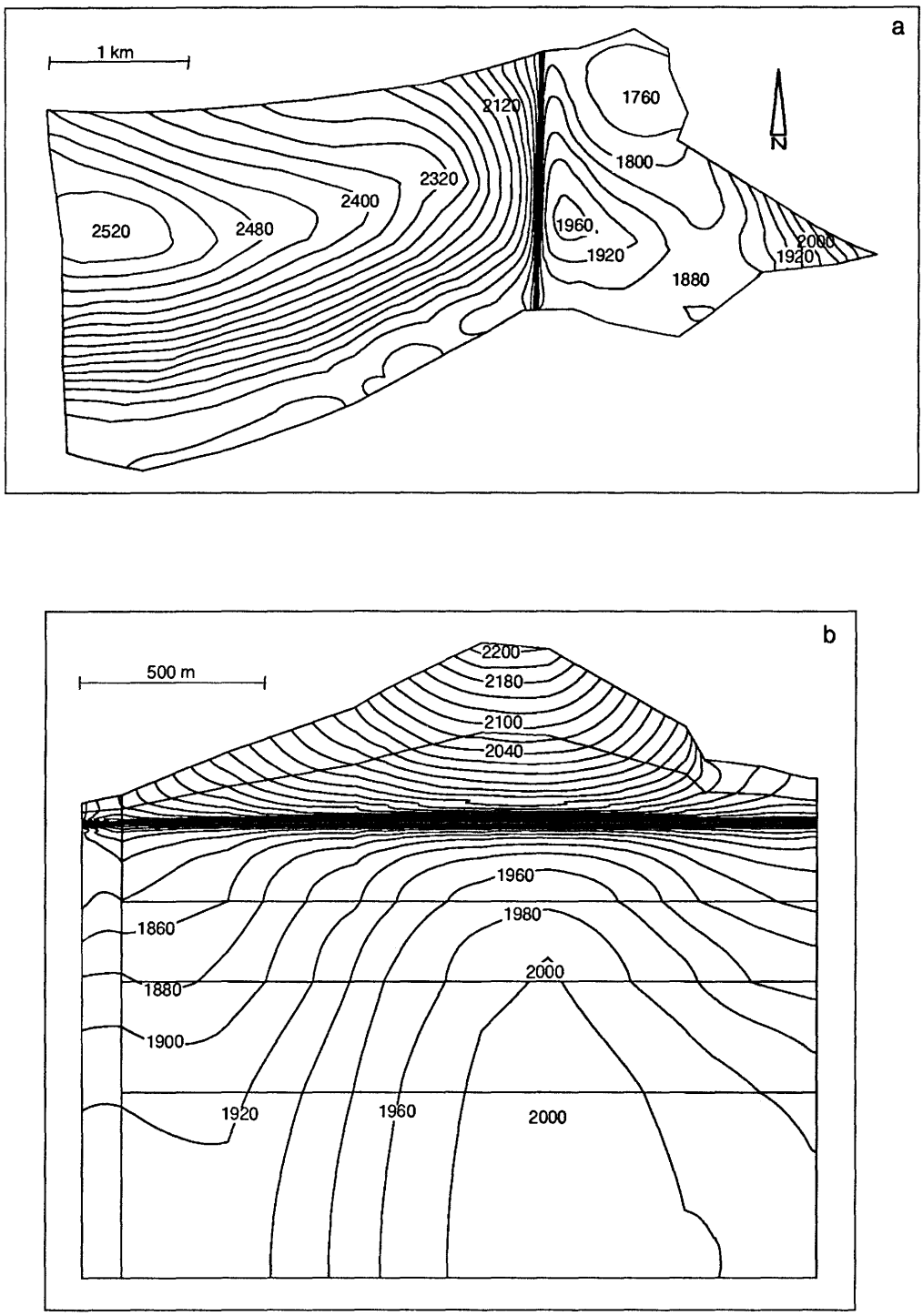

Figure 3.37 Transient results with tunnel at t=500 years for: (a) a horizontal section; and (b) a vertical section parallel to the tunnel. GTS base case.

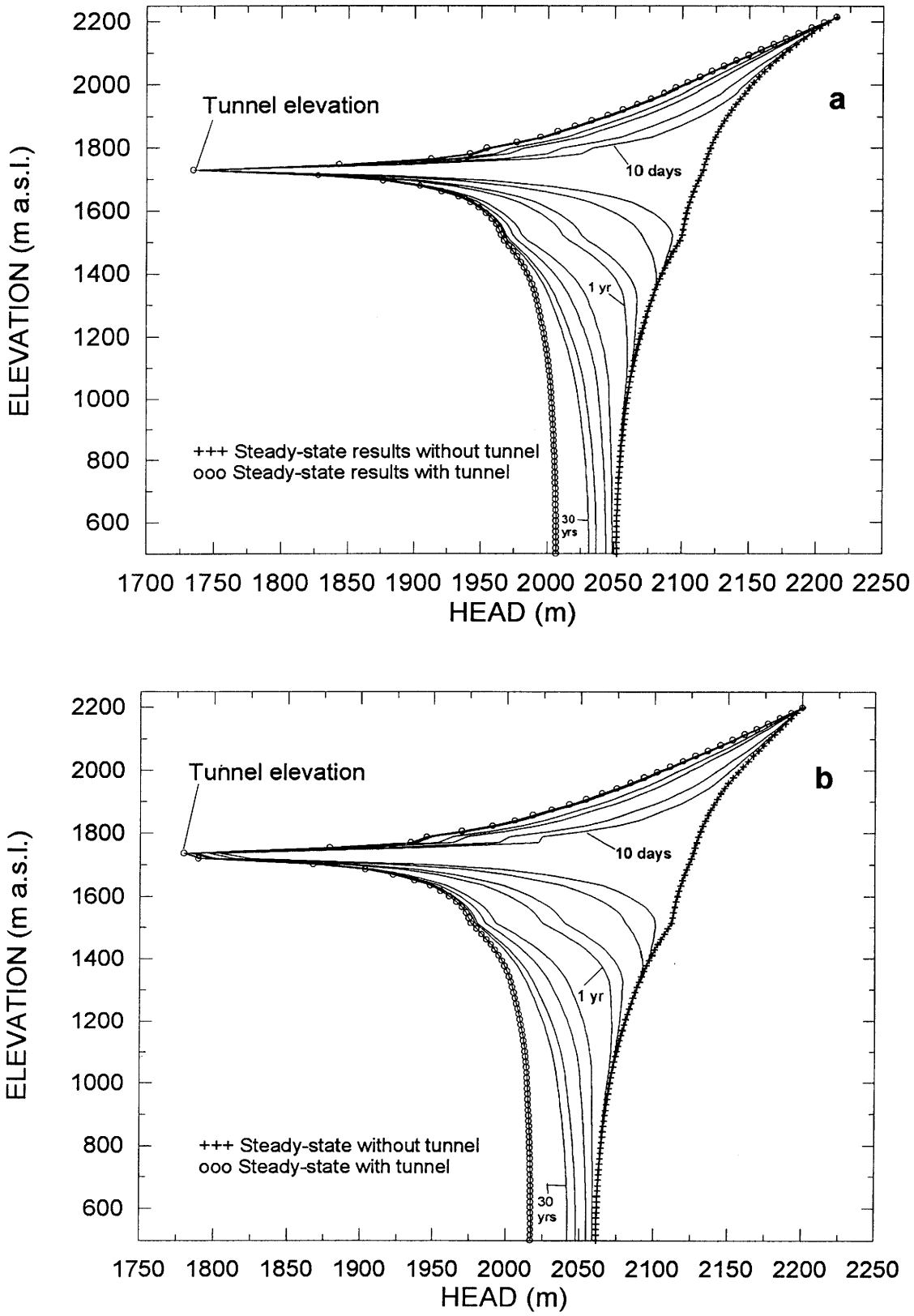

Figure 3.38 Evolution of hydraulic head with time for a selected profiles from top to bottom: (a) node 13230; (b) node 671. GTS base case.

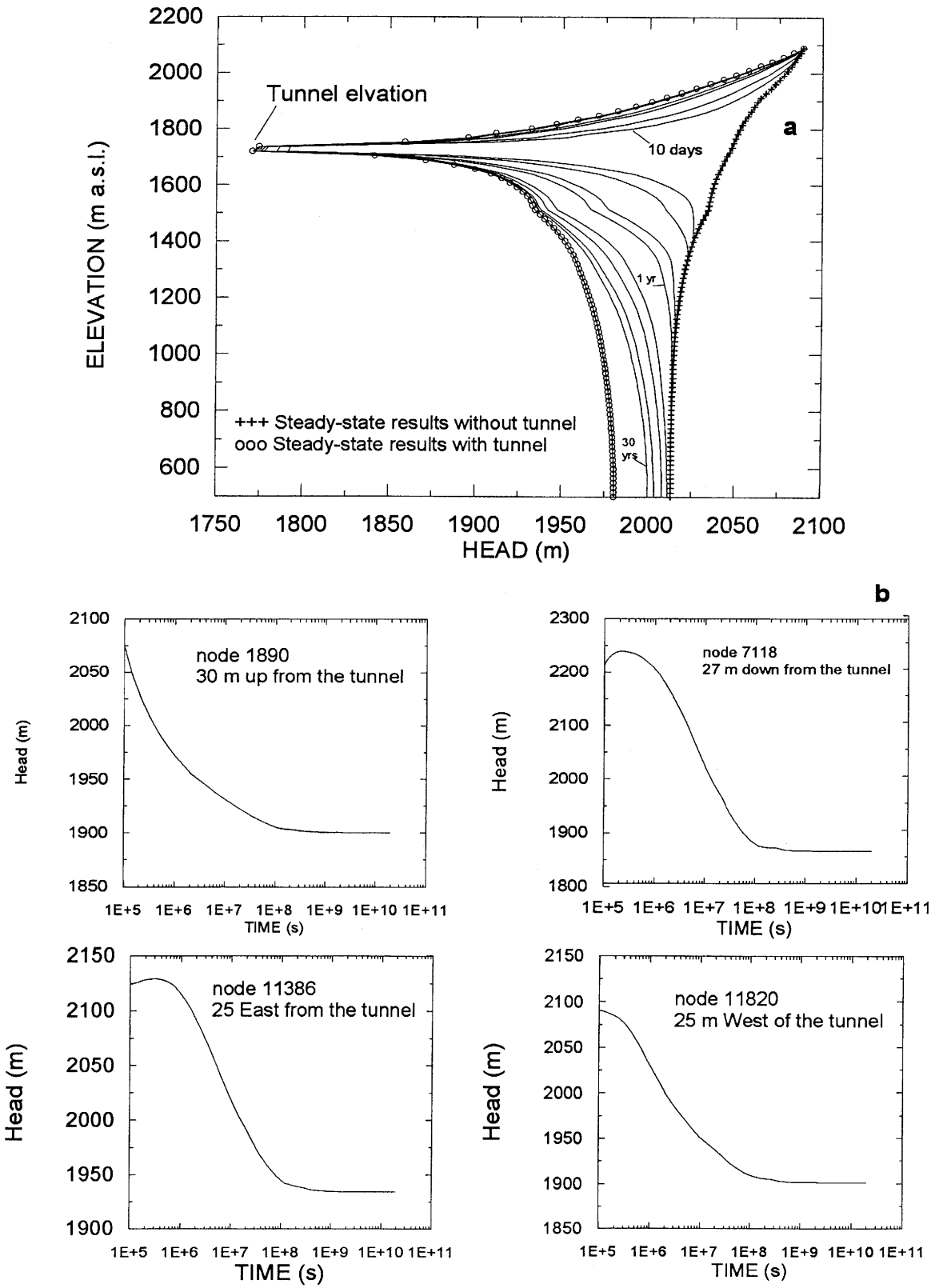

Figure 3.39 Evolution of hydraulic head with time for: (a) vertical profile from top to bottom; node 667; (b) selected points about 25 m from the tunnel. GTS base case.

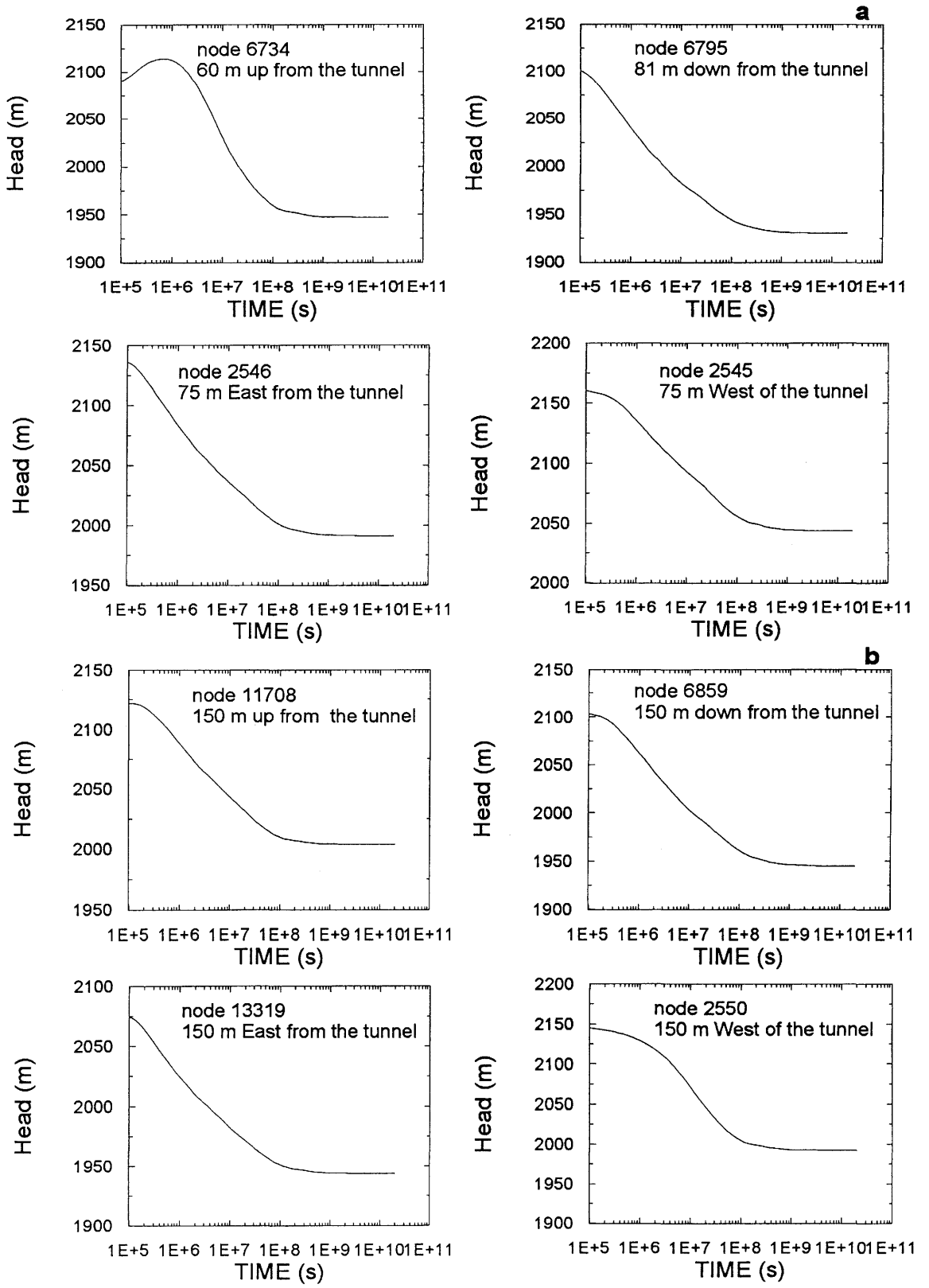

Figure 3.40 Evolution of hydraulic head with time for selected points about: (a) 75 m and (b) 150 m from the tunnel. GTS base case.

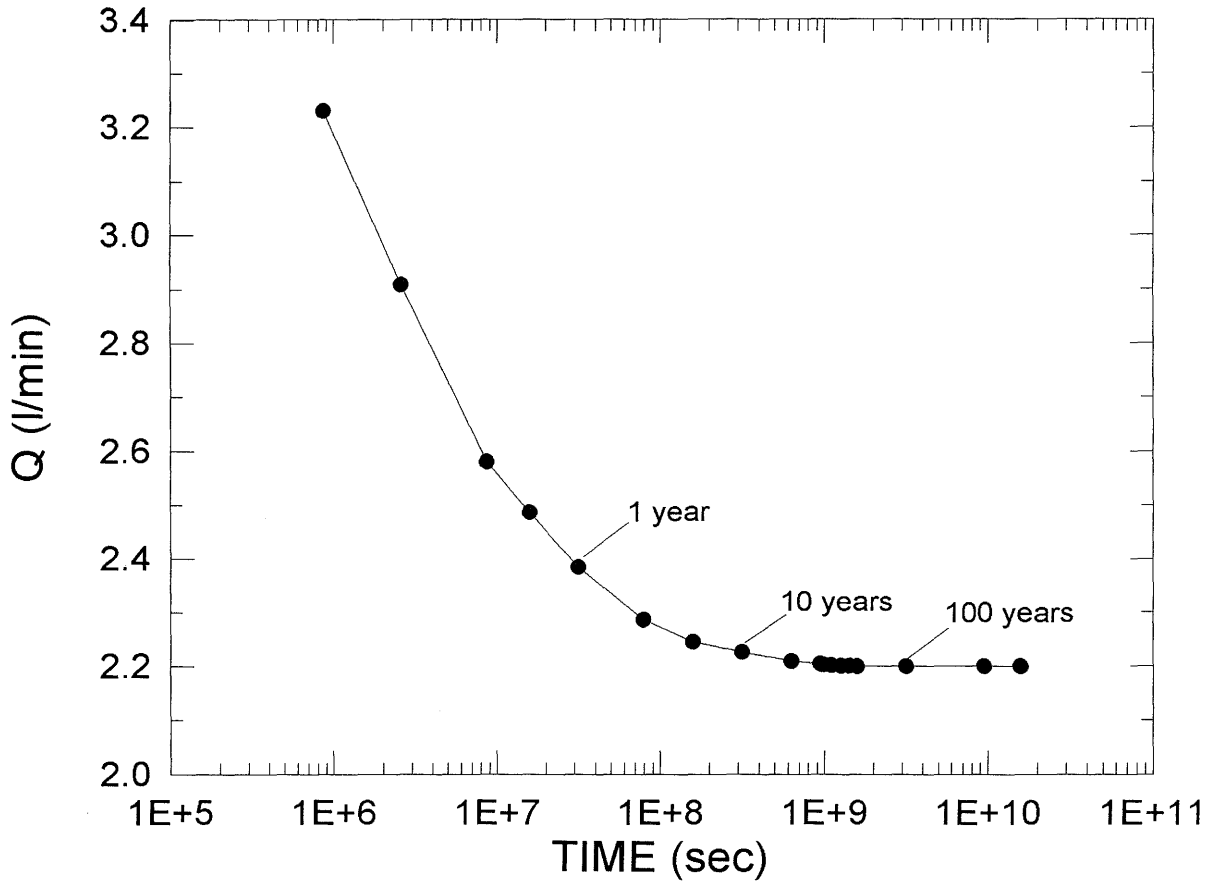

Figure 3.41 Total volumetric fluxes drained by the tunnel for the GTS base case.

3.3.7 Simulation of a fictitious repository

The simulations presented in this Chapter are designed to mimic, from a hydraulic perspective, a site containing a fictitious repository. The sub-regional GTS model (SRM2) was used for these 3D simulations. Figure 3.25a shows the location of the SRM within the GTS regional model RM (see also Chapter 2).

Selection of a section of the tunnel

In order to imitate the presence of a repository, a central section of the KWO 3D tunnel was selected. This section should not include fractures in a 150-m distance. The fractures located at 150-m distance or less from the selected section have been "sealed" for a length of about 150 m around the center of the tunnel. This could be accomplished simply by changing parameter values in the fractures present in the selected section.

Figure 3.42 presents all the elements (2D and 3D) located up to a distance of 150 m around the tunnel. The selected section (roughly at the center of the tunnel) is shown in Figure 3.43 with the corresponding sealed 2D fractures. The tunnel is shown by the horizontal lines colored in green.

Parameter values, boundary and initial conditions

The boundary conditions for the SRM2 are the same as for the base case (§3.3.6). The initial conditions are the three-dimensional steady-state simulation without the tunnel, as presented in subsection 3.3.5. At time=0 the tunnel is activated in the numerical model and the transient calculation begins.

The conductivity values of the 2D fractures shown in Figure 3.43 originally were: 1E-7, 5E-9 and 5E-8 m/s, which correspond to K classes 9, 10 and 11, respectively. The conductivity values for these fractures in the present simulation were changed to 1E-10 m/s, which correspond to the rock matrix conductivity of layer 1, K class 1 in the model (see Table 3.11). The compressibility and specific storativity values were changed to those of the same K class 1. Therefore, the hydraulic diffusivities of these fractures were decreased by 2 to 3 orders of magnitude (see Table 3.12).

Simulation results

Simulated times, CPU time, disk space, and RAM

The initial control parameters for NAMMU were designed as follows:

— Newton-Raphson iterations	3
— Factor for time step increase	1.2
— Initial step size	1E+05 sec

— Final time step	200
— Final time	2.6E+06 sec [30 days]
— Convergence criterion	0.1

The complete transient simulation was carried out by phases in order to provide intermediate results. The calculations were separated into five phases, as follows:

Phase 1 = 0 - 1 month
phase 2 = 1 month - 1 year
phase 3 = 1 year - 10 years
phase 4 = 10 years - 100 years
phase 5 = 100 years - 630 years

The CPU time needed for each phase, the in-core (RAM) and hard disk space, as well as the time steps needed per simulated phase, are given in Table 3.15.

Table 3.15: Summary of computer load for the hypothetical repository case

Simulated Time (phases)	CPU time (Hrs)	Disk Space (Bytes)	RAM size (Mbytes)	Time step per simulated phase
0 - 1 month 1 m - 1 year 1 y - 10 y 10 y - 30 y 30 y - 630 y	13.1 5.60 5.32 3.52 7.63 Total= 35.17	FOR003= 85'681'024 FOR004= 1'380'464 FOR011= 45'465'600 FOR024= 2'113'933 OUTPUT file= 14'168'512 (5 files) Results FEM301 format= 8'670'084 (12 files) Global freedoms= 9'172'942 (5 files) TOTAL = 166'652'559	46	18 9 9 6 11 Total= 53

Simulated Hydraulic heads

In this case, it took from 5 to 10 years for the hydraulic heads to reach a steady-state condition between the tunnel elevation and the top surface at the level parallel to the location of the tunnel. The western part of the model was affected by the presence of the tunnel only at the center, where the "sealed" 2D fractures are located, as shown in the results plotted for 1 and 500 years in Figures 3.44 and 3.45, respectively[2].

[2] A more complete series of 3D transient results are given in RIVERA et al. (1993a).

The vertical head distribution showed that the hydraulic head below the tunnel needs a much longer time to reach a new steady-state condition, i.e., in the order of 500 years or more. In the Figures of vertical cuts parallel to the tunnel, the hydraulic head distribution is clearly marked by the zone of the 2D fractures around the hypothetical repository; there is a clear part above and below the tunnel, where vertical cones of depression are formed. While in the area above the tunnel, the heads reach equilibrium in a relatively short period of time, it takes a much longer time, about 500 years, for the one below the tunnel to reach equilibrium with the tunnel open.

The heading in each of these Figures means:

—POT-REP CASE =	describes this case of an imaginary repository
—lay3_surf.xyz =	describes the coordinate file for the top of layer 3
—lay3_surf.el =	describes the element file for the top of layer 3
—cut_vert.xyz =	describes the coordinate file for the vertical cut parallel to the tunnel
—cut_vert.el =	describes the element file for the vertical cut parallel to the tunnel
—1y.res =	describes the time for which the results are plotted

Figures 3.46 and 3.47a show the results with vertical profiles, through the tunnel from the top to the bottom of the model, for three selected vertical sections approximately at the center of the KWO tunnel. From these, it can be seen that, after 30 years, the heads below the tunnel elevation have not yet reached a steady-state condition, while those above the tunnel reached equilibrium after 5 years.

In Figures 3.46 and 3.47a the results for early times are not very good because of the time discretization and the initial condition of sudden perturbation of the pressure field (i.e., presence of the tunnel). In NAMMU, the numerical solver had to adapt the given initial step size of 1E+5 seconds, until it is stable. On the other hand, starting with smaller initial step sizes does not make sense because of the prescribed initial condition of the tunnel. However, the results for medium to long-term times (months to years) are considered to be plausible.

Simulated volumetric fluxes

In Figure 3.47b the total calculated fluxes through the rock matrix and fractures as a function of time are plotted. In this case 72 % of the volumetric fluxes come from the fractures. After the first year the total flux decreases from 1.82 l/min to about 1.35 l/min; at 10 years it is 1.269 l/min. It continues decreasing at a very low rate; at 100 years it reaches 1.259 l/min, at 500 years it is at 1.258 l/min and is thus practically unchanged, i.e., it has reached a steady-state condition, for the adopted boundaries and hydraulic parameters in the numerical model.

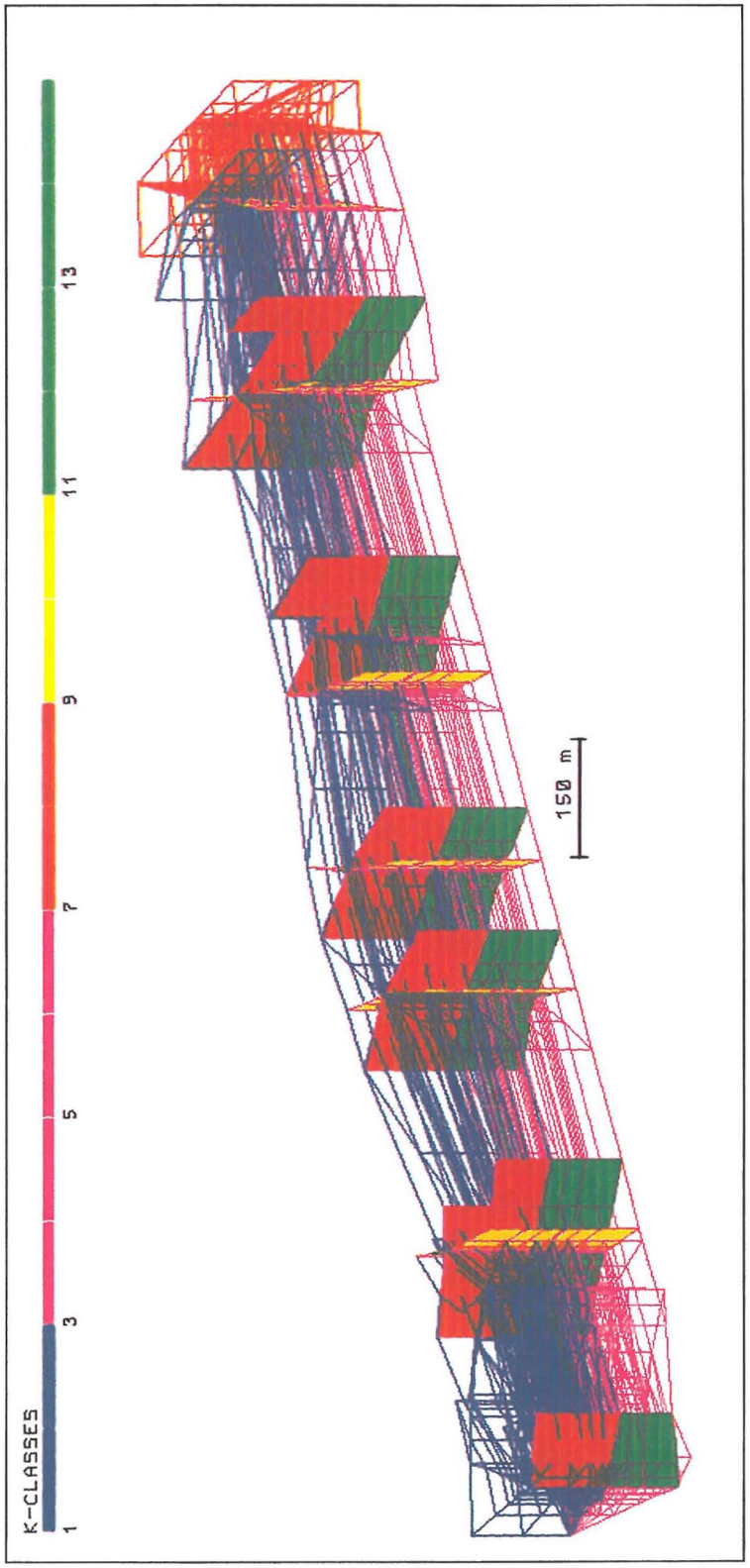

Figure 3.42 2D and 3D elements up to 150-m distance around the discretized KWO tunnel.

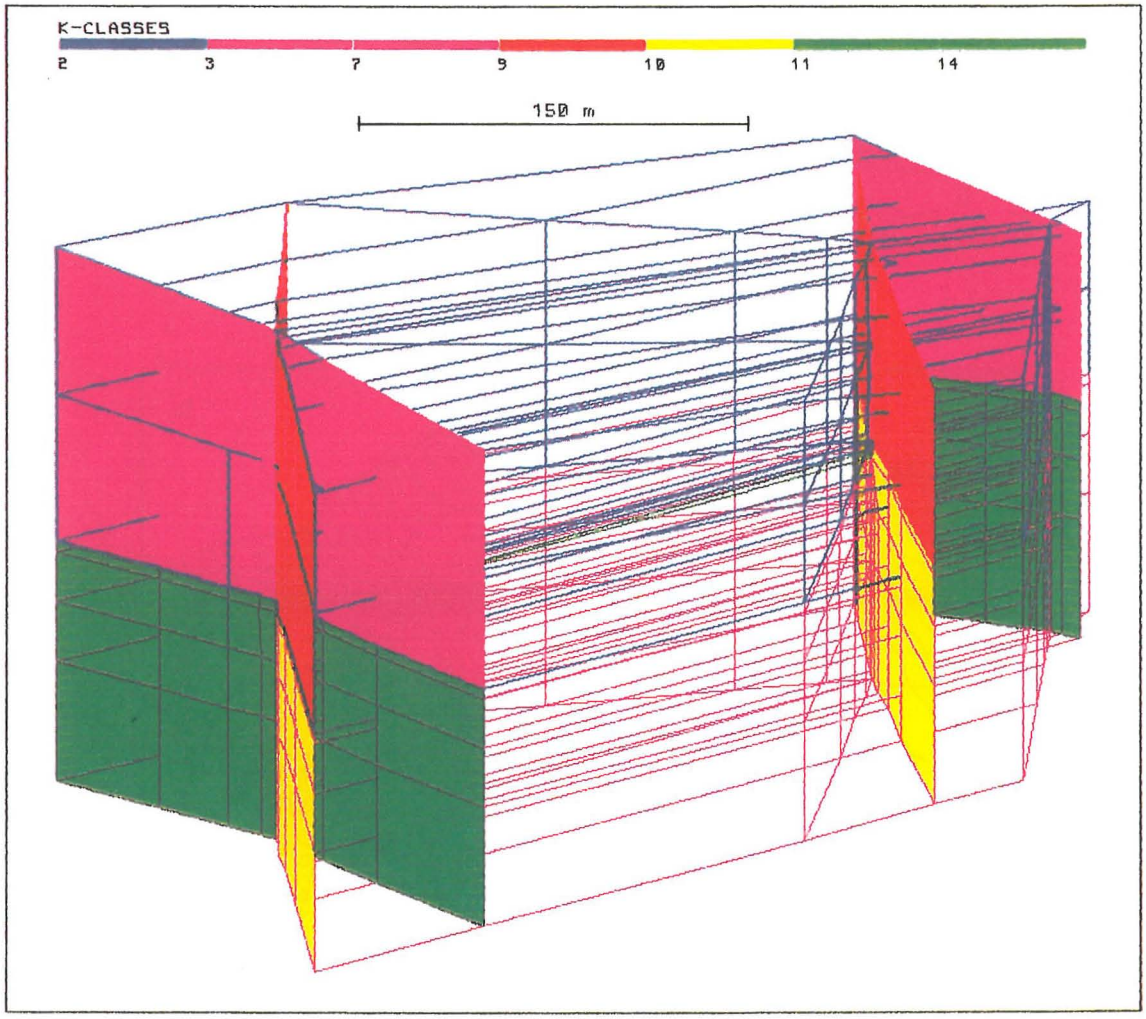

Figure 3.43 Selected section at the center of the tunnel to mimic the hypothetical repository location; the parallel planes are the nearest (sealed) fractures (2D features) to the section.

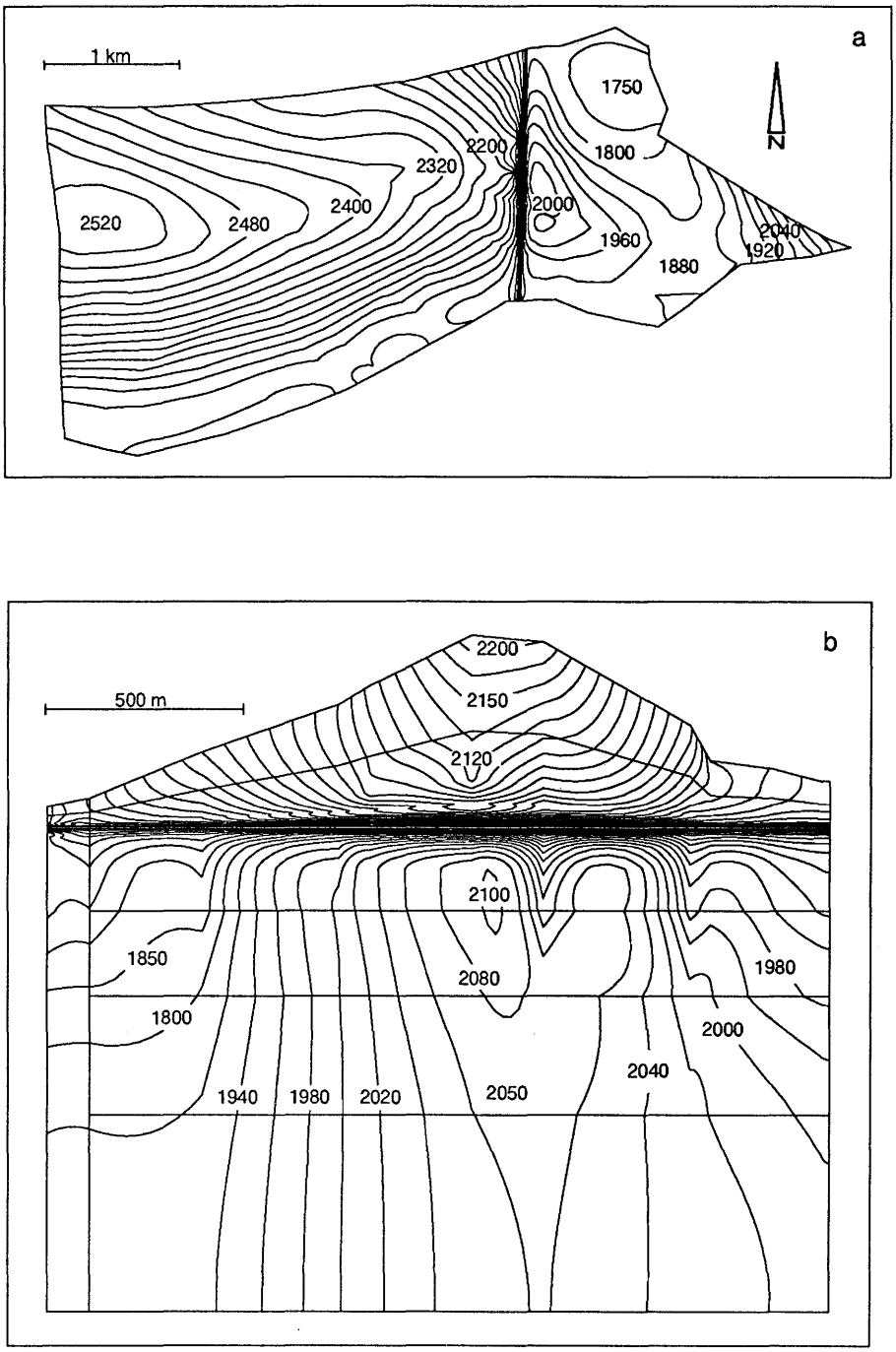

Figure 3.44 Transient results at t= 1 year for: (a) a horizontal section and (b) a vertical section parallel to the tunnel. POT-REP case.

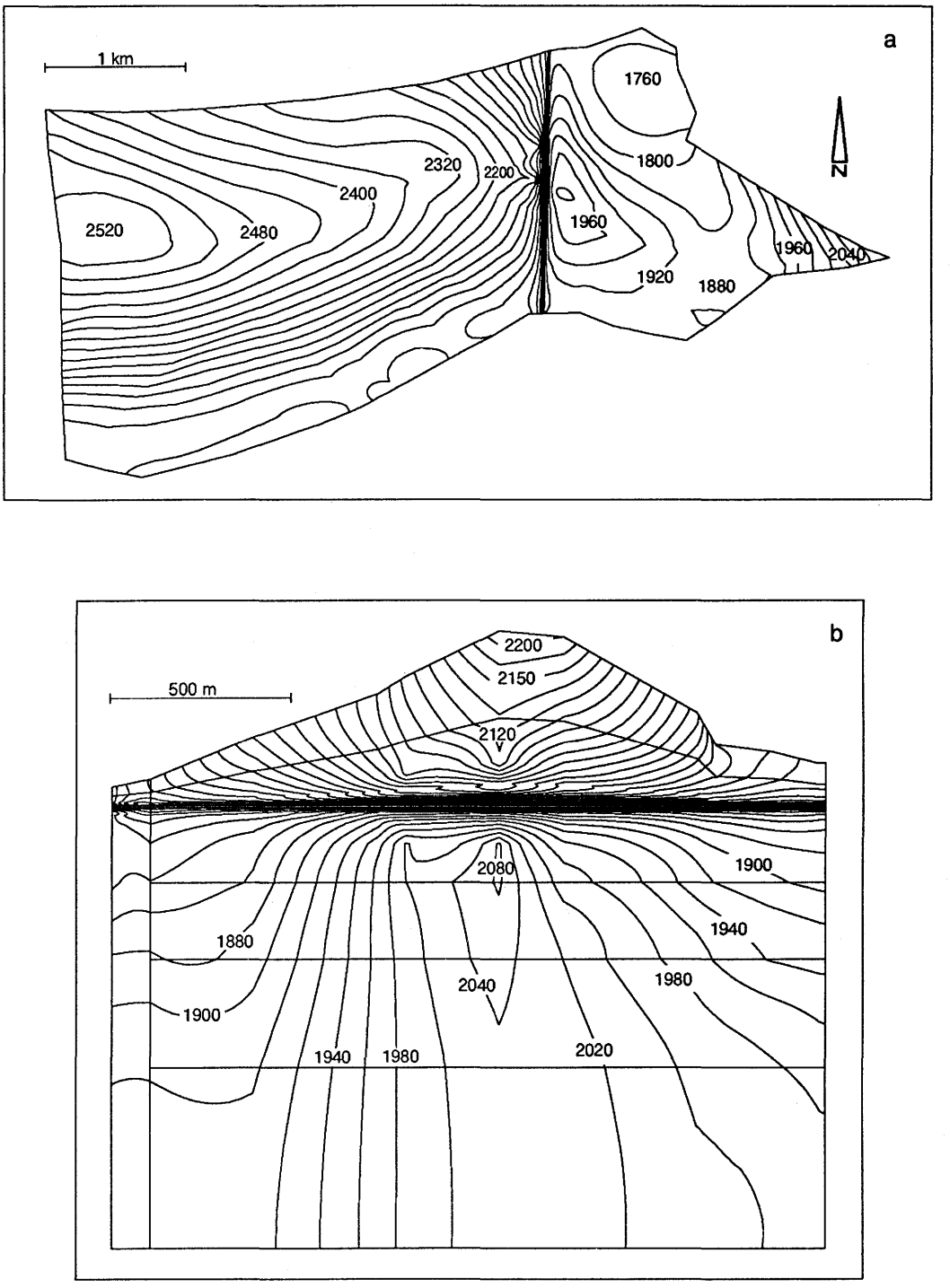

Figure 3.45 Transient results at t= 500 years for: (a) a horizontal section and (b) a vertical section parallel to the tunnel. POT-REP case.

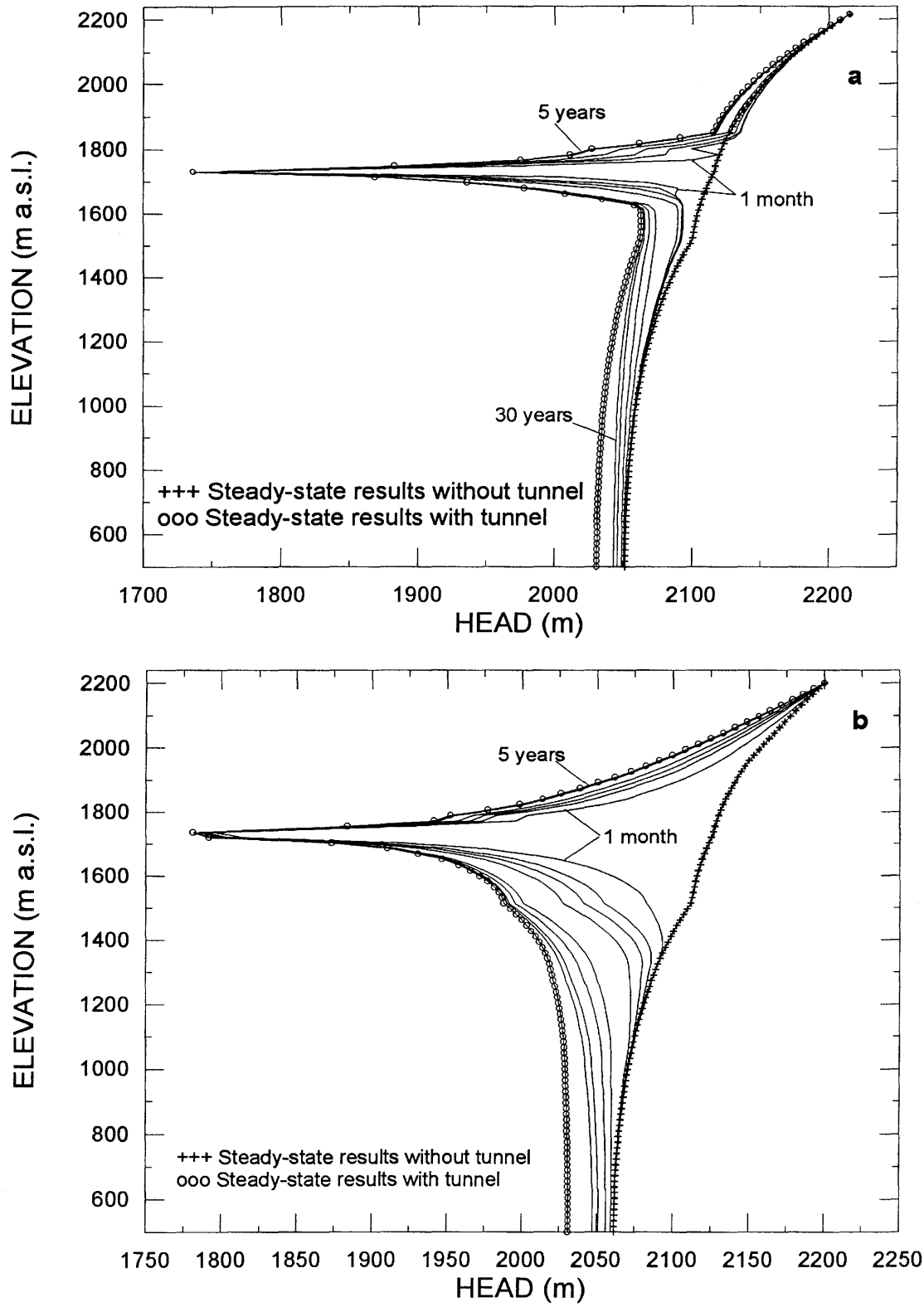

Figure 3.46 Evolution of the hydraulic head with time for a selected vertical profile from top to bottom: (a) node 13230; (b) node 671. POT-REP case.

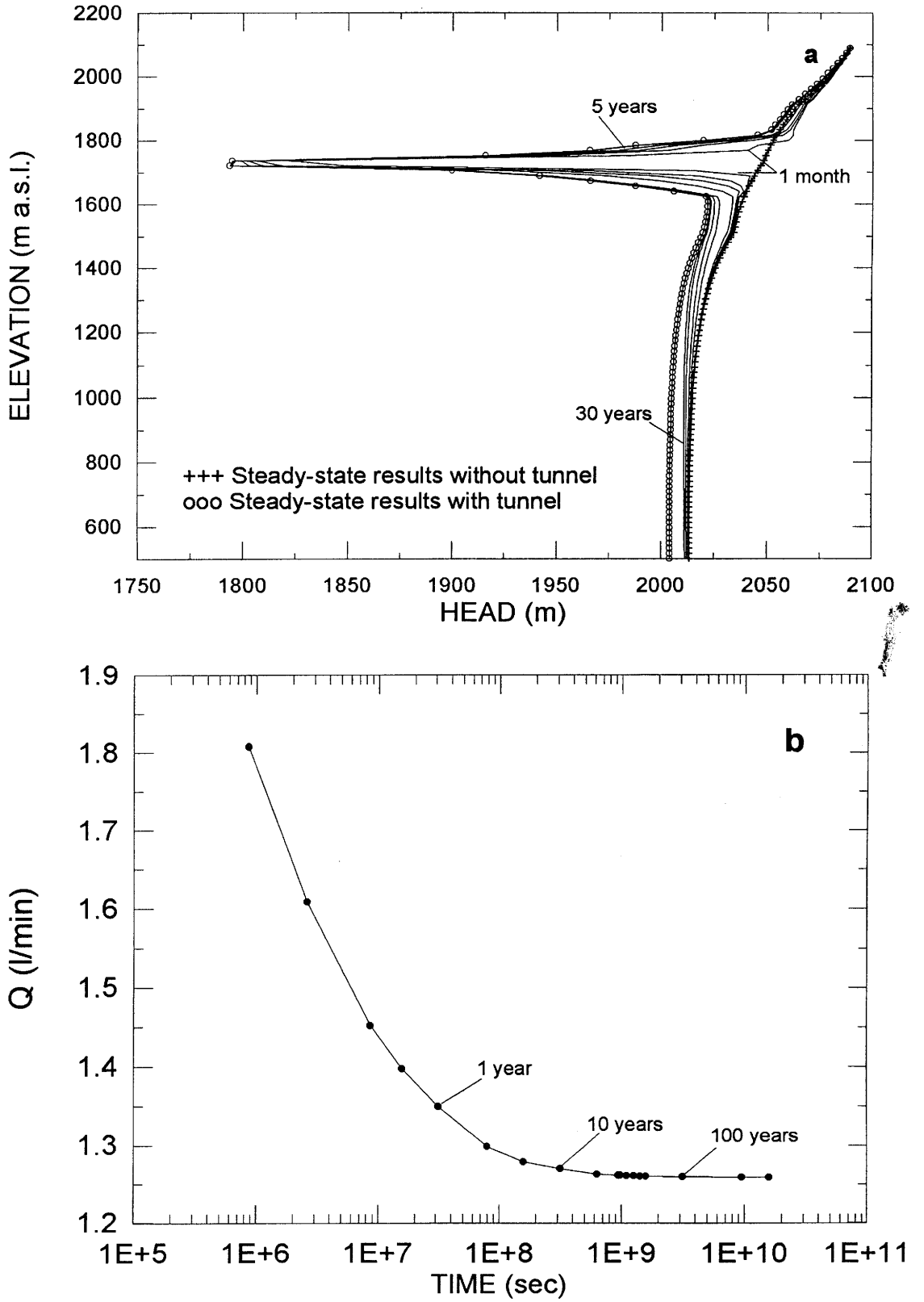

Figure 3.47 (a) Evolution of the hydraulic head with time for a selected vertical profile from top to bottom; node 667; (b) Total volumetric fluxes drained by the tunnel. POT-REP case.

3.3.8 Opening, operation and closure of the fictitious repository

As in the previous subsection, this simulation considers the SRM2 as a fictitious repository site. In this case, however, the transient effects due to the opening, "operation" and closure of such a repository are numerically investigated. Thus, the selected section in the KWO model is simulated, first, for a period of 30 years, representing the "operation" of the fictitious repository; second, the latter is then turned off to simulate its closure, and the transient effects are simulated over a long period of time until the system reaches hydraulic equilibrium.

Parameter values, boundary and initial conditions

The boundary conditions considered in section 3.3.7 remained the same for this case; the initial condition is the transient result at time= 30 years. At this time the tunnel is closed by taking out the boundary condition of atmospheric pressure at its walls. The simulation is carried out in a transient state but with the tunnel being sealed.

The hydraulic parameter values for the fractures around the selected section, and the rest of the material in the model, as defined in section 3.3.7, were not modified. The material with which the tunnel is backfilled up after its closure was simulated with a hydraulic conductivity of 1E-11 m/s, a porosity of 0.1 and a compressibility of 1E-7 Pa^{-1}. The combination of these parameter values results in a diffusivity of 1E-8 m^2/s inside of the backfilled tunnel.

Simulation results

Simulated times, CPU time, disk space, and RAM

The initial control parameters were as follows

—Newton-Raphson iterations	3
—Factor for time step increase	1.2
—Initial step size	1E+05 sec
—Final time step	200
—Initial time	9.5E+08 sec [30 years]
—Final time	2.E+10 sec [630 years]
—Convergence criterion	0.1

Since this case is an extension of the fictitious repository case described in section 3.3.7, only one phase was carried out, from 30 years to 630 years, to complete the transient simulation of the post-closure of the tunnel.

The CPU time needed for this phase, the in-core (RAM) and hard disk space, as well as the time steps needed per simulated phase, are given in Table 3.16.

Table 3.16: Computer load for the operation and closure of the fictitious-repository case

Simulated Time (phases)	CPU time (Hrs)	Disk Space (Bytes)	RAM size (Mbytes)	Time step per simulated phase
0 - 1 month 1 m - 1 year 1 y - 10 y 10 y - 30 y 30 y - 630 y	13.1 5.60 5.32 3.52 27.0 Total= 54.53	FOR003= 85'681'024 FOR004= 1'373'548 FOR011= 47'104'000 FOR024= 2'062'460 OUTPUT file= 14'341'084 (5 files) Results FEM301 format= 14'465'400 (20 files) Global freedoms= 12'446'648 (5 files) TOTAL = 189'920'884	46	18 9 9 6 42 Total= 84

Because the post-closure transient simulation was carried out in one single numerical phase, the total number of time steps increased substantially. The CPU time needed also increased considerably. One of the reasons for this, is the fact that the Gears' method (in NAMMU) used to solve the transient case had to re-adapt the length of the time steps to avoid convergence problems (this is done automatically in NAMMU). Figure 3.48 is a plot of the time steps against the lenght of the time steps in seconds, from 30 years to 630 years.

Simulated Hydraulic heads

Figures 3.49 and 3.50a show the results for vertical profiles through the tunnel, from the top to the bottom of the model, in the same selected vertical sections displayed in previous Chapters. From these, it can be seen that, after the closure of the tunnel, it takes about 70 years for the hydraulic head to recover to a steady-state condition above the tunnel location (400 to 500 m). Below the tunnel and down to the bottom of the model, the hydraulic heads reach equilibrium about 200 years later.

The head recovery is clearly seen at single points where the head evolution is plotted against time at about 25 m, 75 m, and 150 m distance from the tunnel, above, below, to the east and to the west. Figures 3.50b to 3.51 present these plots. At all these distances, the time needed for full recovery of the hydraulic head is about 65 to 70 years after the tunnel was closed.

Simulated volumetric fluxes

Figure 3.52 displays the total calculated fluxes through rock matrix and

fractures to the sealed tunnel as a function of time. After the closure of the tunnel, $t=30$ years in the Figure, the fluxes drop abruptly from 1.25 l/min to 0.04 l/min in about 70 years, i.e., $t=100$ years in the Figure. They remain practically unchanged thereafter.

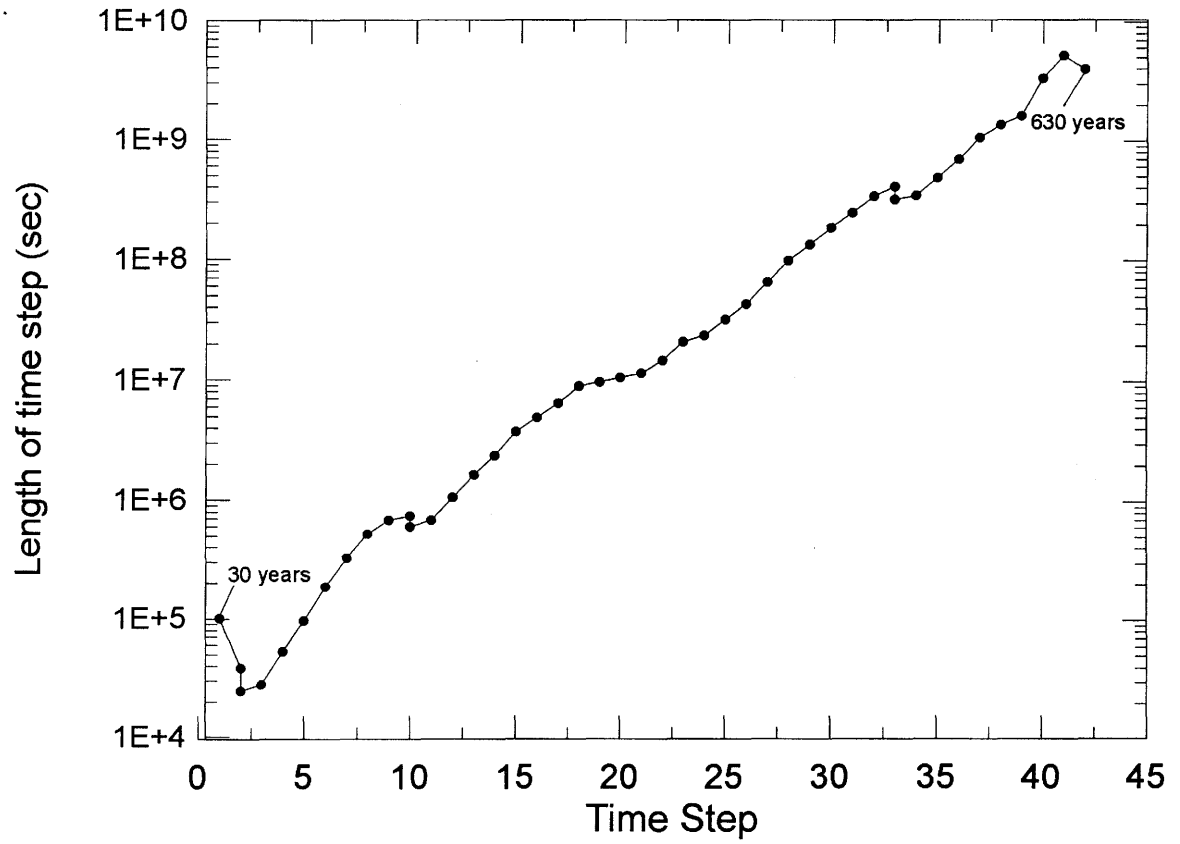

Figure 3.48 Time stepping by Gears' method for the post-closure transient simulation.

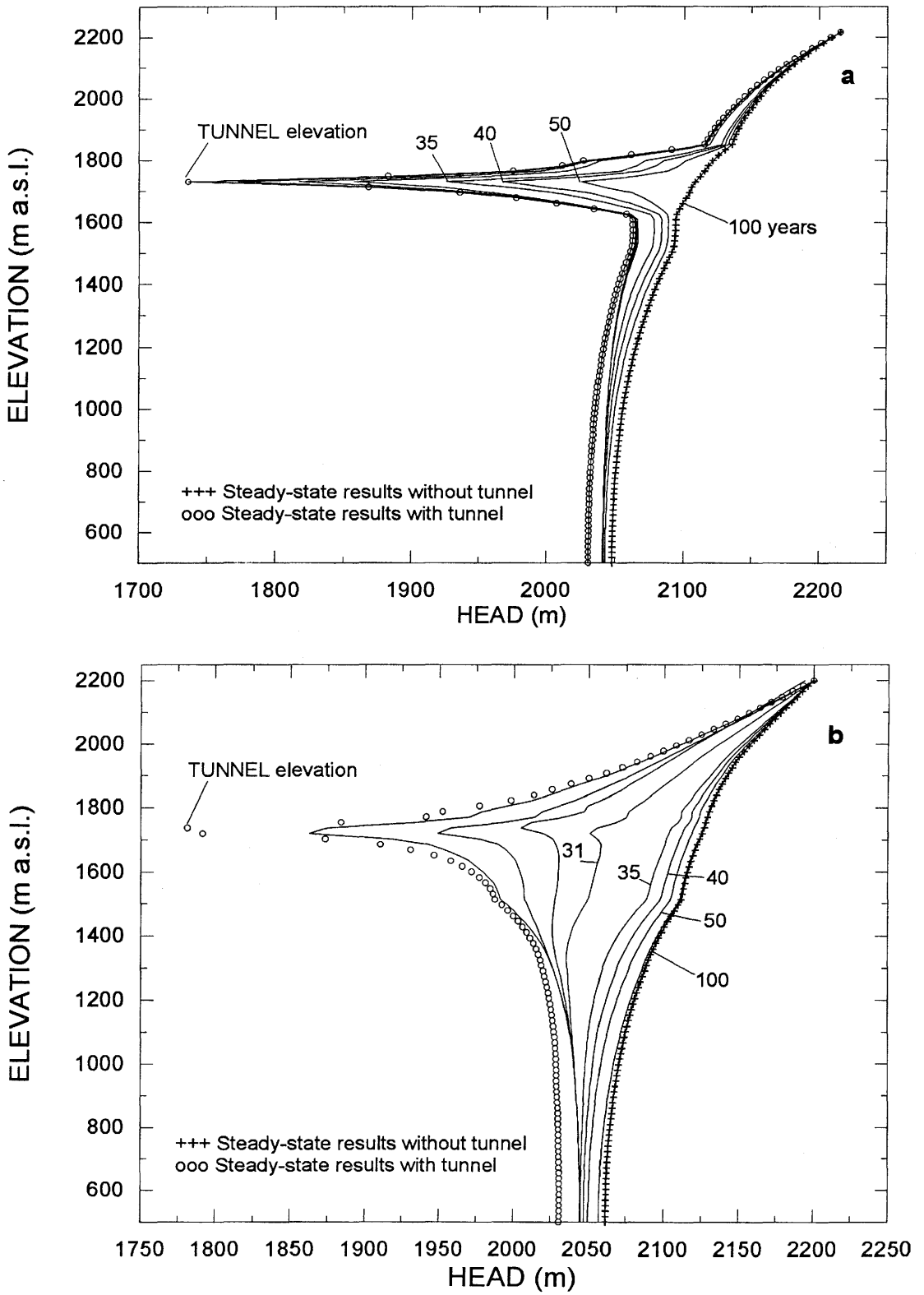

Figure 3.49 Evolution of the hydraulic head with time in the post-closure phase; vertical profiles through: (a) node 13230, and (b) node 671.

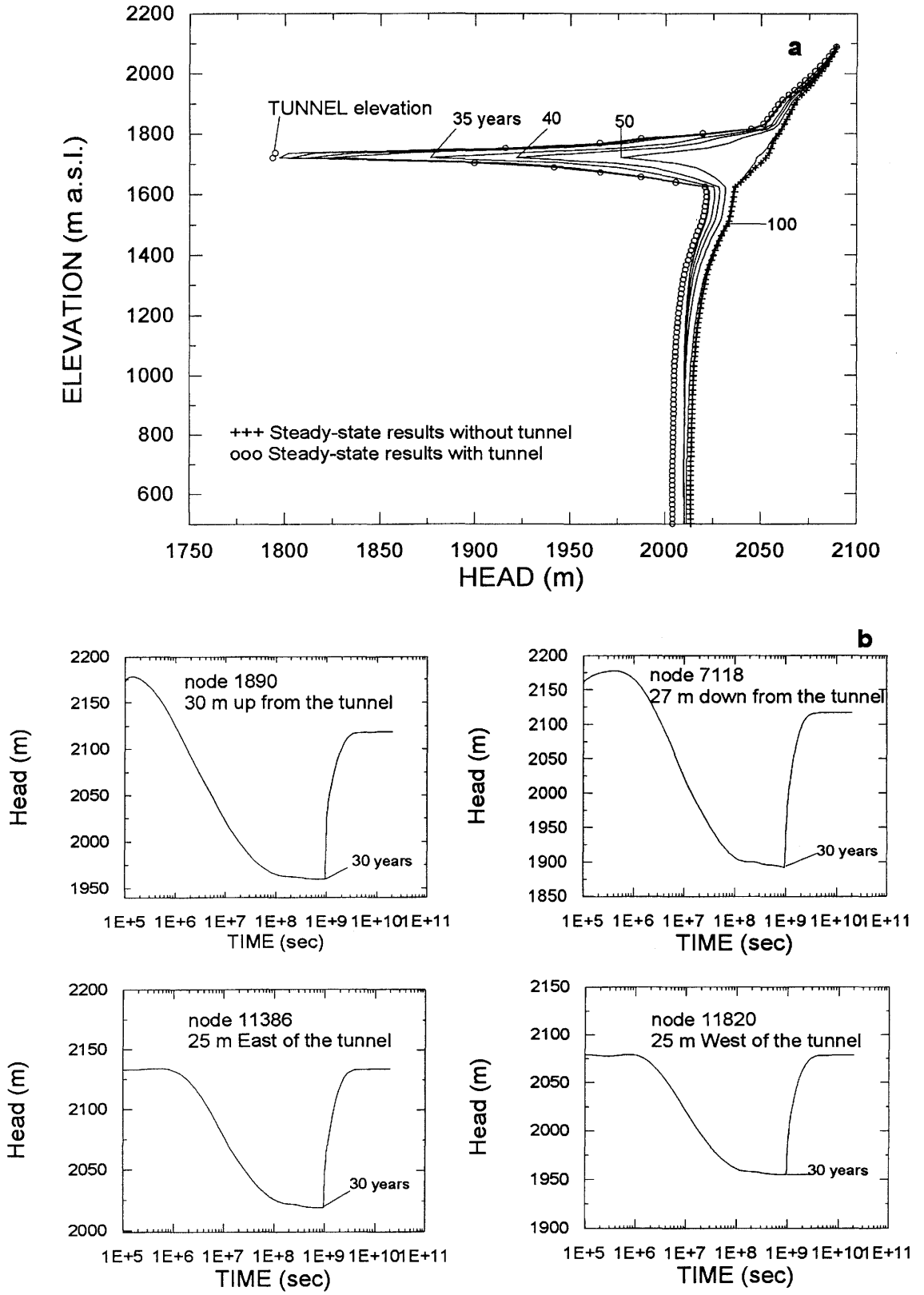

Figure 3.50 (a) Evolution of the hydraulic head with time in the post-closure phase; profile through node 667; (b) Hydrographs at distances of about 25 m around the tunnel.

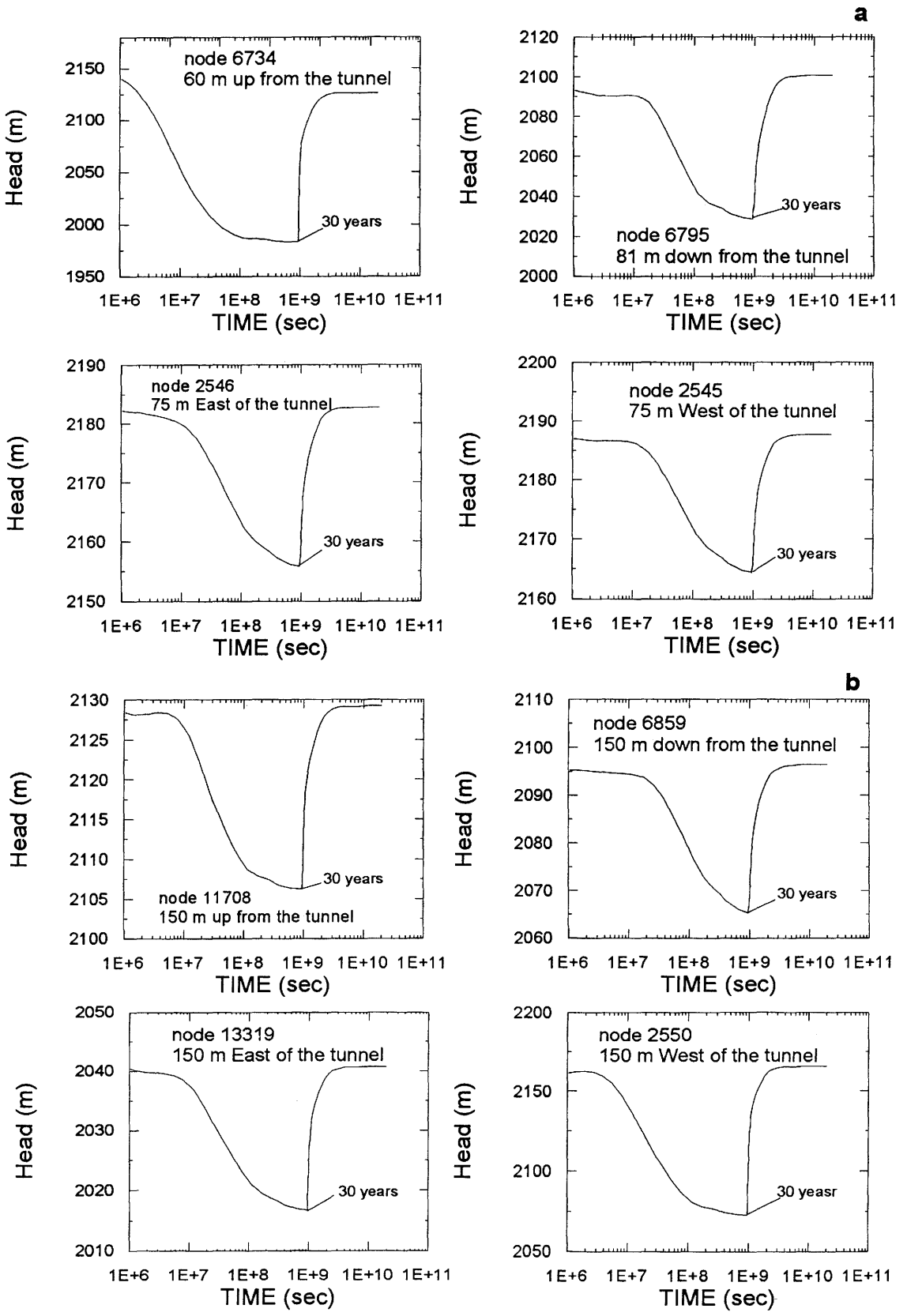

Figure 3.51 (a) Hydrographs at distances of about: (a) 75 m around the tunnel, and (b) 150 m around the tunnel; for the post-closure phase.

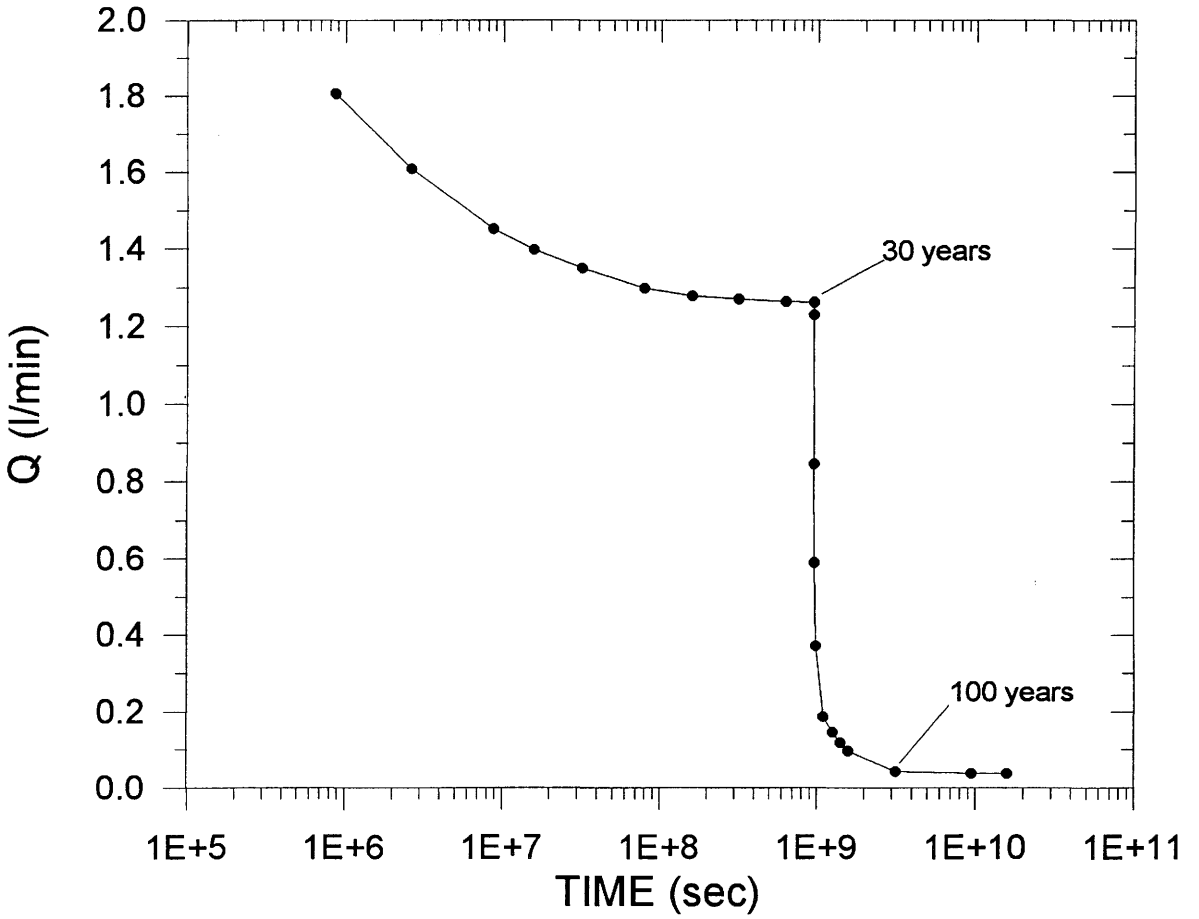

Figure 3.52 Total volumetric fluxes drained by the tunnel in the post-closure phase.

3.4 Consequences for groundwater monitoring in drifts

Based on this study, some practical recommendations can be made, which may be applicable to modeling a real site, where a radioactive-waste repository may be located.

It is strongly recommended that the groundwater influxes into access drifts to the future repository be measured soon (i.e., first days and weeks) after drift construction, and that these observations be continued during the first few years. The hydraulic diffusivity of the medium can be quantified if time-dependent flow and pressure measurements are available.

Additionally, if the transient evolution of measured fluxes and hydraulic heads is available, it could be used to calibrate the site model and provide credible output for the analysis of repository performance. These results will also define the transient hydraulic boundary conditions for the near-field during the post-closure phase.

3.5 Summary and concluding remarks

The transient effects caused by the presence of tunnels were numerically investigated with one-, two- and three-dimensional models.

1-D and 2-D models

Table 3.17 summarizes the results of these numerical investigations in one and two dimensions, with analytical and numerical solutions, and for fixed-head as well as free-surface boundary conditions (§ 3.2.1, § 3.2.2). Some conclusions may be stated for the one- and two-dimensional models.

This study demonstrated the importance of:

- the modeling approach;
- the parameter values, in particular the matrix compressibility;
- the adopted initial conditions;
- the adopted infiltration rates;
- the nature of the space dimensions (1D, 2D).

In the free-surface case, the main uncertainties are related to the parameter values, the discretization of the tunnel (s), and the infiltration rates.

Table 3.17: Summary of the results of transient effects caused by the presence of tunnels with 1D and 2D models

Simulated conditions	Diffusivity ratio ($\kappa = K/S_s$, m^2/s)	Time to reach steady state under the boundary conditions simulated
1 Dimension With fixed-head boundary conditions	0.1 1.E-2 1.E-3 1.E-4 1.E-5	1 month 5 years 30 years 100 years 500 years
2 Dimensions With fixed-head boundary conditions	5.E-4 5.E-5 5.E-6	100 years 500 years 2000 to 3000 years
2 Dimensions With free-surface boundary conditions	5.E-4 5.E-5 5.E-6	~3000 years ~4000 years ~30000 years

The results from the two-dimensional numerical simulations are more or less consistent with the one-dimensional case (calculated with analytical and numerical models) for the case of the fixed-head boundary conditions, as can be seen in Table 3.17. However, for the two-dimensional simulations with the free-surface boundary conditions, the results are very different, with factors of up to 10 depending on the diffusivity coefficient. Given the nature of the adopted boundary conditions in the latter case, the uncertanties in the parameter values are even greater.

Since this is a process-oriented modeling study, the conclusions should be taken as a guide for a 3D site-specific model. No effort was invested in calibrating the 1D and 2D models. Additionally, it appears that a finer discretization of the upper first and second layers (where the free surface is readily moving) is necessary to ensure good numerical convergence. This aspect was not further investigated in the present study.

In the free-surface case, the infiltratrion rate needed to saturate the 2D model have a very low value (1 to 3 mm/y). The precipitation in the region of the Grimsel massif is in excess of 1500 mm per year. The recharge is limited by the rock permeability, which, in the case of Grimsel, is in the order of 1.E-10 m/s (for granite). At this particular loaction a fixed-boundary condition at the top would be adequate.

For other more permeable rocks for example the limestone at the Wellenberg site with a permeability in the order of 1.E-7 m/s, the infiltration rate needed to saturate the model could be orders of magnitude greater (e.g.1'000 to 3'000 mm/y), which is more than the available precipitation for infiltration. In this latter case, a moving free-surface boundary condition at the top of the model would probably be more appropriate. This statement should of course be

further investigated and should also include a good evaluation of the matrix compressibility of this rock.

Finally, a simulation of the head recovery after the sealing of a tunnel was performed for the fixed-head boundary condition (§ 3.2.1). The results showed that, if the tunnel is sealed after 30 years of operation, the hydraulic head in the rock matrix would take about 500 years to recover about 95% of its original condition.

3-D model

For the three-dimensional case, the most relevant aspect was the grid refinement of the existing finite-element mesh to include the 3D tunnel.

Starting from the existing three-dimensional grid of the GTS sub-regional model (SRM), the model grid was refined to accommodate a 3D tunnel into the existing mesh. Given the complexity of the original topology of the SRM, the 3D refinement was not easy to accomplish with the available tools. The topology of the 2D fractures embedded in the SRM had to be modified, which resulted in the modification of the original hydraulic heads in steady state, as discussed in Chapters 2 and 3. The refinement of the SRM to accommodate the KWO tunnel in three dimensions increased the total number of elements by more than a factor of two, and the total number of nodes by almost a factor of three. For this reason, the choice of either the size of the first elements around the tunnel or the time steps for a transient simulation with a 3D model of that size, had to be carefully selected.

From this work we conclude that, in future 3-D models with similar complexity, the discretized 3-D tunnel should be included from the very beginning, when the grid is created following the original geology. Otherwise, it becomes very difficult, if not impossible, to include such a 3D feature in an existing grid without having to modify the original model topology.

Nevertheless, the numerical results with the newly refined SRM are very similar to the previous 3D groundwater flow modeling works at the GTS site. The effects of the hydrodynamic transient behaviour when the tunnel is activated also gave plausible results with the new grid. If one is interested in short-term results (days), the boundary conditions for the head perturbation have to be prescribed as time-dependent, and either the space or the time discretization must be very fine. For grids such as the SRM this may mean a very unpractical grid (i.e., prohibitively fine for a regional model). In the present study the interest was focused more on the medium- to long-term effects; thus the adopted boundary conditions and space discretization are adequate.

The costs of the transient simulations in terms of CPU time, in-core (RAM) and hard-disk spaces with the refined SRM (with the STARDENT computer) are given at the end of each simulated case. They are summarized in Table 3.18

for convenience.

Table 3.18: Computer load of the SRM using NAMMU4

CASE	Simulated Time	CPU Time (Hrs)	Disk Space (Bytes)	Numerical load	RAM Size (Mb)	Time Steps
SSO	Steady-state without Tunnel	1.3	TOTAL = 137'848'116	Max. frontwidth=1252 number of multiplications= 2.4E+9	47	--
GTS base case	630 years	29.07	TOTAL= 169'382'737	Max. frontwidth=1252 number of multiplications= 2.4E+9	47	Total = 56
POT-REP	630 years	Total 35.17	TOTAL = 166'652'559	Max. frontwidth=1252 number of multiplications= 2.4E+9	46	Total = 53
POT-REP2	30 to 630 years	Total = 54.53	TOTAL = 189'920'884	Max. frontwidth=1252 number of multiplications= 2.4E+9	46	Total = 84

Because the crucial factor of any finite-element model is its **problem size**, all the simulated cases were performed with NAMMU version 4. This version was modified to reduce the scratch file sizes produced by NAMMU during the simulation.

In general, the time needed to re-equilibrate to a new steady-state condition after the pressure field had been disturbed by the presence of the tunnel was variable. For the POT-REP case (§3.3.8), it took from 5 to 10 years for the hydraulic heads to reach a steady-state condition between the tunnel elevation and the top surface, at the level parallel to the location of the tunnel. The westernmost part of the model was not very much affected by the presence of the tunnel, given the high topographic relief which conditions the infiltration. The eastern part of the tunnel was more affected, it took from 10 to 20 years to reach the new steady state. The head below the tunnel needed about 500 years to reach equilibrium. The simulation of the recovery time after the closure of the hypothetical repository indicated that it would take about 70 years for the head to recover, under the conditions simulated, above the tunnel location. Below the tunnel ($z < 1400$ m a.s.l.), the time for recovery was from 200 to 300 years depending on the location.

The results of these 3D transient calculations cannot be directly compared to previous 2-D transient simulations because the 2D fractures were not included in the latter.

Finally, the computation of transient volumetric fluxes resulted in values that are below the expected measured fluxes as presented in CHALMERS and CORREA (1993). The magnitude of the volumetric fluxes for the GTS base case ranges from about 3 l/min at the beginning of the transient simulation to about 2 l/min for the steady-state condition. Compared to the measured values of 18 l/min, the calculations underestimated the fluxes by about a factor of 6. However, qualitatively, the 3D transient calculations showed that the area with the highest fluxes drained by the tunnel is located at approximately the same location as where the highest fluxes were measured. We believe that the present sub-regional numerical model is suitable for calibration; i.e., the sum of the measured fluxes could be reproduced with additional runs of model calibration. The calibration of the SRM was carried out and it is presented in Chapter 5 of this report.

CHAPTER 4

COUPLED THERMO-HYDRAULIC EFFECTS

A. Rivera, N.R. Correa and U. Schroeder

4 COUPLED THERMO-HYDRAULIC EFFECTS

4.1 Objectives and scope

Three-dimensional transient simulations were performed with the sub-regional model (SRM) including the KWO tunnel, as presented in RIVERA et al. (1993b), and summarized in Chapter 3. These simulations were done under isothermal conditions, i.e., constant-density fluid.

When there is a thermal gradient due to the presence of a temperature change in the rock formation, thermo-hydraulic (TH) processes may occur in the form of buoyancy flow. In addition, in a repository where high-level radioactive wastes are disposed of, heat release from the near-field may also influence the groundwater flow field. In these cases, both the fractures and the rock matrix play a major role in the thermal conduction phenomena.

The objective of this Chapter is to perform a process-oriented study to evaluate coupled-TH processes to account for the effects of variable-density fluid (due to temperature) in the groundwater flow field, around a fictitious repository.

4.1.1 Generic coupled thermo-hydraulic model

The conditions under which a realistic, generic, coupled-TH model should be built, are shown schematically in Figure 4.1. This would be the ideal conceptual model for the complete SRM conditions.

In order to account for the full procedure of the construction (opening), operation and closure of the repository, time-dependent boundary conditions would have to be applied to the numerical model. These are:

Heat;
H_o = f(x,y,z); initial condition, steady-state groundwater flow without the tunnel;
H= f(x,y,z,t); during opening, operation (decrease in temperature), and closure (increase in temperature) prescribed at the repository walls; and at the top and lateral boundaries.

In this case, H means a source of heat that could be prescribed either as a heat-flow boundary condition (Neumann type), or as a temperature gradient (Dirichlet type). In both cases, these should be time-dependent.

Hydraulic;
P_o = f(x,y,z) initial condition, steady-state groundwater flow without the tunnel for saturated conditions;
P = f(x,y,z,t) during opening, operation (pressure decrease) and closure (pressure increase) at the repository walls and at the lateral boundaries.

In this case, the time-dependent pressure decrease during opening and operation of the fictitious repository is calculated using the numerical model. The Dirichlet-type boundary conditions would prescribe atmospheric pressure at the tunnel walls during the complete period of opening and operation, and fixed pressure at the top and lateral walls of the model. The pressure boundary condition inside the tunnel is then released after its closure. A process is then simulated by the numerical model in which there is a pressure build-up as a function of the hydraulic diffusivity, coupled with the heat transport release by the repository. The coupling is done through the variable-density groundwater flow.

4.1.2 Scope of modeling

In a previous modeling study, a coupled hydro-thermal numerical evaluation was carried out to study the effects of a thermal anomaly, on the groundwater flow field of a two-dimensional cross section in the crystalline basement of Northern Switzerland (RIVERA and RESELE, 1992).

In this case an attempt is made to perform 3D thermo-hydraulic computations for the fictitious repository presented in Chapter 3, where 2D fracture zones are included in the far field. The thermal boundary conditions prescribed at the "repository" walls were adopted from the thermo-mechanical computations for the near-field by OBAYASHI (1993), during Nagra's Krystallin-I program.

Therefore, within the general scope of project MOD to acquire practical know-how with a view to understanding and characterizing groundwater flow in the fractured rock around an imaginary repository, the specific aims of the present modeling work are defined as:

- to determine the feasibility of performing 3D coupled thermo-hydraulic computations with the available computer facilities;
- to perform thermo-hydraulic computations for a representative 3D fictitious repository;
- to compare the resulting groundwater flow field from coupled-TH computations with the isothermal flow field as presented in Chapter 3;
- to conclude on the relevance of the TH effects on groundwater flow in the far-field, as a consequence of the coupled-TH processes originating from the near-field of a fictitious high-level waste repository.

4.2 Feasibility of a three-dimensional computation

4.2.1 Computational limitations with NAMMU

The crucial aspect of any finite-element model is its **problem size**, to which

the required scratch space on hard disk and the total CPU time are roughly proportional. The problem size is given by the product of the total number of degrees of freedoms (i.e., number of nodes times number of variables per node) and the nodal band-width of the mesh. For example in RIVERA et al. (1993b), it was found that the total disk space needed to run the SRM (including the 3D KWO tunnel) was about 160 to 180 megabytes. As explained by those authors, the disk space was reduced by about half by modifying the NAMMU code (version 4). Considering the total number of nodes of 18'279, and since the simulations were done only for constant density with a single variable to solve (hydraulic head), these simulations could still be perfomed with the available disk space for temporary scratch files on COLENCO's *STARDENT* computer.

If coupled TH processes are including in the 3D SRM, the global freedoms would increase by a factor of 2 because there would be at least two variables to solve, i.e., pressure, P, and temperature, T. Depending on the numerical formulation, there is the possibility to adopt an approach in which the three components of Darcy's velocity are included as variables together with P and T. Furthermore, in order to take full advantage of the latest version of NAMMU (release 6.1), it would be necessary to keep the output of the scratch files to their original sizes, that is, the scratch space could not be reduced as in NAMMU4 (see RIVERA et al., 1993b). This would imply that the disk space needed for such a modeling study would account for approximately 430 megabytes as shown in Table 4.1, if only two variables, P and T, are considered.

Table 4.1: Preliminary evaluation of disk space needed for coupled TH modeling with the SRM

Constant-density model (Chapter 3)			Variable-density model (this Chapter)		
Disk space (Mbytes)	Numerical load	RAM (Mb)	Disk space (Mbytes)	Numerical load	RAM (Mb)
FOR003 = 86 FOR004 = 1.4 FOR011 = 45 FOR024 = 2.1 OUTPUT file = 14.1 Results FEM301 = 12.3 Global freedoms = 8.3 TOTAL = 169	Max front-width = 1252	47	FOR003 and FOR011 about 366. All others, about 70. Total about 430	Max frontwidth = 1500	?

From this rough analysis, it follows that it is of paramount importance to have an early adequate design of the problem in hand, before venturing into such a large, highly non-linear 3D modeling study. If the disk space necessary for such a study was indeed the one shown in Table 4.1 (~430 Mbytes), it would still be possible to perform this with the *STARDENT* disk space availability

(~500 Mbytes) for temporary files. However, as will be shown below, it is expected that the SRM's grid needs further refinement in some regions in order to avoid ripples on the scale of the elements in the solution to the finite-element equations due to large element sizes.

Therefore the calculation of coupled TH effects requires an optimum spatial discretization of the finite element mesh. The optimum spatial discretization for coupled TH simulations is determined by several factors, such as fluid density, fluid heat capacity, Darcy velocity, fluid temperature and rock heat conductivity. A good first quantitative indication of the required refinement of the grid may be calculated with the grid Peclet number criteria.

4.2.2 The grid Peclet number criteria

BREDEHOEFT and PAPADOPULOS (1965) initially introduced a method to analyze variation in temperature gradients related to a groundwater flow field of Darcy velocity, **q**, that is constant over an interval of length L between an upper limit Z_o and a basal depth Z_b in a 1D isotropic and homogeneous space, through the use of the vertical Peclet number. This Peclet number is a dimensionless ratio between the heat flow density components due to convection and conduction in the transfer of heat.

Because fluid density is a function of temperature and viscosity, $\rho=(T,\mu)$, the problem in hand is highly nonlinear. In the formulation of the model, the equation for temperature is:

$$\rho_{fluid} C_{fluid} q \cdot \nabla T - \lambda_s \cdot \nabla^2 T = 0 \qquad (4.1)$$

where ρ_{fluid} is the fluid density, C_{fluid} is the fluid heat capacity, q is the Darcy velocity, T is temperature and λ_s is the rock heat conductivity.

When solving the coupled problem numerically with finite elements, and if the Darcy velocities are too high and/or rock heat conductivity is too low, oscillations in the numerical solution would be expected. To avoid this, the grid must be further refined in areas where this situation may occur. However, the resulting grid could be unpractically large. For the sake of simplicity, a compromise must be found in which the refined grid is adequate in terms of computational efficiency, numerical accuracy, mesh density, and type of boundary conditions.

A practical way of designing the most adequate grid to avoid oscillations in the numerical solution, is the use of the grid Peclet number (P_g). The grid Peclet number for equation (4.1) is defined as:

$$P_g = \frac{v \Delta x \rho_{fluid} C_{fluid}}{\lambda_s} \qquad (4.2)$$

and should be < 10. If the grid Peclet number does not satisfy this relation, then oscillations in the solution would be expected; consequently, the grid should be further refined in areas where P_g is too large.

In equation (4.2), Δx represents the lenght of a given element in the flow direction, and v is the average pore-water velocity, given by $v = q/\phi$ with ϕ = rock porosity.

Equation (4.2) was used to calculate the required additional refinement (if any) of the SRM grid. Values for Darcy velocities were taken from the results of the simulations presented in Chapter 3. The calculations were done per layer and the results are visualized with *AVS*, to help define zones where further refinement or shrinking are needed.

4.2.3 Grid Peclet numbers for the sub-regional model

The grid Peclet number was calculated in the three dimensions (x, y and z directions) with a simple approximation (conservative approximation). Equation 4.2 was modified as follows,

$$P_{gi} = \frac{v_i \Delta x_i \rho_f C_f}{\lambda_s} \qquad (4.3)$$

with i = x, y and z indicating the three directions; values for ρ_f and C_f are given in Table 4.2. The calculations were carried out with all elements of the SRM, and analyzed with the help of visualization programs adapted for this purpose.

The following sequence describes the unix shell file which calculates the grid Peclet number in the three directions for the whole model:

- Select one K-class (1 to 14);
- Merge all active nodes of the selected K-class;
- Calculate flux for the selected K-class;
- Create a list of all elements of the selected K-class;
- Loop over all elements of selected K-class;
- Select each element individually;
- Purge coordinates of the individual element;
- Purge flux results for the selected element;
- Calculate the arithmetic mean transport velocity in x, y, z directions for all nodes of the element. Store the results in *velocity.dat* file;

— Calculate the maximum length in x, y, z directions for the element. Store results in *minmax.dat* file; and
— Calculate the grid Peclet number in each direction with equation 4.3.

The results of these calculations are given in three separate files (each for one direction) containing the element number and the corresponding grid Peclet number.

4.2.4 Results of grid Peclet number calculations

Statistical representation

The total number of elements (2D and 3D) in the current SRM grid is 7852. Of these, from 79 % to 85 % have grid Peclet numbers smaler than 10. The statistical distribution of elements with $P_g < 10$ is given in Figure 4.2. About 1130 to 1647 elements would need further refinement. 97 % of these are located in the 2-D features. This is a clear effect of the higher values of Darcy velocity in the 2D elements due to high conductivity values, where advective processes override the conductive processes (eq. 4.2).

Graphical representation

In addition to the statistical results of the grid Peclet number calculations, it is also necessary to identify the zones where the mesh needs refinement. Because of the complex geometry, the results are displayed for 2D and 3D elements separately. In Figure 4.3 the elements with grid Peclet numbers greater than or equal to 10 are represented in red. Figure 4.3 represents grid Peclet numbers only for 3D-elements, while Figure 4.4 shows grid Peclet numbers for the 2D elements.

For the x direction, there are a total of 62 3-D elements (colored red in Figure 4.3a) with P_{gx} is greater than or equal to 10. For the z direction, there are 49 elements (red) with P_{gz} numbers greater than or equal to 10.

In Figure 4.4a the grid Peclet numbers for all 2-D elements in x direction are plotted. Blue colors indicate grid Peclet numbers smaller than or equal to 10. All other colors indicate grid peclet numbers greater than 10. In the Figure, red color indicates grid peclet numbers equal to or greater than 100. Finally Figure 4.4b shows the same results for the z direction.

4.2.5 Concluding remarks and recommendations

This study is a first quantitative analysis of the sizes of a 3D grid needed to perform a coupled groundwater flow and heat transfer simulation where fluid density is dependent on temperature. Because this is a 3D problem in which

the real groundwater flow directions and the corresponding flow velocities for each element is dependent on the purpose of model application, we followed a simple approach that would allow us to have control and a better understanding of the problem.

Thus, an unsolved problem is a more realistic estimation of the elements' length in each direction (Δx_i in 4.3). Additionally, a more rigorous derivation of the grid Peclet number for a combination of the three directions should be done. In our approach we assumed that Δx_i is the size of the mesh in the main direction of the flow given by Darcy's vectors, and we used the one-dimensional formulation separately for each x, y and z direction. Because of this, we may have overestimated the calculation of the P_g. However, the results are on the conservative side.

Our first conclusion is that coupled TH processes cannot be modeled with the current SRM grid because it contains a large number of 2D elements which would present numerical oscillations during the solution of the problem. These 2D elements would have to be refined 2 or 3 times, consequently leading to a total number of elements that our current hardware can not handle.

Based on the above-mentioned reasons, two possibilities were foreseen:

(A) The simulation could be done including only the 3D elements, in which case the grid refinement would be minor and it would be possible to handle it with the available hardware.

(B) The simulation could be done for a selected part of the SRM grid, which includes the KWO tunnel. This region could then consider both 3D and 2D elements.

However, the second option would still need further detailed analysis to design and carry out the required grid refinement. This was performed for the analysis presented in the following section (§ 4.3)

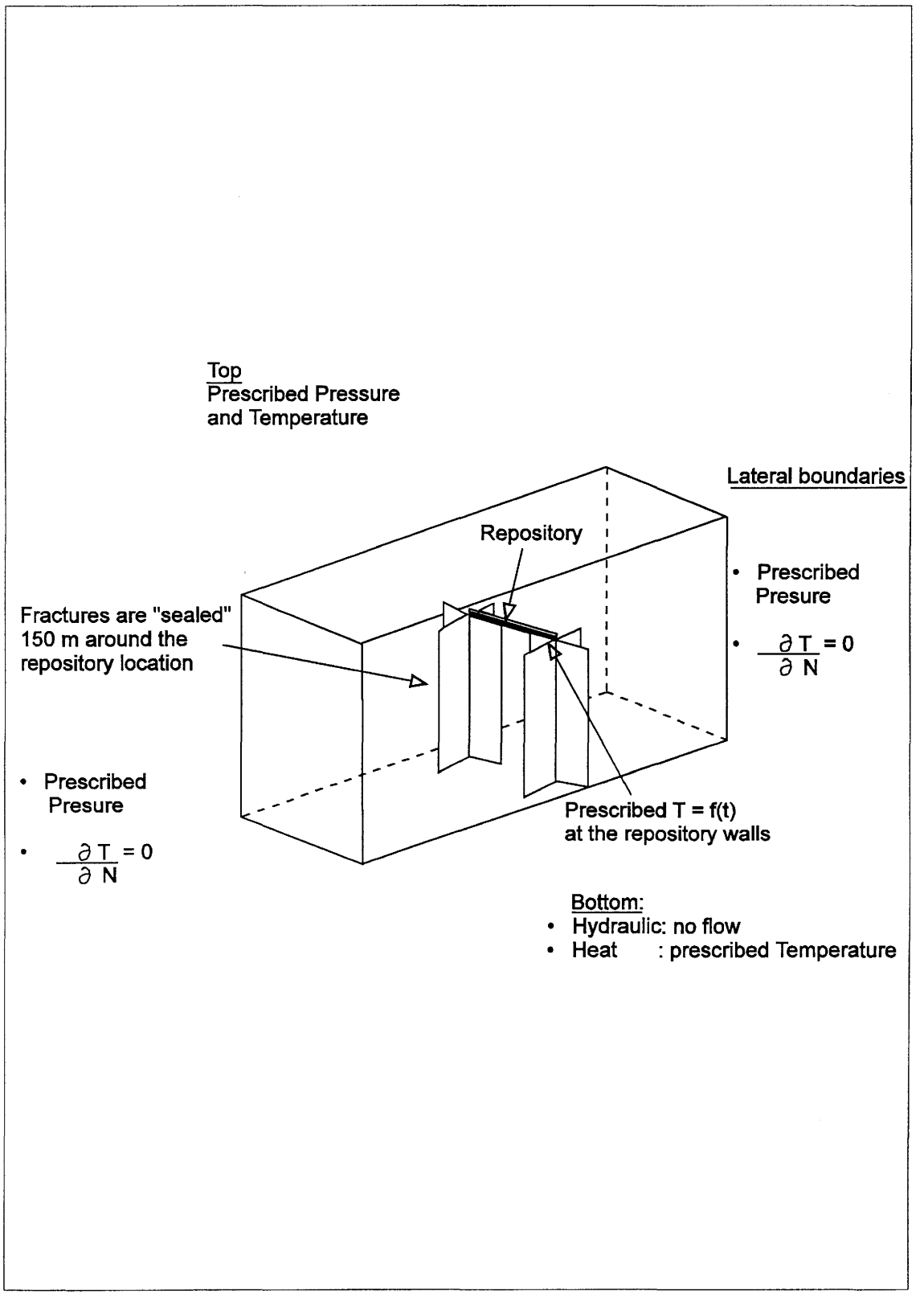

Figure 4.1 Schematic representation of the SRM with boundary conditions for coupled TH simulations.

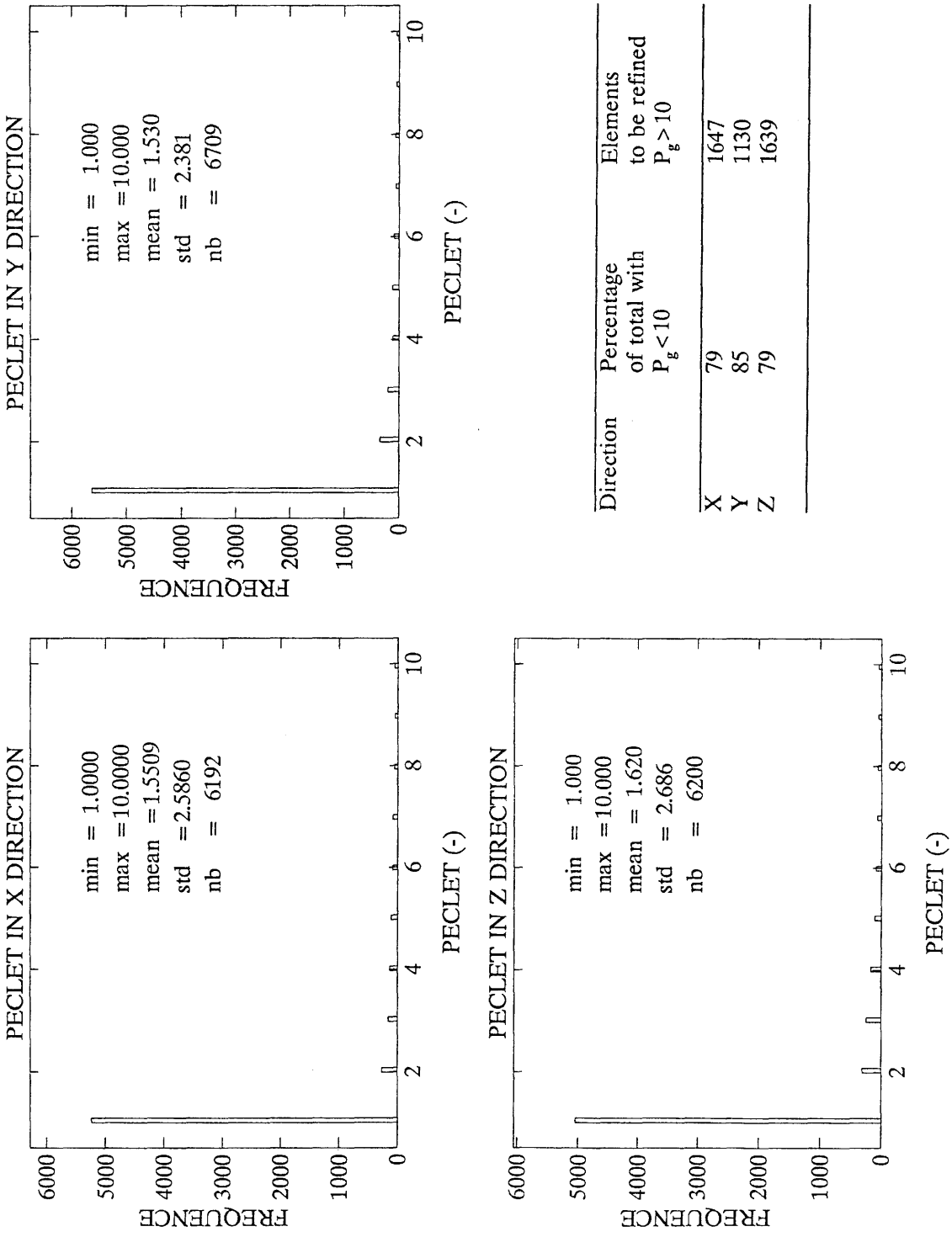

Direction	Percentage of total with $P_g < 10$	Elements to be refined $P_g > 10$
X	79	1647
Y	85	1130
Z	79	1639

Figure 4.2 Statistical distribution of P_g for all the elements of the SRM grid.

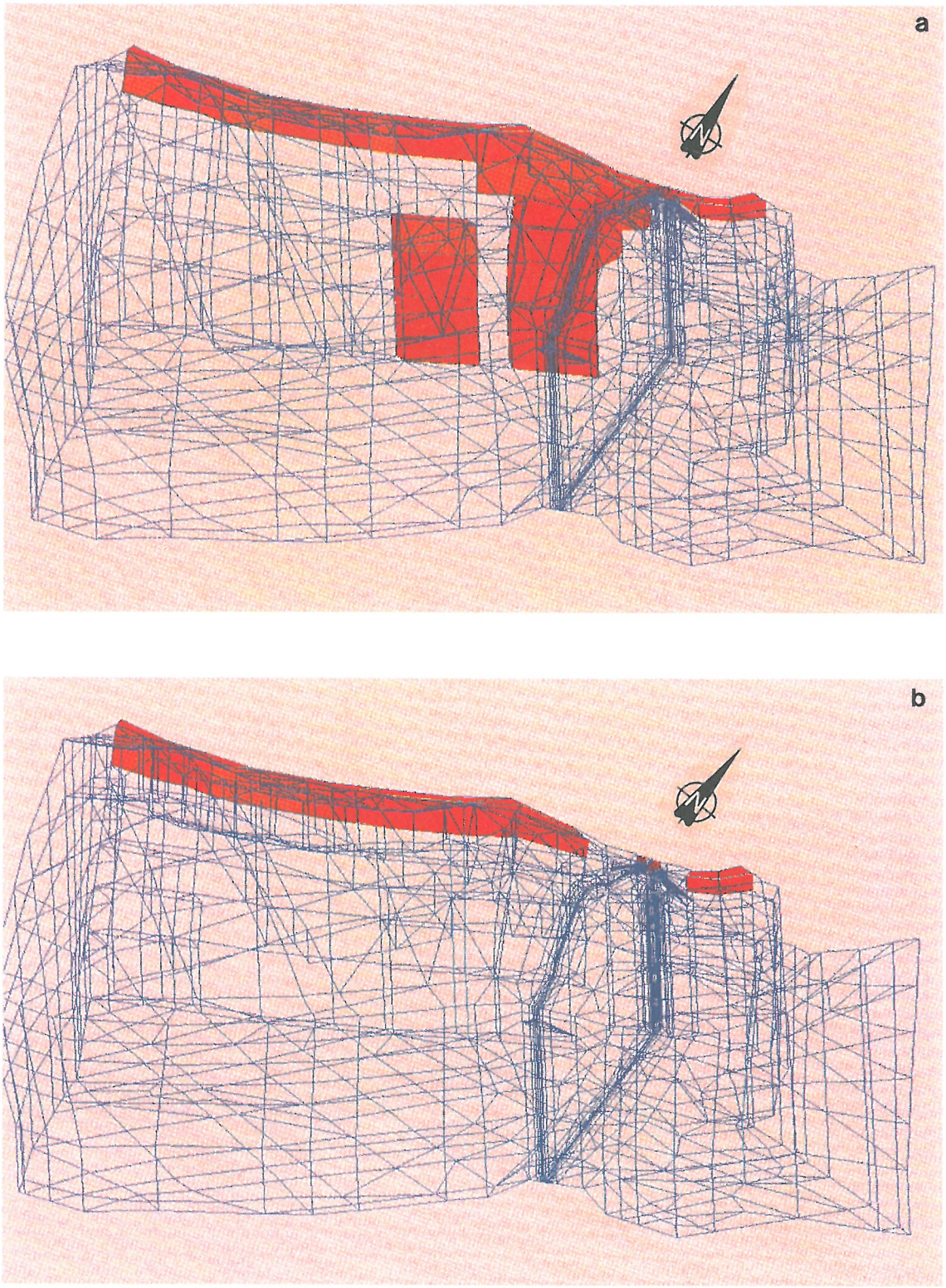

Figure 4.3 Location of 3D elements with $P_g > 10$ (in red); all other elements have $P_g \leq 10$; for: (a) x direction, and (b) z direction.

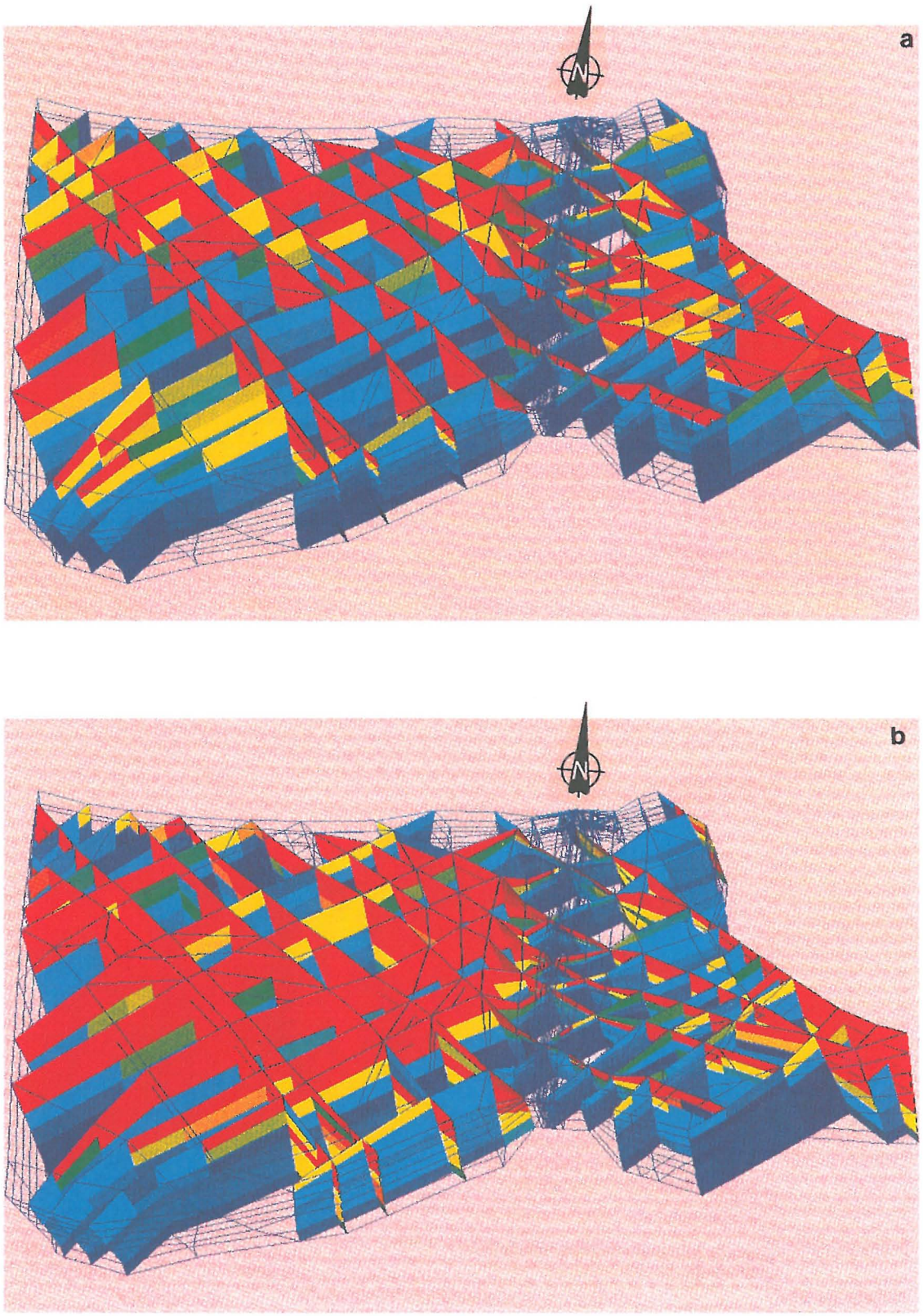

Figure 4.4 Location of 2D elements with $P_g \leq 10$ (in blue); all other elements have $P_g > 10$; for: (a) x direction, and (b) z direction.

4.3 Steady-state coupled thermo-hydraulic computation

Following the analysis of the grid Peclet number criteria, the second option was adopted (§ 4.2.5). A part of the SRM was selected and an attempt was made to perform a coupled thermo-hydraulic simulation including a heat source prescribed in a fictitious repository.

4.3.1 Selection of a region from the sub-regional model

A part of the 3D grid from the sub-regional GTS model (SRM), as presented in Chapter 3 (see Figure 3.25a), was selected. The selection includes the refined part of the SRM that was used to simulate transient effects due to the presence of the KWO tunnel in three dimensions. It includes the full length of the KWO tunnel, part of the Baechlisbach shear zone to the north, part of the Räterichsboden to the north-east, part of the Grimsel lake to the south, and the western boundary is cut at an elevation of approximately 2320 m a.s.l. (Juchlistock massif). Figure 4.5 shows a plan view of the selected part of the SRM.

The new grid is approximately 1000 m wide (west-east) and 2000 m long (north-south); it contains 5'518 elements and 13'824 nodes. Although the surface area was reduced to about a fifth of the SRM, the number of nodes and elements was only reduced by about 24 % and 30 %, respectively. This is because the selected part contains the full refined area of the SRM (§ 3.3.4 and Table 3.9).

4.3.2 Hydraulic boundary conditions and parameter values

The hydraulic boundary conditions were derived directly from a SRM simulation. The model was assumed to be saturated; thus, the hydraulic head at the top is prescribed to be equal to the topographic elevation ($h=z$) everywhere in the selected part. The east and west lateral walls of the model have a prescribed head derived from the 3D transient calculation after the closure of an imaginary repository, as presented in section 3.3.8. Finally, the southern wall and the bottom of the model have no-flow boundary conditions.

Since it is assumed that the repository is sealed after 30 years of operation, the three-dimensional tunnel, as simulated in Chapter 3, is not hydraulically activated after that time. The hydraulic parameter values are the same as the ones used in the sub-regional model (see Tables 3.11 and 3.12). The hydraulic conductivity of the backfill material in the tunnel is $K=1.E\text{-}11$ m/s.

4.3.3 Hydraulic calculation

A hydraulic calculation was necessary to verify the new grid with the adopted boundary conditions and parameter values before attempting a coupled TH simulation. A three-dimensional steady-state run was performed with the new

grid and with the tunnel not being activated.

Figure 4.6 shows the results of this run in a horizontal section (top of layer 3), and in a vertical cross-section parallel to the tunnel.

These results are in good agreement with results from a steady-state run with the full SRM grid. Only a qualitative comparison is possible in this case. Figure 4.6 can be compared with Figure 4.7 from RIVERA et al. (1993b), reproduced here for convenience.

4.3.4 An attempt to simulate coupled thermo-hydraulic effects

Once the new grid had been checked and accepted, a first attempt was made to simulate steady-state coupled thermo-hydraulic effects due to the release of heat from an imaginary repository. The following model is the simplest conceptual model that can be posed without changing the reality of the generic problem. The basic assumptions are:

1 — Three-dimensional fluid flow is coupled with heat transfer.
2 — An equivalent porous medium is assumed except where major fractures zones are represented as discrete features with permeabilities at least 10^3 times that of the surrounding rock matrix.
3 — Thermal equilibrium exists between fluid and solid phases (conservative assumption).
4 — The basal boundary is horizontal and impermeable with a conductive heat flux or a natural thermal gradient, applied along the boundary.
5 — Lateral boundaries for heat transfer are impermeable and insulated.
6 — The upper boundary of the domain is the top surface where mean air temperature is prescribed.
7 — Fluid density and viscosity vary as a function of temperature and pressure, while thermal conductivity and specific heat capacity of the fluid are assumed to be constant.

Additional assumptions to evaluate the influence of heat release from the fictitious repository on sub-regional groundwater flow are:

1 — The near-field of the "repository" is a long-term source of heat.
2 — A conductive heat flux is prescribed at the walls of the 3D repository to mimic the heat release from the near field, or;
3 — A time-varying boundary condition ($\sim T_o$ = 80 °C, OBAYASHI, 1993) for heat transfer is prescribed at the walls of the 3-D tunnel after sealing, if a transient simulation is performed.

If the results from the first set of simulations (i.e., natural thermal gradients) show that the transfer of heat is negligible (i.e., it does not affect sub-regional groundwater flow), then only the heat release from the repository is simulated.

A section of the three-dimensional KWO tunnel was selected to represent the repository. This is the same 150-m long section as previously selected in the 3D transient simulations with an imaginary repository as described in RIVERA et al. (1993b) and presented in Chapter 3 of this document (§ 3.3.7 and § 3.3.8).

The hydraulic diffusivity (κ) of the matrix (3D elements), 2D and 1D features are fixed according to the parameter values presented in Tables 3.11 and 3.12. The thermal parameter values are defined in Table 4.2:

Table 4.2: Thermal simulation parameter values

BHF	Basal heat flow	40-50 mW/m^2
ΔT	Thermal gradient	0.01 - 0.02 °C/m
T_o	Reference surface temperature	0.1 °C
ρ_o	Reference fluid density	998.2 kg/m^3 (for T=20°C)
μ	Viscosity	1.E-3 Pa s (for T=20°C)
λ_s	Solid thermal conductivity	2.51 W/m °C for rock mass; 2.9 W/m °C for fractures
λ_f	Fluid thermal conductivity	0.6 W/m °C
c_f	Specific heat capacity of water	4186 J/kg °C
ρ_s	Rock density	2600 kg/m^3
ϕ_r	Porosity of basal unit	0.01 - 0.02
ϕ_f	Porosity of fractures	0.10 - 0.11
$(\rho_f C_f)$	Volumetric heat capacity	4.185E+6 J/m^3 °C

The boundary conditions for heat transport are (see Figure 4.1):

- The vertical temperature (T) distribution in the model is initialized to correspond to the natural thermal gradient in the region. This gradient is calculated by the model by prescribing T=0.1 °C at the surface, corresponding to the mean annual air temperature at the GTS, and T=34 °C at the bottom of the model (z=500 m asl), which corresponds to a natural thermal gradient of ΔT =0.01 to 0.02 °C/m.
- The initial value for temperature, in the model, is zero everywhere; the numerical model then calculates the temperature distribution everywhere in the simulated region according to the prescribed temperatures at the top and bottom.
- The four side walls are isolated against horizontal heat flow, i.e., $\partial T/\partial n=0$.
- The heat release from the "repository" is represented by a fixed temperature of 80 °C, according to OBAYASHI (1993), prescribed at the walls of the selected 3D section of the tunnel.

All the numerical calculations were carried out with NAMMU (release 6.1, 1993). An approach was first attempted, where only two variables (P and T)

were used with an initial run. Even though the Darcy velocity field is affected by the variations in the fluid density, the former was left to be calculated separately. The reasons for this are that if the Darcy velocity field is to be solved simultaneously, one would have to account for five variables, namely pressure, temperature and the three components of the velocity field. In this case, the computer space needed for this three-dimensional coupled calculation with five variables would fall outside the limits of the available computer space in COLENCO's hardware. The preliminary scoping evaluation of the disk space needed (§ 4.1, Table 4.1) indicated that the available disk space was the limiting factor, and that is even when considering only two variables (P and T).

After constructing the numerical model with the adopted hydraulic and thermal boundary conditions described above, and the additional parameter values presented in Table 4.2, a first run was designed as follows:

— Initial guess =	P=1E+5 Pa, T= 0°C
— Maximum front width =	1500
— Maximum no. of iterations =	10
— Convergence criterion =	1E-4
— Maximum nodes per element	20
— Nodes =	14'000
— Elements =	5'600
— Global freedoms =	30'000
— Solve for residual pressure, P^R	

The residual pressure rather than the pressure was adopted as a variable, because the residual pressure is a convenient variable for variable-density flows, being proportional to the groundwater head variable for constant-density flows: $P^R=P^T-P_o+\rho_o \cdot g \cdot (z-z_o)$, where P^T is the total pressure and P_o is a reference pressure.

Because the problem in hand is non-linear, the numerical solver needs to iterate. This is done in NAMMU with Newton-Raphson iterations. The convergence criterion in NAMMU is carried out by considering the behaviour of the quantity called *RSTEP*. This is a measure of the magnitude of the largest change in the unknown nodal values (degrees of freedom) over an iteration. It is equal to the ratio of the magnitude of this change to the largest degree of freedom. *RSTEP* is calculated for each Newton-Raphson iteration. Once the iterations are sufficiently close to the solution they converge quadratically and *RSTEP* correspondingly decreases quadratically.

In NAMMU, the coupled groundwater flow and heat transport process is solved simultaneously; in addition, the model is three-dimensional, resulting in a very large matrix to solve. After several trials and adjustments of the limits of the real and integer spaces, the final values for the model size accepted by the solver to assemble and solve the necessary matrices were:

— Real workspace = 6'000'000 bytes;
— Integer workspace = 700'000 bytes; and
— Maximum front width = 2300.

The first numerical simulation was carried out with the *STARDENT* computer. Because other concurrent jobs, and because the disk space availability for temporary files was not enough, the simulation could not be accomplished.

A second attempt was performed with a *DEC 3000* series 800 computer with an alpha processor. This computer has a total memory of 128 MB and disk space capacity of 3 GB; it performed about 4 times faster than the *STARDENT* computer for the present problem.

The results of this second attempt are described in Table 4.3.

Table 4.3: Results of the second attempt to run coupled TH processes in 3D

UNIT	SPACE (Bytes)	RAM (Mb)	CPU (hrs)	Newton-Raphson iteration	RSTEP
FOR003	114'774'400			1	124
FOR004	1'085'412			2	2.08
FOR011	510'197'400			3	0.83
FOR024	1'536'000			4	5.85
			~44	5	1.14
Total		53	~44	6	169.9
				7	2.14
				8	29.98
				9	127.8
				10	74.3

The units in the first column of Table 4.3 are the scratch files needed during the complete simulation. The original guess on computer load (see Table 4.1), were then highly underestimated, both in the numerical load (front width) as well as in the required memory and hard disk space. From the RSTEP values it was clear that after the fourth Newton-Raphson iteration the problem was not going to converge. It started to oscillate and no matter how many more iterations had been done, the problem would not converge.

One reason for the non-convergence is due to the fact that the setting of the front width (2300) was still not big enough for the problem in hand; the front width in the numerical matrix started to increase after the fourth iteration. Several other attempts were done by increasing the sizes of the front width

and the necessary real work space until the limits of the computer's memory were reached. The limiting values were:

— Real workspace = 15'000'000 bytes
— Integer workspace= 7'000'000 bytes
— Maximum front width = 3500
— RAM = 95 MB
— Total space occupied by temporary files = 803 MB

For a computer load greater than this, the computer's virtual memory would be reached and the numerical model could not be run.

4.4 Concluding remarks

The requirements on numerical load and computer capacity, for a complex three-dimensional coupled thermo-hydraulic model indicated that, with the available software and hardware facilities, such a problem can not be solved.

We believe that the main factors are the problem size and its non-linear nature. Additionaly, the required complexity (2D+3D elements) of the conceptual model exceeded the available computer facilities and type of numerical code (NAMMU). This type of problem probably could only be run with a supercomputer (e.g., *CRAY YMP-4D*), or with a different numerical approach (e.g., parallel processing and/or pre-conditioned conjugate gradient method). The NAMMU developers are currently taking actions to adapte it for running in computers with parallel architecture and with the use of the PCCG. Further numerical investigation is beyond the scope of this work.

Finally, even if the present model could be run, it may still be necessary to refine the existing grid according to the grid Peclet number analysis presented in section 4.2.2. As a consequence, some specific aims of the scope of modeling for coupled-TH computations remain open questions.

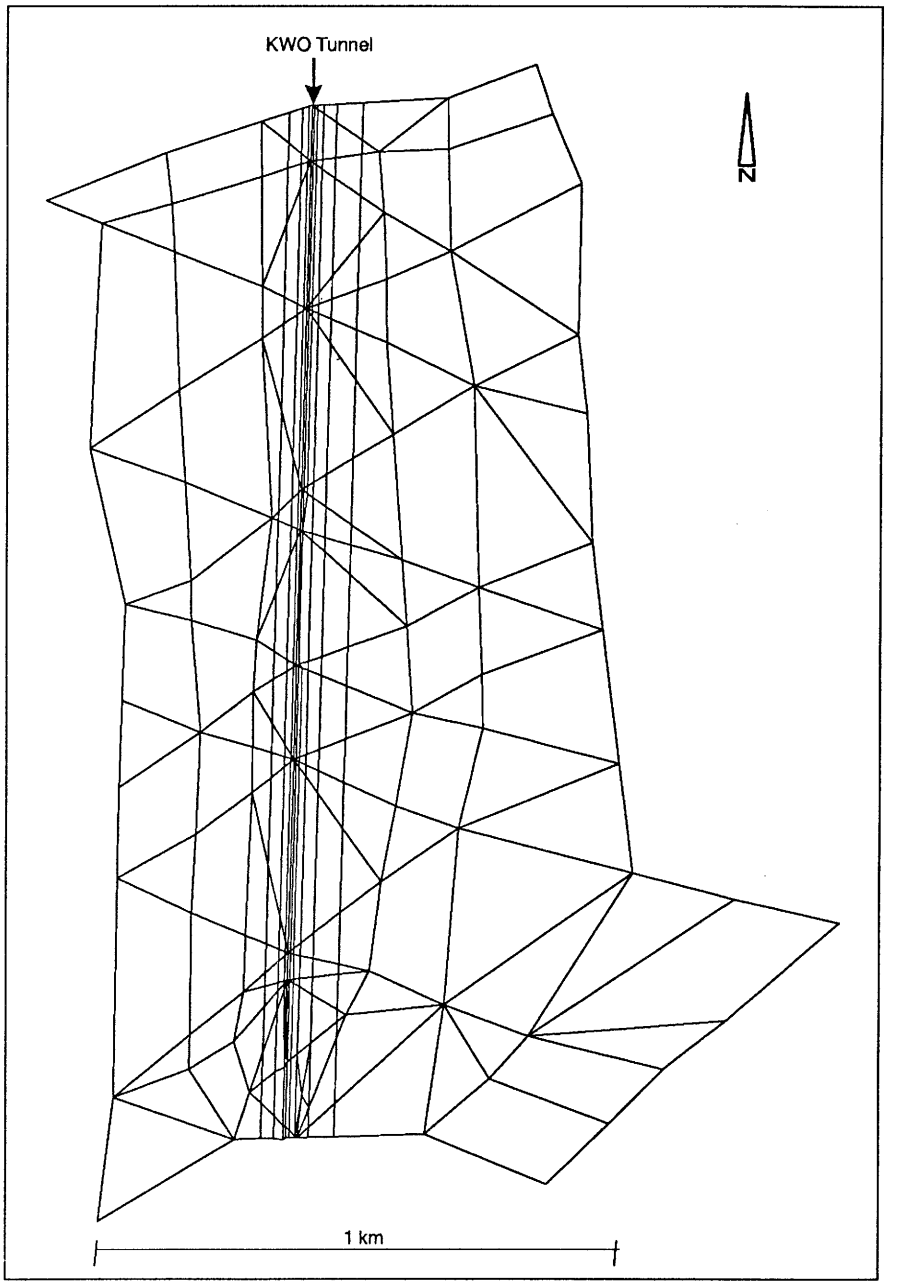

Figure 4.5 Plan view of the selected part of the SRM used for modeling coupled-TH processes (see Figure 3.25a).

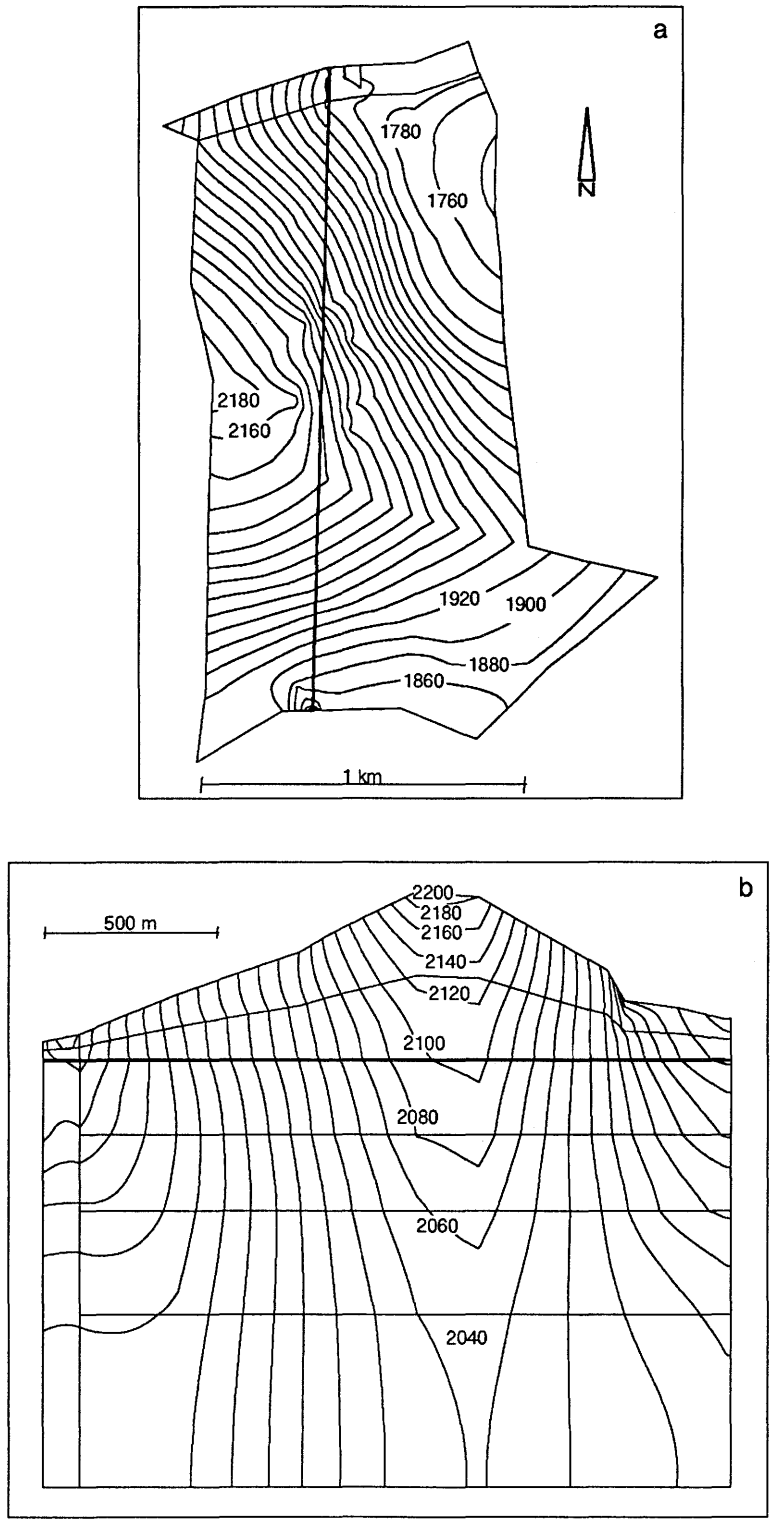

Figure 4.6 Steady-state results with the new grid for: (a) a horizontal section (top of layer 3); and (b) a vertical section parellel to the tunnel. Tunnel not activated.

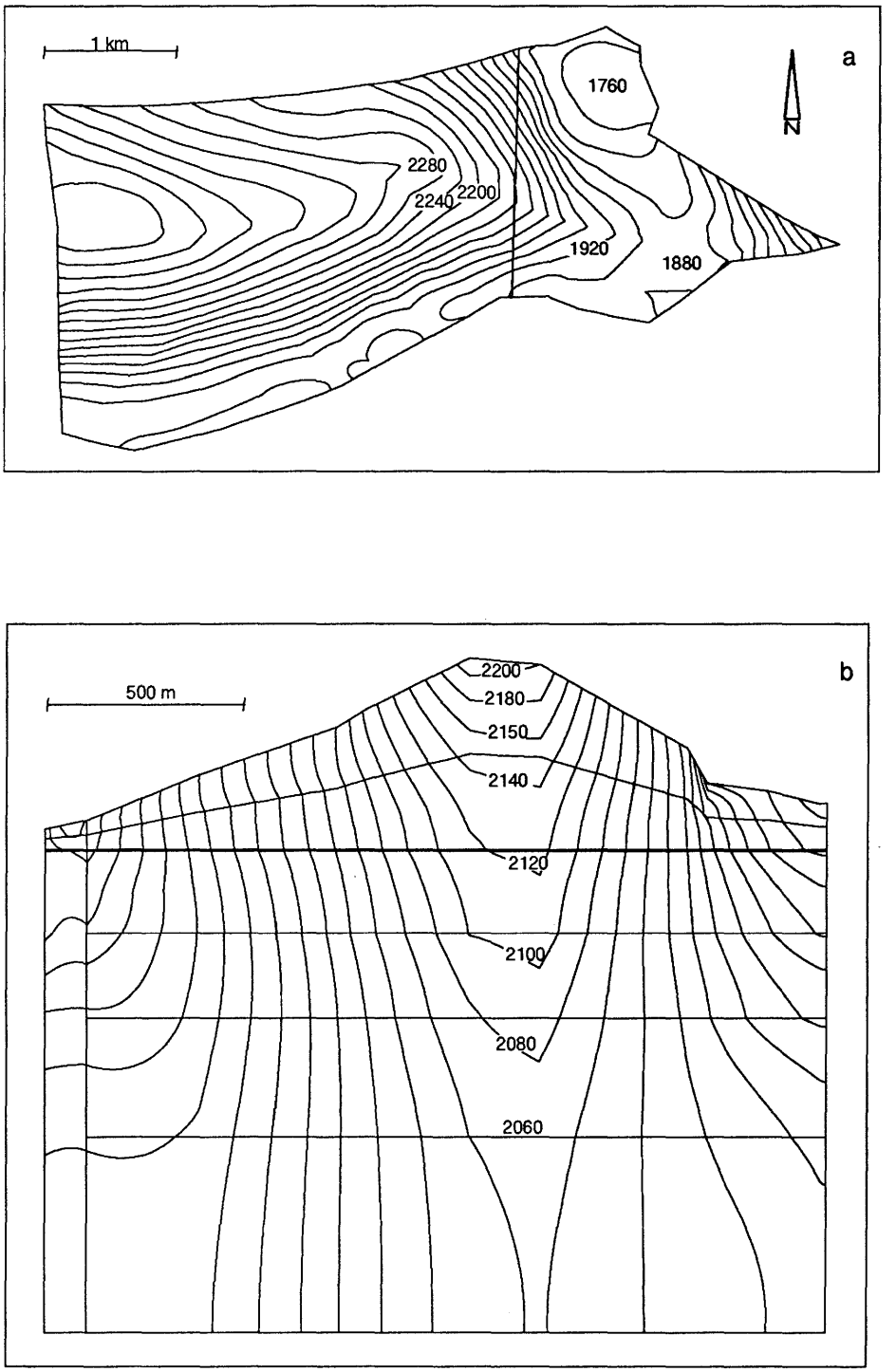

Figure 4.7 Steady-state results with the SRM for: (a) a horizontal section (top of layer 3); and (b) a vertical section (from RIVERA et al., 1993b).

CHAPTER 5

CALIBRATION OF THE SRM WITH THE KWO TUNNEL

U. Kuhlmann, N.R. Correa and A. Rivera

5 CALIBRATION OF THE SRM WITH THE KWO TUNNEL

5.1 Scope and objectives

Important modeling tools were developed during the previous phase of project MOD as described in Chapter 2. In previous works, the regional and the embedded local 3D models were calibrated in steady-state using lumped parameters and measurements.

A calibration of a transient sub-regional model (similar to the one presented in Chapter 3 for an imaginary repository) would have been a feasible, challenging and interesting exercise. As shown in section 3.3, and discussed later in Chapter 5.3, the most important phase of the groundwater transients effects around the KWO tunnel had already elapsed by the time the observation of the hydraulic data began with the aim of exploring the site for the construction of the Grimsel Test Site.

The initial idea of performing a transient calibration was discarded because no evidence of significant transient effects could be derived from the data available at the KWO tunnel. The calibration presented in this report demonstrates the application of further improvements in the modeling concepts and tools actually available (see section 1.3 and Chapter 3). They are applied to the new GTS sub-regional model to demonstrate and test a part of the modeling strategy proposed in section 1.3.

Therefore, within the general scope of project MOD, namely testing and developing know-how in order to understand and characterize groundwater flow in fractured rock, the specific objectives of the present modeling efforts were defined as:

- to test one part of the strategy for model calibration/validation as presented in section 1.3, based on the GTS sub-regional model;
- to demonstrate the reliability, range of accuracy, and possibilities of the proposed modeling approach by means of comparing simulated with discrete measured flows along the KWO tunnel;
- to assess the hydrogeological parameter values resulting from the previous modeling efforts made on a larger and smaller scale (see Chapter 2);
- to provide new estimates of the hydrogeological model parameters on the sub-regional scale of the GTS.

5.2 Methodology

5.2.1 Direct Problem

The numerical modeling in this calibration study was performed with the CASA code which enables the automatic estimation of the hydrological and hydrogeological model parameters (KUHLMANN, 1992). In essence, the

computer program searches for optimum parameter values by the repeated solution of the so called *Direct Problem.* For saturated groundwater flow this consists of solving the following equation which has been simplified according to the problem in hand:

$$\text{div}\,(K \cdot \nabla h) = S\,(\partial h/\partial t) + q \qquad (5.1)$$

subject to appropriate initial and boundary conditions. h [m] represents the potential head, K [m/s] is the isotropic conductivity (or transmissivity [m^2/s] for 2d-features), S [-] is the storage coefficient and q [m/s] denotes sources and sinks. Equation (5.1) is solved numerically by means of the Galerkin Finite Element Method coupled with implicit Finite Differences in time. Discretization in space is achieved by applying isoparametric elements with second order shape functions. The difficult problem of hydrogeological parameterization can be treated using either conventional zonation or defining the hydrogeological properties pointwise in combination with a kriging interpolation scheme (see section 1.3).

5.2.2 Inverse problem

The *Inverse Problem* consists of estimating model parameters from measurements made on the system response and from appropriately weighted prior information on the parameters. In CASA the inverse problem is formulated within the framework of the statistical Maximum Likelihood (ML) estimation method and largely follows an approach proposed by CARRERA (1984). ML theory leads to the following negative Log-Likelihood-Function to be minimized with respect to the geohydrological parameters

$$S = \sum_i Z_i/\sigma_i^2 + \sum_i M_i \ln \sigma_i^2 + \sum_i \ln |V_i| + M \ln (2\pi) \qquad (5.2)$$

where

$$\begin{aligned} Z_i &= r_i^T V_i^{-1} r_i \\ M &= M_h + M_Q + M_p = \sum_i M_i \end{aligned} \qquad (5.3)$$

$$r = \begin{pmatrix} r_h \\ r_Q \\ r_p \end{pmatrix} = \begin{pmatrix} z_h - z_h^* \\ z_Q - z_Q^* \\ p - p^* \end{pmatrix} \qquad (5.4)$$

M denotes the total number of available measurements and prior estimates and represents the sum of the subsets M_i where the index i refers to the type of the data subsets i {h, Q, p} (i.e. head, flow rate, model parameters). V_i represents symmetric, positive definite matrices, which account for *a priori* covariance within the individual groups of data. σ_i^2 denotes positive scalars

often taken as unknown statistical parameters to be estimated by the inverse scheme. The sums Z_h and Z_Q, (5.3), quantify the discrepancies between the computed performance measures z_i and the vector of measurements z_i^* and are often termed as *'fit' criteria,* Z_p (5.3), on the other hand, quantifies the deviations between the actual values of model parameters p and their prior estimates p^* representing a plausibility measure of the estimation results (*plausibility* or *penalty criterion*).

If the error structure is assumed to be known i.e. given $\lambda_i = \sigma_h^2/\sigma_i^2$, minimizing the Log-Likelihood Function (5.2) is equivalent to minimizing

$$Z = \sum_i \lambda_i Z_i \qquad (5.5)$$

CASA minimizes (5.5) applying alternative optimization algorithms such as the Levenberg-Marquardt algorithm or a Quasi-Newton method. In case a global and unique minimum is detected, those model parameters are estimated which are most likely to reproduce the measurements based on a given model structure. Details of the approach can be found elsewhere (e.g., KUHLMANN, 1992; CARRERA & NEUMAN, 1986a,b,c).

5.3 Observed data

Flow rate measurements were carried out between 1983 and 1987 at 15 points along the KWO tunnel (CHALMERS & CORREA, 1993, § 3.3.1.1). Most of the measured fluxes reached a quasi-steady state for approximately the last two years. Table 5.1 shows the averaged steady-state values as used in the inverse runs below. These flow rates have been observed at locations where fault zones intersect the KWO access tunnel. In the simulated tunnel of the SRM, the intersection lines with the 2D-fracture zones do not exactly correspond with the real observation points. Therefore, the assumed inflow locations had to be slightly shifted according to the existing SRM mesh. The error structure of the flow measurements is assumed to be known with a standard deviation of 5% related to the averaged value.

Table 5.1: Quasi steady-state flow rates measured in the KWO tunnel

Distance m	Inflow l/min	Distance m	Inflow l/min
709	1.45	2'171	0.46
927	0.15	2'244	1.48
1'698	1.10	2'280	1.37
1'755	1.11	2'288	2.01
1'792	0.24	2'300	0.36
1'845	0.30	2'302	0.78
2'076	6.65	2'314	0.47

5.4 Model parameters and prior information

The SRM as described in Chapter 3 (base case) includes 13 zones, each defined by a different conductivity/transmissivity class. Table 5.2 lists the set of parameters as used for inverse run IMOD-1. Note that the hydraulic conductivities of the crystalline layers 1 and 2 and the conductivities of the layers 4, 5 and 6, respectively, are lumped into one single parameter.

Table 5.2: Model parameters for run IMOD-1.

Description	Parameter	Prior Information m^2/s
3d-Layer 1&2	3dLa1	1.00E-10
3d-Layer 3	3dLa3	1.00E-11
3d-Layer 4&5&6	3dLa4	5.00E-12
Shear-Layer 1	ShLa1	1.00E-08
Shear-Layer 2	ShLa2	1.00E-09
K-Fracture Zones 1	KFra1	1.00E-07
K-Fracture Zones 3	KFra3	5.00E-08
S-Fracture Zones	SFrac	5.00E-09

This original parameter structure does not distinguish between individual fractures so that the K- and the S- fracture family both have only one single parameter. In order to be able to reproduce the inflow distribution along the tunnel in a more quantitative way, a second inverse run has been performed. Here, each 2D feature intersecting the KWO tunnel is represented by its own transmissivity parameter. Table 5.3 summarizes the model parameters used for run IMOD-2. The a priori standard deviation (related to the log-values of the parameters) was assumed to be 1 [log (m/s)].

Table 5.3: Model parameters as for run IMOD-2.

Description	Parameter	Prior Information m^2/S
3d-Layer 1 & 2 & 3	3dLa1	1.00E-10
3d-Layer 4 & 5 & 6	3dLa4	5.00E-12
Shear-Layer 1 & 2	ShLa1	1.00E-08
K-Fracture tm427-1397	KFr22	1.00E-07
K-Fracture tm1948	KFr34	1.00E-07
S-Fracture tm711	SFr24	5.00E-09
S-Fracture tm1058	SFr26	5.00E-09
S-Fracture tm1397	SFr30	5.00E-09
S-Fracture tm1580	SFr32	5.00E-09
S-Fracture tm1948	SFr34	5.00E-09

5.5 Calibration results

The computed inflow rates from run IMOD-1 along the KWO tunnel are plotted in Figure 5.1a. Each computed peak corresponds to an intersection of a fracture with the access tunnel. Due to the existing parameter structure (same transmissivity for each fracture) the model computes an averaged inflow for each fracture, not being able to distinguish between more and less water-bearing fractures. As a result, the high peak at approximately tm2000 is very poorly reproduced. Nevertheless, the sum of the inflows (cumulative inflow) as shown in Figure 5.1b agrees fairly well.

The effects of the re-parametrization (see section 5.4) realized in run IMOD-2 are shown in Figures 5.2a and 5.2b. Here, the agreement of the inflow is acceptable at least up to a distance of 2000 m from the tunnel entrance. Because in the existing mesh none of the fractures intersects the tunnel beyond tm2000, the model still fails to match the observed high flow rates in this domain. The introduction of either an additional fracture or a new conductivity class would solve this problem. This task can be readily performed using the discretization tools presented in section 3.3.4. The resulting model parameters estimated by run IMOD-2 together with their approximated 95% confidence intervals, are illustrated in Figure 5.3.

5.6 Run-time environment

The computations were carried out on a Sun Sparc10 workstation. Due to the iterative preconditioned conjugate gradient matrix solver (PCCG) in CASA, the solution of the FE-system depends heavily on the conditions to be simulated (parameters, boundary conditions). The SRM with its 18275 nodes and 7820 elements took between 200s and 300s of CPU time per system solution (i.e., steady-state direct problem). CPU-time needed for one step of the parameter estimation algorithm is N+1 times the forward solution time if Levenberg-Marquardt minimization is used, where N is the number of model parameters. In summary, the inverse solution based on IMOD-1 took about 4.5 hours (10 parameter iterations) and IMOD-2 required less than 13 hours of CPU time (12 Jacobian evaluations, 28 forward solutions).

5.7 Summary and conclusions

The inverse modeling efforts presented here are based on the 3D sub-regional model (SRM) simulating groundwater flow from the surface into the KWO access tunnel. The study aimed at calibrating the SRM on the basis of flow rate measurements available along the KWO tunnel (see Chapter 3).

Two variants of the model were investigated each corresponding to a different parametrization of the hydraulic conductivity-transmissivity. Because the inflow mainly occurs at locations where fractures intersect the tunnel, the original parameter structure of the previous model failed to resolve the

heterogeneous inflow distribution. This is a consequence of the assumed uniform transmissivities for both the K- and S- fracture family. In the second inverse run, the resolution of the fracture transmissivities (assigning model parameters for each fracture) significantly improved the agreement between observed and computed flow rates along the KWO tunnel. Further improvement of the model performance would require a comprehensive mesh modification (introduction of new fractures or shifting of existing fractures), which is beyond the scope of this study.

Figure 5.3 shows a good agreement for the previous and final model parameters in the relatively less permeable zones of the SRM. Larger differences in the final parameter values result for the more permeable 2D fracture zones. These discrepancies can be explained by the different treatment of the flow data available in the KWO tunnel: discrete values along the tunnel against integrated (lumped) data in the previous modeling work. This result shows the importance of discriminating the available data both in space and in time (if transient data were available). This modeling exercise demonstrates very clearly the possibilities for carrying out hydrodynamic repository site modeling with the tools and concepts available.

The calibration of subsequent model variants, improving the model performance, demonstrates the iterative nature of the hydrodynamic modeling work. The usefulness of previous model results was demonstrated in providing "a priori" information on the parameter values of the two-dimensional fracture zones that control the hydrodynamics of the sub-regional model. The uncertainty in the calibrated parameter values would have been reduced had the transient effects of the flow and head data been measured with accuracy at the tunnels, caverns, and from the site surface.

An appropriate design of sampling strategies aimed at obtaining transient hydraulic data during the construction of tunnels and caverns would help to improve the model structure, its reliability and its prediction capacity for the post-closure phase. With further modeling efforts it would have been possible to reduce the remaining differences between the simulated and observed flow data at the KWO tunnel, but this exercise is beyond the scope of this work. Last but not least, with current modeling tools and concepts, we consider such further modeling efforts to be necessary and, most important, feasible in the case of a "true" repository site model.

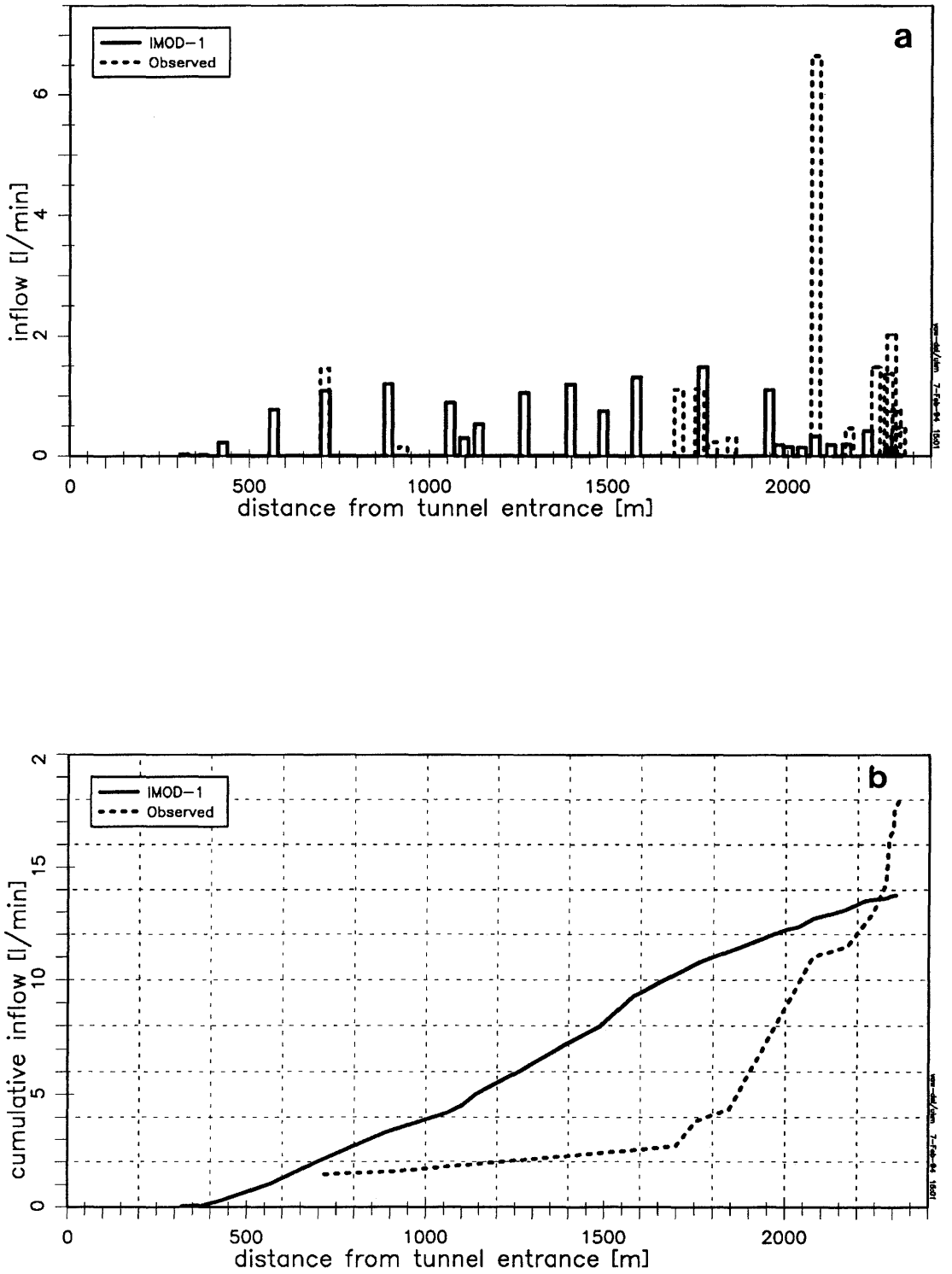

Figure 5.1 Run IMOD-1: (a) Computed and observed inflow rates; (b) computed and observed cumulative inflow rates.

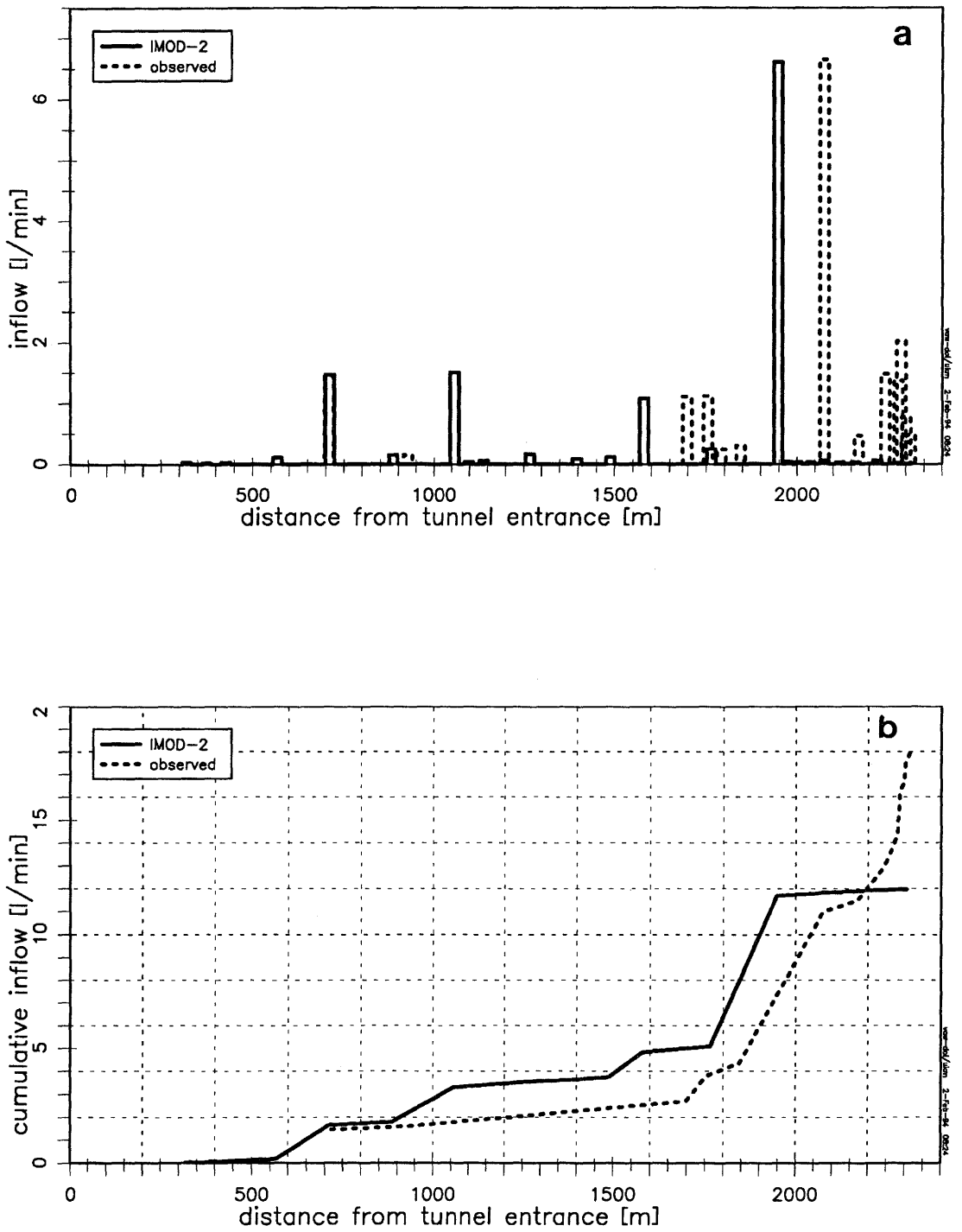

Figure 5.2 Run IMOD-2: (a) Computed and observed inflow rates; (b) Computed and observed cumulative inflow rates.

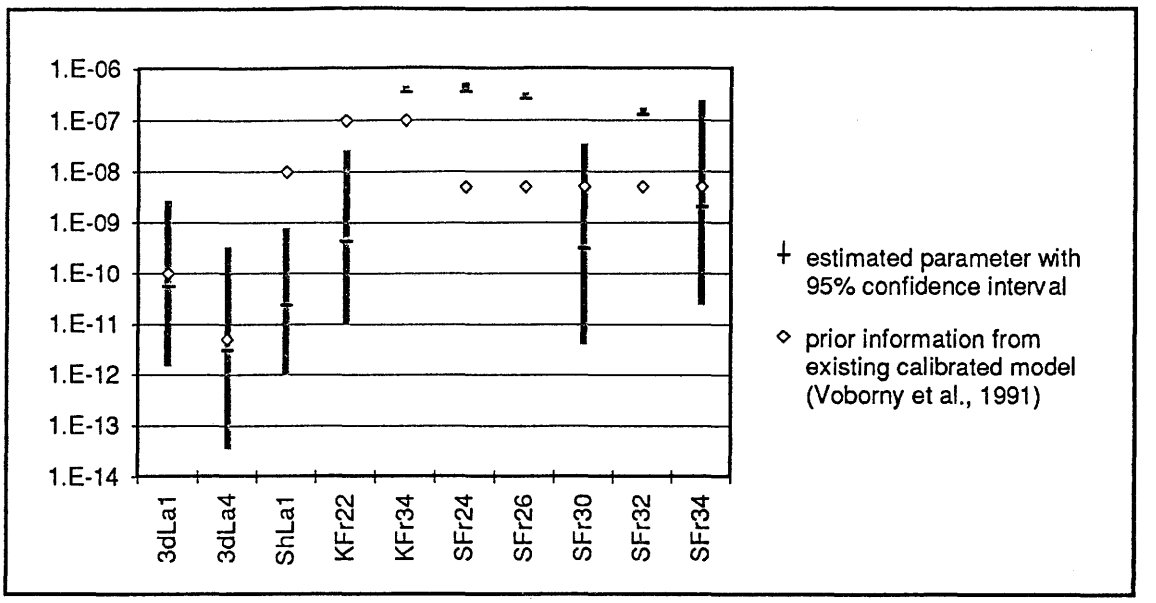

Figure 5.3 Computed parameter values with 95 % confidence intervals (run IMOD-2).

CHAPTER 6

GENERAL CONCLUSIONS AND RECOMMENDATIONS

A. Rivera and N.R. Correa

6 GENERAL CONCLUSIONS AND RECOMMENDATIONS

The evaluation of the transient effects caused by the presence of tunnels demonstrated the importance of: the modeling approach; the parameter values (in particular the matrix compressibility), the adopted initial conditions and infiltration rates; and, the nature of the space dimensions of the model (1D, 2D, 3D). In the two-dimensional free-surface case, the main uncertainties are related to the parameter values, the discretization of the tunnel (s), and the infiltration rates.

The results from the one- and two-dimensional analytical and numerical calculations are consistent for fixed-head boundary conditions. However, for the 2-D simulations with free-surface boundary conditions, the results are different with factors of up to 10, depending on the diffusivity coefficient used. A 2-D simulation of the head recovery after the sealing of a tunnel, for fixed-head boundary condition, showed that if the tunnel is sealed after 30 years of operation, the pressure in the rock matrix would take about 500 years to recover about 95% of its original condition.

For the three-dimensional case, the most relevant aspect was the grid refinement of the existing finite-element mesh to include the 3-D tunnel. Given the complexity of the original topology of the grid, the 3-D refinement was not easy to accomplish. From this work we conclude, that in future 3-D models with similar complexity, the discretized 3-D tunnel should be included from the very beginning, when the grid is created following the original geology. Otherwise, it becomes very difficult, if not impossible, to include such a 3D feature onto an existing grid as the one in the GTS, without having to modify the original model topology.

For the 3-D model, the time needed to reequilibrate to a new steady-state condition after the pressure field was disturbed by the presence of the tunnel, was uneven. It took from 5 to 10 years for the hydraulic heads to reach a steady-state condition between the tunnel elevation and the top surface. The western-most part of the model was not very much affected by the presence of the tunnel given the high topographic relief which condition the recharge. It took from 10 to 20 years to reach steady-state at eastern part of the tunnel. The hydraulic head below the tunnel needed about 500 years to reach equilibrium. The simulation of the recovery time after the closure of a fictitious repository, indicated that it would take about 70 to 100 years for the head to recover, around the tunnel location.

The results of the 3-D transient calculations are more plausible than the previous 2-D transient simulations because several 2-D fractures were included in the former.

For the automatic calibration of the SRM, two variants were investigated, each

corresponding to a different parametrization of the 2D fractures for hydraulic conductivity/transmissivity. Because the inflow mainly occurs at locations where fractures intersect the tunnel, the original parameter structure of the previous model failed to resolve the observed heterogeneous inflow distribution. These discrepances can be explained by the different treatment of the flow data available in the KWO tunnel: discrete values along the tunnel against integrated (lumped) data in the previous modeling work. This result shows the importance of discriminating the available data both in space and in time (if transient data were available). This modeling exercise demonstrated very clearly the possibilities for successfully carrying out an hydrodynamic repository site modeling with the tools and concepts available.

The calibration of subsequent model variants, improving the model performance, demonstrated the iterative nature of the hydrodynamic modeling work. The uselfulness of previous model results was demonstrated in providing "a priori" information on the parameter values of the two-dimensional fracture zones that control the hydrodynamics of the sub-regional model. The uncertainty in the calibrated parameter values would have been reduced had the transient effects of the flow and head data been measured with accuracy at the tunnels, caverns, and from the site surface.

An appropriate design of sampling strategies aimed at obtaining transient hydraulic data during the construction of tunnels and caverns would help to improve the model structure, its reliability and its prediction capacity for the post-closure phase. With the actual modeling tools and concepts, we consider such further modeling efforts as necessary, and most important, feasible in the case of a "true" repository site model.

The scoping of the numerical load and computer capacity, for the simulation of a three-dimensional coupled thermo-hydraulic model, indicated that with the available software and hardware facilities, such a problem can not be solved. Thus, the significance of the thermal effects in this case remains an open question that needs to be solved in the future.

We believe that the main limiting factors are the problem size and its non-linear nature. Additionaly, the heterogeneity of the conceptual model and its three-dimensional nature make it impossible to run with the available computer facilities and type of numerical code. This type of problem probably could only be run with a supercomputer (e.g., *CRAY YMP-4D*), or with a different numerical approach (e.g., parallel processing and/or pre-conditioned conjugate gradient method). The program NAMMU is currently underway to adapte it for effectively running in computers with parallel architecture and with the use of the PCCG. Further numerical investigation was beyond the scope of this work. Even if the present model could be run, it may still be necessary to refine the existing grid according to the grid Peclet number analysis.

We conclude that the main goals of project MOD phase III were achieved. The

methodologies and tools developed during this work, as well as the modeling strategy and actual simulations, can be useful for future site-specific hydrodynamic modeling studies within the scope of NAGRA. Automated inverse modeling has proven to be a powerful tool for model calibration. The scoping of computer load and grid discretization, for large problems (3D) with complex hydrogeology and transient or coupled problems, can be used to better design future specific studies. In one word, it is believed that considerable know-how and experience have been acquired related with the hydrogeologic behaviour of low permeable heterogeneous medium around underground constructions.

Finally, some practical recommendations may be relevant for modeling a real site where a radioactive-waste repository is planned.

- It is strongly recommended that the groundwater influxes into access drifts to the future repository be measured soon (e.g., first days and weeks) after construction. These data can be used later for performance assessment and for a reliable detailed calibration of a site-specific numerical model.

- Additionally, if the evolution with time of measured fluxes and heads is available, this information could be used as credible input for the analysis of the post-closure phase of the repository, i.e., for setting the boundary conditions for the near-field in the transient phase. Furthermore, the hydraulic diffusivity of the medium surrounding the drifts could be quantified if time-dependent flow and pressure measurements are available.

7 ACKNOWLEDGEMENTS

The work reported here was carried out under contract with NAGRA. Special recognition for fruitful comments and discussions goes to J. Troesch (VAW-ETH), W. Huerlimann (Colenco) and S. Vomvoris (Nagra). The technical review of F. Pasquier contributed to improving the presentation of this report.

Finally, we thank L. McKinley for her editorial comments.

8 REFERENCES

BREDEHOEFT, J.D. and I.S. PAPADOPULOS, 1965. Rates of vertical groundwater movement estimated from the earth's thermal profile, *Water Resour. Res.*, 1(2), 325-328.

CARRERA, J., 1984. Estimation of aquifer parameters under transient and steady- state conditions, Dissertation, University of Arizona, Tucson.

CARRERA, J. and S.P. NEUMAN, 1986a. Estimation of aquifer parameters under transient and steady-state conditions: 1. Maximum Likelihood Method incorporating prior information, *Water Resour. Res.*, vol. 22(2), 199-210.

CARRERA, J. and S.P. NEUMAN, 1986b. Estimation of aquifer parameters under transient and steady-state conditions: 2. Uniqueness, stabillity and solution algorithms, *Water Resour. Res.*, vol. 22(2), 211-227.

CARRERA, J. and S.P. NEUMAN, 1986c. Estimation of aquifer parameters under transient and steady-state conditions: 3. Application to synthetic and field data, *Water Resour. Res.*, vol. 22(2), 228-242.

CHALMERS B.W. and N.R. CORREA, 1993. FLG: Hydraulic information at the sub-regional scale of the Grimsel Test Site. Nagra Internal Report, Nagra, Wettingen, Switzerland.

FINSTERLE, S, 1991. Programm zur Verfeinerung von Finite-Elemente-Netzen, version UIAG. ETH Zürich.

FOSTER, C. and L. SMITH, 1988. Groundwater flow systems in montanious terrain, 1. Numerical modeling technique. *Water Resour. Res.* 24(7) 999-1010.

FREEZE, R.A. and J.C. CHERRY, 1979. Groundwater. Prentice Hall, Englewood Cliffs, New Jersey.

FRICK, U., W.R. ALEXANDER, B. BAEYENS, P. BOSSART, M.H. BRADBURY, CH.BÜHLER, J. EIKENBERG, TH. FIERZ, W. HEER, E. HOEHN, I.G. MCKINLEY, and P.A. SMITH, 1992. Grimsel Test Site, The Radionuclide Migration Experiment - Overview of Investigations 1985 - 1990. NTB 91-04, Nagra, Wettingen.

HÜRLIMANN, W., 1994. FRACMESH, a program for the generation of Finite-Element meshes for the hydrodynamic modeling of fractured rocks. NTB 93-36, Nagra, Wettingen, Switzerland.

HÜRLIMANN, W., A. RIVERA, S. MISHRA and N. CORREA, 1992. Project MOD III Status Report 1991, Nagra Internal Report, Nagra, Baden, Switzerland.

IAEA, 1982. Radioactive Waste Management Glossary, International Atomic Energy Agency, IAEA-TECDOC-264, Vienna.

IAEA, 1988. Radioactive Waste Management Glossary, 2nd edition, International Atomic Energy Agency, IAEA-TECDOC-447, Vienna.

KUHLMANN, U., 1992. Inverse Modellierung in geklüfteten Grundwasserträgern, Versuchsanstalt für Wasserbau, Hydrologie und Glaziologie, Mitteilung Nr. 120, Zürich.

MARSILY, G. de, 1986. Quantitative hydrogeology, groundwater hydrology for engineers, Chapter 11, Academic Press Inc.

NAGRA, 1985a. Grimsel Test Site: Overview and Test Programs. - Nagra Technical Report NTB 85-46, Baden, Switzerland.

NAGRA, 1985b. Felslabor Grimsel: Übersicht und Untersuchungs- programme. Nagra Technischer Bericht NTB 85-47, Baden, Switzerland

NAMMU, 1993. NAMMU User Guide, Release 6.1 (L.J Hartley and C.P.Jackson) AEA Technology Decomissioning & Waste Management, Harwell, UK.

NEUMAN, S.P. and P.A. WITHERSPOON, 1970. Finite element method of analyzing steady-state seepage with a free surface. *Water Resour. Res.* 6(3), 889-897.

OBAYASHI CORPORATION, 1993. Kristallin-1: Repository layout study based on rock mechanics considerations. Preliminary calculation of temperature distributions around an emplacement tunnel. Final report of task 3-3; Obayashi Corporation, Tokyo, Japan.

RIVERA, A. and G. RESELE, 1992. Analytical and numerical evaluations of variable-density groundwater flow in northern Switzerland. Nagra Internal Report, Nagra, Wettingen.

RIVERA, A., W. HÜRLIMANN, J. TRÖSCH, U. KUHLMANN, F. MÜRI and N. CORREA, 1993a. Project MOD-III status report 1992. Transient effects, boundary conditions, validation concepts. Nagra Internal Report, Nagra, Wettingen.

RIVERA, A., U. SCHRÖDER, and N. CORREA, 1993b. Project MOD: three-dimensional groundwater transient calculations with the sub-regional model including the KWO tunnel. Nagra Internal Report, Nagra, Wettingen.

SUN, N.-Z. and W. W.-G. YEH, 1990a. Coupled inverse problems in groundwater modeling: 1. Sensitivity analysis and parameter identification, *Water Resour. Res.*, Vol. 26(10), 2507-2525.

SUN, N.-Z. and W. W.-G. YEH, 1990b. Coupled inverse problems in groundwater modeling: 2. Identifiability and experimental design, *Water Resour. Res.*, Vol. 26(10), 2527-2540.

SUN, N.-Z. and W. W.-G. YEH, 1992. A stochastic inverse solution for transient groundwater flow: Parameter identification and reliability analysis, *Water Resour. Res.*, Vol. 28(12), 3269-3280.

TRÖSCH, J., 1990. Beschreibung des dreidimensionalen, stationären und instationären Grundwasserprogramms GW3D. ETH Zürich.

USUNOFF, E., J. CARRERA and S.F. MOUSAVI, 1992. An approach to the design of experiments for discriminating among alternative conceptual models, *Advances in Water Resources*, Special Issue: Validation of Geo-hydrological Models, Vol.15(3),199-214.

VOBORNY, O., P. ADANK, W. HÜRLIMANN, S. VOMVORIS and S. MISHRA, 1991. Grimsel Test Site: Modeling of groundwater flow in the rock body surrounding the underground laboratory, NTB 91-03, Baden, Switzerland.

YEH, W. W.-G. and N.-Z. SUN, 1990. Variational sensitivity analysis, data requirements, and parameter identification in leaky aquifer systems, *Water Resour. Res.*, Vol. 26(9), 1927-1938.